3-22-2017

Spatio-temporal Dynamics of Soil Composition and Accumulation Rates in Mangrove Wetlands

Joshua L. Breithaupt
University of South Florida, josh.breithaupt@gmail.com

Spatio-temporal Dynamics of Soil Composition and Accumulation Rates in Mangrove Wetlands

by

Joshua L. Breithaupt

A dissertation submitted in partial fulfillment
of the requirements for the degree of
Doctor of Philosophy
College of Marine Science
University of South Florida

Co-Major Professor: Joseph (Donny) M. Smoak, Ph.D.
Co-Major Professor: Robert H. Byrne, Ph.D.
Pamela Hallock Muller, Ph.D.
Brad E. Rosenheim, Ph.D.
Stephen E. Davis III, Ph.D.

Date of Approval:
March 8, 2017

Keywords: Mangroves, Accretion, Carbon Burial, Sea-Level Rise, Timescale, Everglades

Acknowledgments

This research was funded by the University of South Florida College of Marine Science fellowships provided by Anne and Werner Von Rosenstiel and the St. Petersburg Downtown Partnership Endowed Fellowship in Coastal Science, and under STAR Fellowship Assistance Agreement no. F13B20216 by the U.S. Environmental Protection Agency (EPA). This manuscript has not been formally reviewed by EPA. The views expressed are solely those of the author, and EPA does not endorse any products or commercial services mentioned in this publication. Material research support was provided by the National Science Foundation under South Florida Water, Sustainability & Climate grant 1204079, the US Fish & Wildlife Service's State Wildlife Grants Program (#F13AF00982), and NASA-JPL "Vulnerability Assessment of Mangrove Forest Regions of the Americas" [LSU subcontract #1452878]. Discussions with faculty and students in the Florida Coastal Everglades Long Term Ecological Research program (supported by the National Science Foundation under grant DEB-1237517) are gratefully acknowledged.

Co-author assistance was provided by the following: Chapter 1: Joseph M. Smoak, Victor H. Rivera-Monroy, Edward Castañeda-Moya, Ryan P. Moyer, Marc Simard, & Christian J. Sanders; Chapter 2: Joseph M. Smoak, Christian J. Sanders, & Tiffany Troxler; Chapter 3: Joseph M. Smoak, Robert H. Byrne, Matthew N. Waters, Ryan P. Moyer, & Christian J. Sanders.

Table of Contents

List of Tables iii

List of Figures iv

Abstract vi

Introduction 1
Context and Objectives 1
References 3

Chapter 1: Partitioning the relative contributions of organic matter and mineral sediment to accretion rates in carbonate platform mangrove soils 7
Abstract 7
1. Introduction 8
2. Methods 10
2.1 Study area 10
2.2 Soil gravimetric measurements 12
2.3 Radiometric dating, rate calculations, & statistical comparisons 13
2.4 Modeling SOM and SIM contributions to accretion 14
3. Results 16
3.1 Gravimetric results and soil classification scheme 16
3.2 Radiometric results 16
3.3 Rates of SOM, SIM, and accretion 17
3.4 Model results 18
4. Discussion 19
4.1 SOM and SIM are non-additive contributors to soil volume 19
4.2 SOM drives accretion; SIM drives bulk density 20
4.3 Accretion and historical rates of sea-level rise 22
4.4 Estimating future accretion requirements compared with sea-level rise 23
5. Conclusions 24
References 25
Tables 32
Figures 37

Chapter 2: Spatial variability of organic carbon, calcium carbonate and nutrient burial rates spanning an estuarine gradient in the coastal Everglades 43
Abstract 43
1. Introduction 44
2. Methods 46
2.1 Study Area 46
2.2 Mangrove above-ground vegetation characterization 47
2.3 Soil characterization and dating 48
2.4 Estimating $CaCO_3$ dissolution rates from $CaCO_3$:TP ratios 49
2.5 Statistical analyses 50
3. Results 50

3.1 Above-ground vegetation characteristics 50
3.2 Site soil characteristics 51
3.3 Soil fluxes 51
3.4 $CaCO_3$:TP and carbonate dissolution 52
4. Discussion 53
4.1 Spatial variability of above-ground vegetation and belowground rates 53
4.2 Carbon Burial Efficiency 55
4.3 Potential $CaCO_3$ dissolution 57
4.4 Regional Carbon budget implications 60
References 61
Tables 70
Figures 73

Chapter 3: Bias in timescale assessments of coastal wetland sea-level rise vulnerability 79
Abstract 79
1. Introduction 79
2. Methods 83
2.1 Literature review 83
2.2 Regional focus 83
2.3 Regional environmental categories 84
2.4 Timescale definitions 85
2.5 Data analysis and interpretation of literature data 86
2.6 Case study locations 88
2.7 100-year projections of accretion and elevation change balances as a function of local SLR 88
3. Results 89
4. Discussion 91
References 96
Tables 104
Figures 106

Conclusions 113
Key Findings 113
Future directions 114

Appendix 1 117
List of acronyms, abbreviations and uncommon terms 117

List of Tables

Table 1.1: Average loss-on-ignition (LOI) percentage and dry bulk density (DBD) by site for each river/transect. 32

Table 1.2: 100-year mean rates of accretion, soil organic matter (SOM), and soil inorganic matter (SIM) accumulation by Site. See footnotes for explanation of uncertainties. 33

Table 1.3: Multiple linear regression statistics and coefficients (Top-down model) for the fluxes of organic matter (SOM) (kg m^{-2} yr^{-1}) and mineral sediment (SIM) (kg m^{-2} yr^{-1}) vs. accretion rates (cm yr^{-1}) for each soil class. 34

Table 1.4: Linear regression statistics for modelled vs. observed average accretion rates (by soil class) of samples from this dataset with ^{210}Pb ages of 10-, 50- and 100-years. 34

Table 1.5: Mean (± 95% C.I.) density-normalized accretion rates with local rates of sea level rise (recorded at Key West, FL & Progreso, Mexico) over the most recent 10-, 50-, and 100-year periods. 35

Table 1.6: Required SOM and SIM accumulation rates necessary to achieve accretion targets by soil class calculated using Equation 1 and terms from Table 3. 36

Table 2.1: Mean (± 1SE) soil content of organic carbon (TOC), calcium carbonate ($CaCO_3$), and nutrient ratios by site and site classification. 70

Table 2.2: 100-year mean accumulation rates of organic carbon, total nitrogen, total phosphorous, and calcium carbonate by site and by site classification. 71

Table 2.3: Regression statistics for 100-year mean soil fluxes vs. upstream distance (x). 71

Table 2.4: Core-specific mean TP fluxes, baseline and slope molar $CaCO_3$:TP along with interval-specific and total core estimates of $CaCO_3$ dissolution rates. 72

Table 3.1: Description of methods used to measure accretion and surface elevation change in coastal wetlands, along with strengths, weaknesses, and assumptions of each 104

Table 3.2: Definition of terms related to measurements of accretion and elevation change in coastal wetlands 105

Table 3.3: Mean and standard deviation (SD) of length of record (years) and sample number for elevation change and sediment accretion rates (SAR) for each timescale by region 105

List of Figures

Figure 1.1 Map of soil core locations in Florida, USA and the Yucatan Peninsula in Mexico: Ten Thousand Islands (A), Everglades National Park (B), Celestun Lagoon (C), and Sian Ka'an (D). 37

Figure 1.2 Mean (± 1 Std. Dev.) LOI and DBD for soil core intervals by Soil Class. 38

Figure 1.3 100-year mean accumulation and accretion rates (± 1 SE) by soil class. 38

Figure 1.4 Accretion rates for soil core intervals (≤ 100 years old) as a function of a) organic (SOM) & and b) inorganic matter (SIM) accumulation rates. 39

Figure 1.5 a) Total Dry Bulk Density as a function of the SOM & SIM fractions of Dry Bulk Density. b) Dry Bulk Density as a function of SIM accumulation rates, and c) Dry Bulk Density as a function of the SOM accumulation rate. 40

Figure 1.6 Depth profiles (cm) of excess ^{210}Pb activities (dpm g^{-1}) & total core inventories (dpm cm^{-2}). 41

Figure 1.7 Bottom-up model of mangrove cores from this dataset; DBD = 1 / (LOI / k_1 + (1 - LOI) / k_2)) 42

Figure 2.1 a) Everglades National Park and b) WSC core sampling locations on the Shark, Harney, and Broad Rivers. 73

Figure 2.2 Above-ground biomass characteristics by site for each river and soil class 73

Figure 2.3 Mean (± 1 SE) burial rates by site classification 74

Figure 2.4 Plots of $CaCO_3$:TP vs. age/depth by site 75

Figure 2.5 Above-ground biomass as a function of soil total phosphorous (black circles) compared with model from Castañeda-Moya et al. (2013) (dashed line) 76

Figure 2.6 Organic carbon burial and soil C respiration (Troxler et al., 2015) as a fraction of site-specific above- and belowground mangrove carbon net primary productivity (CNPP) (Castañeda-Moya et al., 2013) 76

Figure 2.7 Comparison of maximum $CaCO_3$:TP ratios in WSC cores with regional ratios measured at different depths, and surface samples (0-4cm) from sites across southwest Florida 77

Figure 2.8 Molar $CaCO_3$:TP as a function of soil organic matter (OM%) for a) individual soil core intervals, and b) samples throughout Florida Bay and SW Everglades compiled from Kang & Trefry (2013) 77

Figure 2.9 Regressions of molar $CaCO_3$:TP with the flux of $CaCO_3$ (black circles; R^2: 0.58) and TP (gray circles; R^2: 0.26) 78

Figure 2.10 Mean above-ground vegetation characteristics by site classification 78

Figure 3.1 Timescales of processes affecting change of soil body accretion and elevation in coastal wetlands, and the methods used to measure them 106

Figure 3.2 Location of regions examined in this study 107

Figure 3.3 Average rates of elevation change (Elevation Δ) and sediment accretion (SAR) by timescale for each region 108

Figure 3.4 Comparison of average rates of accretion and elevation change for sub-decadal and decadal timescales for environmental categories within each region 108

Figure 3.5 Conceptual model of timescale hierarchies of soil body rates as a function of depth/age 109

Figure 3.6 Timescale dependence of 100-year soil body balances relative to local sea-level 110

Figure 3.7 Site-specific timescale hierarchies 111

Figure 3.8 Case studies: raw accretion and elevation data (total mm relative to initial benchmark) 112

Abstract

Coastal wetlands are globally important environments for biogeochemical cycling and are the object of intensive research related to the sequestration and exchange of carbon with oceans, continents, and the atmosphere. Wetland soil core records of organic carbon (OC) provide insights about future ecosystem responses to global change by identifying temporal variability in the context of environmental changes including sea level rise (SLR), anthropogenic reductions in freshwater flow, and landscape-scale disturbance events. My studies of Gulf of Mexico mangroves involved the use of radiometrically-dated soil cores to identify spatial and temporal accumulation trends of various constituents including organic and carbonate carbon, and macro-nutrients. My dissertation includes a literature review to assess the timescales of these processes and refine global perspectives on coastal wetland vulnerability.

The contributions of organic and mineral matter to soil accretion (mm yr^{-1}) was measured to (a) quantify how the supply of each may allow regional mangroves to keep pace with various SLR scenarios and, (b) assess wetland carbon sink capacity and stability in southwest Florida and the Yucatan Peninsula of Mexico. Mangroves in this region are largely devoid of terrigenous mineral sediments, and it has been hypothesized that storm surge-driven accretion of marine sediments could improve the capability of these locations to keep pace with SLR. Rates of accretion and organic matter accumulation were statistically similar across all four study regions, whereas mineral deposition rates ranged over two orders of magnitude. The volumetric contribution of mineral sediment to accretion is minimized by its high density. Organic matter, whose porous structures allow for highly variable densities, can contribute to a wide range of accretion rates and is a strong predictor of accretion. Future sustainability of these wetlands is

more strongly dependent on the balance between soil organic matter production and preservation than the provision of storm-derived mineral sediments.

To understand how OC sequestration will respond to SLR, the spatial and temporal variability of OC burial rates (g m^{-2} yr^{-1}) were examined across ecosystem gradients in salinity, nutrient availability and mangrove productivity in the coastal Everglades. Results showed relatively little spatial variability and indicated that OC burial in the region is slow compared to rates in mangroves globally. However, significant regional differences in OC burial were observed in the context of primary productivity. Over a centennial timescale, mid-stream sites sequestered roughly 22% of annual net primary production and upstream sites preserved less than 10%. Least efficient sequestration occurs in the oligohaline ecotone, where increases in groundwater salinities and the potential for sulfate reduction have been recorded in the past decade. These findings indicate a significant slowdown in OC burial, and suggest that accelerating SLR will cause a substantial loss of historically sequestered carbon. The loss and potential out-welling of this carbon (including particulate and dissolved organic matter, dissolved CO_2, and carbonate alkalinity) has important and complex implications for neighboring marine ecosystems including coral reefs and seagrass meadows.

Several recent high-profile publications have used 5–15 years of soil accumulation rates to model wetland SLR-vulnerability outcomes over the next 50–100 years. To provide perspectives on these models, data that were generated from observations on multiple timescales (sub-annual to millennial) around the globe were used in a meta-analysis to determine the role of observational timescale on assessment outcomes. This analysis focused on rates of accretion and elevation change because of the wide availability of these data. Results demonstrate that rates of soil-body change exhibit a dependence on the length of time over which observations are made. Timescale hierarchies are driven by post-depositional diagenesis, ecosystem state changes, and regional effects primarily related to hydrology and sediment supply. Longer periods of observation utilizing multiple geochronological methods are needed to differentiate trend-changes

from apparent changes that, in fact, may be due to regular periodicity. A conceptual model is presented that categorizes and explains timescale hierarchies in a soil's geochemical history.

Introduction

Context and Objectives

There is growing consensus that anthropogenic activities have altered coastal biogeochemical cycles in the industrial age, with mounting evidence for the transformation of coastal systems from sources to sinks of carbon (Bauer et al., 2013; Cai, 2011). Although mangroves only cover between 138,000 and 152,000 km^2 globally (Spaulding et al., 2010; Giri et al., 2011), they provide disproportionately high contributions to environmental, societal, and economic processes both in the sub-tropical regions where they exist as well as around the globe. In addition to providing habitat and nursery grounds for numerous fauna (Nagelkerken et al., 2008), natural resources for human communities, and stabilization and protection of shorelines from storm surge (Alongi, 2008; Zhang et al., 2012), the past two decades have seen a steadily increasing body of literature focused on the substantial contribution these forests make to the global carbon budget (Bouillon et al., 2008; Kristensen et al., 2008). Mangrove wetlands are estimated to store more organic carbon (OC) in belowground standing stocks than do the entire ecosystems in boreal, temperate or tropical upland forests (Donato et al., 2011) and they continue to bury carbon at annual rates exceeding those of terrestrial forests (Breithaupt et al., 2012; Mcleod et al., 2011). There is great urgency to the attention given to mangroves because these coastal wetlands are being deforested at alarming rates, with between 30-50% of areal coverage lost since the 1940s (Mcleod et al., 2011). Not only is a globally significant carbon sink being lost, but their land-use conversion returns CO_2 to the atmosphere. Understanding of OC stocks and burial rates in mangroves informs research that quantitatively estimates the global impact to atmospheric CO_2 levels due to projected mangrove deforestation and peat loss, or alternatively, the carbon offset potential that may be achieved through mangrove conservation (Alongi, 2011; Pendleton et al., 2012; Siikamäki et al., 2012).

In addition to direct anthropogenic causes of mangrove deforestation, including wood harvesting, construction of aquaculture shrimp ponds, and coastal development, it is sea-level rise and modifications of coastal hydrology (Krauss et al., 2014; Lewis et al., 2015; Lovelock et al., 2015) that pose a pressing and immediate threat to mangroves. While a moderate amount of sea-level rise is a natural and beneficial control on mangrove sedimentation and vertical growth, the accelerated rates anticipated in the coming century exceed historical records of mangrove vertical growth. While coastal wetland vulnerability literature has often noted the potential for landward migration to evade the threat of permanent submergence, there are consequences of such migrations that have yet to be examined. One such question has to do with the vulnerability of the currently sequestered stocks of soil carbon, many which have accumulated over thousands of years (Donato et al., 2011; Yao and Liu, 2017), and the uncertainty of their fate when the overlying vegetation dies and is no longer able to hold it in place. Maximum estimates of the impacts on carbon cycles may assume a worst-case scenario in which all the soil carbon will be oxidized and returned to the atmosphere, although remobilization and export to nearby marine ecosystems is also possible. In addition to questions regarding this vulnerability, there are also temporal trade-offs that will affect other ecosystem services of mangroves. Because mangroves experience year-round growth, the implication of upslope migration (as opposed to lateral expansion) are that older, more mature sections of forest near the seaward edge will be replaced by younger immature forests on the landward front. There are sure to be substantial trade-offs in ecosystem function because of such mismatched replacements. Recent soil carbon research suggests that it may take as much as 20 years for a newly established mangrove wetland to reach a level of maturity for peat accumulation to begin (Osland et al., 2012; Yando et al., 2016).

There were three over-arching research objectives for this dissertation. (1) The first was to quantify the respective soil accretion contributions made by organic matter and mineral sediment in mangrove wetlands where there is limited supply of allochthonous material. This kind of quantitative analysis has been conducted for coastal and freshwater tidal marshes throughout North America (e.g., Nyman et al.,

1990; Neubauer, 2008; Morris et al., 2016), but this work represents the first such analysis for mangrove wetlands. Results from this research enable assessments of the vertical growth capacity of mangrove soils, and provide a means of assessing vulnerability relative to regional projections of sea-level rise. (2) Efforts to constrain local carbon budgets are being undertaken in numerous coastal environments around the world because of great variability in the rates of production, export, and sequestration, and the need to provide greater precision in global carbon models (Bauer et al., 2013). Although the southwest Everglades represent one of the most well-studied mangrove carbon budgets in the world, with numerous studies focused on the overall budget as well as its individual components that date back over 20 years, there are still many questions and large uncertainties in the mass balance (Troxler et al., 2013 and references therein). This research quantified the long-term (~100-yr) organic carbon burial rates across a landscape gradient exhibiting substantial aboveground biomass variability that reflects the P-limitation in the estuary. In addition to OC, this research examined the spatial variability of carbonate burial rates and provided a first-order estimate of potential dissolution rates. (3) Finally, the third chapter considered the role that timescale plays in assessments of the vertical change capacity for both mangroves and coastal marshes. The findings from this research have implications for what kind of methods are employed to evaluate the vulnerability of coastal wetlands relative to sea-level rise.

References

Alongi, D., 2008. Mangrove forests: Resilience, protection from tsunamis, and responses to global climate change. Estuar. Coast. Shelf Sci. 76, 1–13. doi:10.1016/j.ecss.2007.08.024

Alongi, D.M., 2011. Carbon payments for mangrove conservation: ecosystem constraints and uncertainties of sequestration potential. Environ. Sci. Policy 14, 462–470. doi:10.1016/j.envsci.2011.02.004

Bauer, J.E., Cai, W.-J., Raymond, P. a., Bianchi, T.S., Hopkinson, C.S., Regnier, P. a. G., 2013. The changing carbon cycle of the coastal ocean. Nature 504, 61–70. doi:10.1038/nature12857

Bouillon, S., Borges, A. V., Castañeda-Moya, E., Diele, K., Dittmar, T., Duke, N.C., Kristensen, E., Lee, S.Y., Marchand, C., Middelburg, J.J., Rivera-Monroy, V.H., Smith, T.J., Twilley, R.R., 2008. Mangrove production and carbon sinks: A revision of global budget estimates. Global Biogeochem. Cycles 22, 1–12. doi:10.1029/2007GB003052

Breithaupt, J.L., Smoak, J.M., Smith, T.J., Sanders, C.J., Hoare, A., 2012. Organic carbon burial rates in mangrove sediments: Strengthening the global budget. Global Biogeochem. Cycles 26, 1–11. doi:10.1029/2012GB004375

Cai, W.-J., 2011. Estuarine and Coastal Ocean Carbon Paradox: CO2 Sinks or Sites of Terrestrial Carbon Incineration? Ann. Rev. Mar. Sci. 3, 123–145. doi:10.1146/annurev-marine-120709-142723

Donato, D.C., Kauffman, J.B., Murdiyarso, D., Kurnianto, S., Stidham, M., Kanninen, M., 2011. Mangroves among the most carbon-rich forests in the tropics. Nat. Geosci. 4, 293–297. doi:10.1038/ngeo1123

Giri, C., Ochieng, E., Tieszen, L.L., Zhu, Z., Singh, A., Loveland, T., Masek, J., Duke, N., 2011. Status and distribution of mangrove forests of the world using earth observation satellite data. Glob. Ecol. Biogeogr. 20, 154–159. doi:10.1111/j.1466-8238.2010.00584.x

Krauss, K.W., McKee, K.L., Lovelock, C.E., Cahoon, D.R., Saintilan, N., Reef, R., Chen, L., 2014. How mangrove forests adjust to rising sea level. New Phytol. 202, 19–34. doi:10.1111/nph.12605

Kristensen, E., Bouillon, S., Dittmar, T., Marchand, C., 2008. Organic carbon dynamics in mangrove ecosystems: A review. Aquat. Bot. 89, 201–219. doi:10.1016/j.aquabot.2007.12.005

Lewis, R.R., Milbrandt, E.C., Brown, B., Krauss, K.W., Rovai, A.S., Beever, J.W., Flynn, L.L., 2015. Stress in mangrove forests: Early detection and preemptive rehabilitation are essential for future successful worldwide mangrove forest management. Mar. Pollut. Bull. 109, 764–771. doi:10.1016/j.marpolbul.2016.03.006

Lovelock, C.E., Cahoon, D.R., Friess, D. a., Guntenspergen, G.R., Krauss, K.W., Reef, R., Rogers, K., Saunders, M.L., Sidik, F., Swales, A., Saintilan, N., Thuyen, L.X., Triet, T., 2015. The vulnerability of Indo-Pacific mangrove forests to sea-level rise. Nature 526, 559–563. doi:10.1038/nature15538

Mcleod, E., Chmura, G.L., Bouillon, S., Salm, R., Björk, M., Duarte, C.M., Lovelock, C.E., Schlesinger, W.H., Silliman, B.R., 2011. A blueprint for blue carbon : toward an improved understanding of the role of vegetated coastal habitats in sequestering CO2 9, 552–560. doi:10.1890/110004

Nagelkerken, I., Blaber, S.J.M., Bouillon, S., Green, P., Haywood, M., Kirton, L.G., Meynecke, J.-O., Pawlik, J., Penrose, H.M., Sasekumar, a., Somerfield, P.J., 2008. The habitat function of mangroves for terrestrial and marine fauna: A review. Aquat. Bot. 89, 155–185. doi:10.1016/j.aquabot.2007.12.007

Osland, M.J., Spivak, A.C., Nestlerode, J. a., Lessmann, J.M., Almario, A.E., Heitmuller, P.T., Russell, M.J., Krauss, K.W., Alvarez, F., Dantin, D.D., Harvey, J.E., From, A.S., Cormier, N., Stagg, C.L., 2012. Ecosystem Development After Mangrove Wetland Creation: Plant-Soil Change Across a 20-Year Chronosequence. Ecosystems 15, 848–866. doi:10.1007/s10021-012-9551-1

Pendleton, L., Donato, D.C., Murray, B.C., Crooks, S., Jenkins, W.A., Sifleet, S., Craft, C., Fourqurean, J.W., Kauffman, J.B., Marbà, N., Megonigal, P., Pidgeon, E., Herr, D., Gordon, D., Baldera, A., 2012. Estimating Global "Blue Carbon" Emissions from Conversion and Degradation of Vegetated Coastal Ecosystems. PLoS One 7, e43542. doi:10.1371/journal.pone.0043542

Siikamäki, J., Sanchirico, J.N., Jardine, S.L., 2012. Global economic potential for reducing carbon dioxide emissions from mangrove loss. Proc. Natl. Acad. Sci. U. S. A. 109, 14369–74. doi:10.1073/pnas.1200519109

Troxler, T., Gaiser, E., Barr, J., Fuentes, J., 2013. Integrated carbon budget models for the Everglades terrestrial-coastal-oceanic gradient: Current status and needs for inter-site comparisons. Oceanography 26, 98–107.

Yando, E.S., Osland, M.J., Willis, J.M., Day, R.H., Krauss, K.W., Hester, M.W., 2016. Salt marsh-mangrove ecotones : using structural gradients to investigate the effects of woody plant encroachment on plant – soil interactions and ecosystem carbon pools 104, 1020–1031. doi:10.1111/1365-2745.12571

Yao, Q., Liu, K., 2017. Dynamics of marsh-mangrove ecotone since the mid-Holocene : A palynological study of mangrove encroachment and sea level rise in the Shark River. PLoS One 12. doi:10.1371/journal.pone.0173670

Zhang, K., Liu, H., Li, Y., Xu, H., Shen, J., Rhome, J., Smith, T.J., 2012. The role of mangroves in attenuating storm surges. Estuar. Coast. Shelf Sci. 102–103, 11–23. doi:10.1016/j.ecss.2012.02.021

Chapter 1:
Partitioning the relative contributions of organic matter and mineral sediment to accretion rates in carbonate platform mangrove soils

Abstract

In coming decades, the global rate of sea-level rise (SLR) is projected to accelerate beyond rates observed over the past several millennia when mangrove wetlands have expanded in tropical, sub-tropical and temperate regions. There is substantial uncertainty about how distinct mangrove ecotypes inhabiting a wide range of geomorphic settings will respond to SLR acceleration, including the thresholds at which they will submerge permanently. In this study the relative contributions of soil organic and inorganic matter (SOM and SIM) to ^{210}Pb-derived accretion rates were examined at 23 mangrove sites in southwest Florida, USA and the Yucatan Peninsula in Mexico. These sites are situated atop carbonate platforms where there is wide variation in the availability of SIM (generally marine marl). To account for this variability, research sites were classified by SIM presence based on soil loss-on-ignition (LOI) values: organic sites (LOI>70%), intermediate sites (LOI=40–70%) and mineral sites (LOI<40%).

SOM accumulation rates were largely the same in the three soil classes in the past century ($p<0.05$); however, SIM accumulation rates in the intermediate and mineral sites were approximately 5 and 20 times greater, respectively, than rates in the organic sites. Despite this substantial difference in total mass accumulation rates, accretion rates were not statistically different between soil classes ($p<0.05$). Our analysis revealed that the rate of SOM accumulation is the best predictor of accretion rates, while the rate of SIM accumulation primarily predicts soil dry bulk density. These findings indicate that SOM and SIM do not contribute additively to soil volume. This is contrary to findings from North American coastal wetlands broadly, and suggests a unique characteristic of carbonate platform mangrove soils that lack a regular, substantive supply of terrigenous SIM.

Overall, accretion rates in the FL sites and a Yucatan site on the Caribbean Sea are maintaining pace with regional rates of SLR over the past 100-year and 50-year timespans, whereas the sites in Celestun Lagoon, MX (located on the Gulf of Mexico) exhibit an accretion deficit. Estimates of regional SLR rates range from 4.6 to 12.2 mm yr^{-1} by the year 2060. Based on accretion rates observed in the past century, some of these sites may be able to keep pace with the lower SLR estimate, but there is no evidence that any of these sites can match the higher rate.

1. Introduction

Many ecologically and economically valuable ecosystem services provided by coastal wetlands depend on their long-term equilibrium with relative sea-level rise (SLR) (Ellison and Stoddart, 1991; Woodroffe et al., 2016). A net result of SLR is the creation of accommodation space for the substrate to add mineral and organic materials from different sources under variable hydroperiod conditions. Additionally, SLR is a key regulator of mangrove productivity that adds organic matter at the soil surface and within the active root zone (McKee et al., 2007). The interaction of long-timescale SLR and short-timescale hydroperiod contribute to the depth, frequency, and duration of inundation that control sub/anoxic conditions that are favorable for long-term preservation of SOM. Conversely, if the rate of soil accumulation fails to keep pace with SLR, the wetland surface will gradually become submerged, permanently altering the soil biogeochemistry and structure and functioning of the local vegetation community (Cahoon et al., 2003; Lewis et al., 2015; McCloskey & Liu, 2013).

Soil accretion in coastal wetlands occurs by the net addition of organic and mineral materials resulting from a range of biophysical processes (Furukawa and Wolanski, 1996; Lynch et al., 1989; Nyman et al., 2006). Mineral sediments are delivered via riverine and/or longshore-tidal transport and storm-surge events (Castañeda-Moya et al., 2010; Smith et al., 2009; Smoak et al., 2013; Whelan et al., 2009). Sources of SOM include the *in situ* production of above- and below-ground (root) biomass (Castañeda-Moya et al., 2013, 2011; McKee et al., 2007), benthic algae (McKee et al., 2007; Sanders et al., 2014), as well as contributions of allochthonous material including marine vegetation such as seagrass

and macro algae or terrestrial vegetation and upland forest litter (Gonneea et al., 2004). The contribution of organic and mineral materials to accretion is dependent not only on the quantity, quality, and timing of their delivery or *in situ* production, but also on the size fractions and relative volumes occupied by each component.

The relative accretion contributions made by SOM and SIM have been well documented in freshwater, brackish and salt-marsh dominated environments (DeLaune et al., 1983; Turner et al., 2006; Neubauer, 2008; Nyman et al., 1990). Overall, these studies have found that organic matter is the dominant driver of accretion. Similar research is lacking in mangrove wetlands (Callaway et al., 1997). Some exceptions include work that has focused on mangroves trapping and collecting sediments (Furukawa and Wolanski, 1996; Kumara et al., 2010) and the contribution of different types of organic matter production and degradation to accretion and elevation change (Krauss et al., 2014).

Mangroves are distributed along temperate, subtropical and tropical coastlines in a range of distinct geomorphological settings (Woodroffe, 1992), and therefore exhibit highly variable productivity (Bouillon et al., 2008) and availability of mineral sediments. Because of these environmental differences, it is critical to evaluate not only overall accretion rates, but also the relative contribution made by different sources of material in each region. The objectives of this research were to evaluate the spatial variability of accretion rates in mangroves of southwest Florida and the Yucatan Peninsula of Mexico, and subsequently to quantify the accretion rate contributions made by SOM and SIM. Mangroves in south Florida and the Yucatan Peninsula are located in karstic, carbonate platform environments where the direct contribution of mineral sediment by rivers is limited or absent. This contribution contrasts with other geomorphic settings inhabited by mangroves such as river deltas where riverine inputs are the dominant driver of mineral sediment delivery and nutrient loading (Woodroffe, 1992). Specifically, the following hypotheses were evaluated: 1) organic matter is the dominant driver of accretion rates in both regions, and 2) the soil-volume contributions made by organic and mineral sediments are additive such that accretion rates will be highest where the combined mass of organic and mineral matter is greatest.

2. Methods

2.1 Study Area

Twenty-three soil cores were collected from four locations: two in south Florida [Ten Thousand Islands (TTI) and Everglades National Park (ENP)] and two in the Yucatan Peninsula, Mexico [Celestun Lagoon (CSTN) and Sian Ka'an Biosphere Reserve (SK)] (Fig. 1, Table 1). Observed gradients in coastal vegetation and hydrology in these karstic environments are the result of the underlying Pleistocene carbonate bedrock. The supply of terrigenous SIM is minimal and groundwater is the dominant input of freshwater into the coastal zone (Saha et al., 2011; Stalker et al., 2014).

Soil cores were collected in ENP in March 2013 along transects of different length on the Shark (25 km), Harney (14 km), and Broad Rivers (11 km) (Fig.1B). Transects in ENP represent landward decreases in salinity, tidal range, soil total phosphorous (Castañeda-Moya et al., 2013; Childers et al., 2006), and storm-derived marine sediments (Castañeda-Moya et al., 2010; Smith et al., 2009), all of which contribute to a landward decrease in soil bulk density, nutrient density, and mangrove above-ground biomass and productivity (Castañeda-Moya et al., 2013; Chen and Twilley, 1999). The sampling methodology was intended to be representative of transect position along each estuary, and soil cores were collected approximately 30–50 m from the bank of the river or tidal creek at each location.

The TTI cores were collected along a 6 km transect to the east of the Faka Union Canal near the Ten Thousand Islands National Wildlife Refuge in June 2014 (Fig. 1A). Hydrology at the TTI sites is mostly tidally-dominated. Throughout the latter half of the 20th Century the flow of water from the Picayune Strand to the north was heavily modified; as a result water is almost exclusively channelized in its delivery to the Faka Union Canal (Krauss et al., 2011).

Soil cores were collected from CSTN and SK in August 2012 (Fig. 1C & D). Celestun Lagoon is 21 km in length and is surrounded by ~19,000 ha of mangrove forests (Adame et al., 2014; Herrera-Silveira, 1996). Although the lagoon does not receive surficial freshwater drainages, the landscape is

dominated by cenotes (natural sinkholes) resulting from the dissolution of the limestone bedrock that provides a surface connection to subterranean groundwater (Stalker et al., 2014). Study sites in this region are not situated along a linear estuarine gradient as is found in the Everglades. However, like the Everglades sites, the supply of sediment is predominantly from the marine side (i.e., re-suspension, storm surges) rather than the upper watershed. Mangrove forests in the Celestun region represent a mosaic of fringe and basin stands surrounding the lagoon, and scrub mangroves in the interior (Zaldivar-Jimenez et al., 2010). The cenote features are surrounded by tall (~15–25 m) *Rhizophora mangle* and *Laguncularia racemosa* mangroves interspersed with freshwater vegetation. The freshwater spatial footprint around inland cenotes is limited to 50–100m; beyond this distance the mangrove species *Avicennia germinans* forms monospecific stands due to higher pore water salinity (> 40 ppt). The Sian Ka'an Biosphere Reserve is located on the Caribbean side of the Yucatan Peninsula (Fig. 1D). This region is also influenced by groundwater flow supplied through cenotes as well as marine exchange, and the landscape is dominated by scrub and fringe mangrove wetlands characterized by distinct forest structural attributes (Adame et al., 2013).

Because the Yucatan soil cores are not located along a linear landscape gradient (such as was present in TTI and ENP), the core sampling methodology was designed to be representative of the heterogeneous spatial distribution of above-ground mangrove biomass. Core PET was taken approximately 600 m from the lagoon near a cenote spring (i.e., *petén*) (Zaldivar-Jimenez et al., 2010). Core SIP (*Isla Pajaros*) was retrieved in a broad expanse of *R. mangle* scrub mangroves also approximately 600 m from the lagoon. Core AG was taken in a monospecific stand of *A. germinans* approximately 300 m inland from the lagoon; high soil carbonate content was observed at this site. Core BP (Big Patch) was also collected near a cenote, and was approximately 200 m from the head of the lagoon (Fig. 1C). Core SK was taken from the Caribbean coast, approximately 70m from the ocean in a fringe-dominated mangrove stand (Fig. 1D).

Most of the south Florida sites included a mix of the three dominant mangrove species that are present in the neotropics, with site differences in tree diameter (breast height, DBH), basal areas, and stem densities (Castañeda-Moya et al., 2013; Krauss et al., 2014). Exceptions in vegetation species composition in South Florida are for ENP sites WSC-1, 2, 3, & 7 (Fig. 1B) where the forests are dominated by *R. mangle* with some individuals of *L. racemosa* and *Conocarpus erectus* (buttonwood), but also include upland, freshwater vegetation such as leather ferns (*Acrostichum aureum L.)*, sawgrass (*Cladium jamaicense*) and spikerush (*Eleocharis sp*.). In the CSTN location, the BP core was collected in a mixed mangrove forest; the SIP core was collected in a broad expanse of scrub *R. mangle*, while the PET core was taken amidst very tall (~28 m), high biomass *R. mangle* near a freshwater cenote spring. The AG core was collected in a mono-specific stand of *A. germinans*. The Core SK was collected in the interior of a fringe mangrove stand co-dominated by *R. mangle* and *A. germinans*.

2.2 Soil Gravimetric Measurements

For the Florida sites, soil cores were collected with a PVC suction-coring device (10 cm diameter x 50 cm length) (*sensu* Meriwether et al., 1996) and sectioned in 2-cm intervals for the top 10 cm of each core, and then into 1-cm intervals until the 40-cm depth. The different sectioning depths were used to accommodate the less compacted nature of the surface sediments. Upon sectioning, aliquots of 2.3 cm diameter were collected, using a sharpened aluminum pipe, for measurements of dry mass and loss-on-ignition (LOI). For the Mexico sites, soil cores were collected using a PVC suction-coring device (14.6 cm diameter x 40 cm length) (Meriwether et al., 1996). Cores were extruded and sectioned into 2 cm intervals using a custom-made incremental soil-core extruding apparatus. Soil dry mass was measured after drying in an oven at 105°C for 24 hours. Total soil organic matter (SOM) was calculated via loss-on-ignition (LOI) at 550°C for three hours (Davies 1974). Mineral sediment (SIM) was calculated as total dry mass minus LOI mass. Each was reported as either percentage of total dry mass or as a flux (g m^{-2} yr^{-1}).

Four types of soil density measurements were considered in our analysis for comparative purposes. First, *dry bulk density* (DBD) was calculated as total dry mass divided by the initial wet volume of the sample (g cm^{-3}). Second, the SOM and SIM fractions of DBD were calculated as the LOI fraction × DBD (SOM fraction) or (1-LOI fraction) × DBD (SIM fraction) for each interval. Thirdly, *self-packing densities* represent the *in situ* volume occupied by SOM or SIM structures that include soil, roots, branches, leaves, and rocks. The method for estimating self-packing densities is described in section 2.4.2. Fourthly, *particle densities* represent the respective mass: volume ratios of the SOM and SIM minus the mass and volume occupied by water and gas; this measurement represents only the mass and volume of the solid particles for each constituent, and is typically measured using crushed, homogenized soil material in a pycnometer. The previously reported particle densities for coastal wetlands are 1.1–1.2 g cm^{-3} for SOM and 2.4–2.6 for SIM (DeLaune et al., 1983; Turner et al., 2006).

2.3 Radiometric Dating, Rate Calculations, & Statistical Comparisons

Radiometric dating was achieved by measuring ^{210}Pb via gamma spectrometry and applying the Constant Rate of Supply (CRS) model. For a detailed account of the procedures and instruments used for sample preparation and gamma counting, see Breithaupt et al. (2014) and Smoak et al. (2013). Uncertainties for accretion rates and mass fluxes were calculated based on propagation of the gamma counting errors for soil interval ages and mass accumulation rates (Binford, 1990). Two of the cores with low inventories of excess ^{210}Pb (cores AG and SK from Mexico) were dated using the Constant Initial Concentration (CIC) model (Smoak and Patchineelam, 1999). A low inventory in these locations likely indicates that some portion of the record is missing, and therefore invalidates use of the CRS model (Appleby and Oldfield, 1978). With the CIC model, a net rate of sediment mass accumulation can be derived based on a best fit for the regression of the natural log of excess ^{210}Pb vs mass depth. The correlation coefficient for this relationship is used as an indication of the extent to which a core has experienced temporally-variable deposition events or vertical mixing (Smoak and Patchineelam, 1999). A good fit is not only unnecessary for application of the CRS model, but also precludes its usefulness

because the model is intended to identify a change in rates throughout the profile, which would not occur with a perfect fit (Appleby and Oldfield, 1978).

The SOM and SIM accumulation rates refer to the mass of soil added per unit area, and are reported in units of g or kg m^{-2} yr^{-1}. Accretion rates refer to vertical soil addition and are reported in units of mm or cm yr^{-1}. To correct for potential auto-compaction, accretion rates for each soil interval were multiplied by the proportion of that interval's DBD to the average DBD of the five bottom-most dated intervals (Lynch et al., 1989). No correction was made if an interval's DBD was greater than that averaged at depth (Smoak et al., 2013). In our analysis, either both values are provided for comparison or, unless stated, accretion rates are not normalized.

Statistical differences in 100-year mean rates of accretion, and SOM and SIM accumulation were obtained using Welch's 1-way ANOVA with post hoc Games-Howell pairwise comparisons using Minitab 17. Welch's test is a robust analysis for detecting difference when the assumption of homogeneity of variance is not met; additionally rates were log-transformed prior to analysis.

2.4 Modeling SOM and SIM contributions to accretion

The accumulation rates of SOM and SIM for individual soil intervals were used as variables in multiple linear regression models to predict accretion rates for organic, intermediate, and mineral soil classes (Fig. 2). The models were used to predict the volume of soil that can be created from a given mass of SOM or SIM. The equation for the multiple linear regression is:

$$Accretion = m_1 \times SOM\ flux + m_2 \times SIM\ flux + b \qquad (Eq. 1)$$

where accretion is reported in units of cm yr^{-1}, the SOM and SIM accumulation rates are reported in units of kg m^{-2} yr^{-1}, and m_1 and m_2 are the respective organic and mineral accumulation coefficients. The b term has been interpreted to represent the volume occupied by pore fluids and gases (Nyman et al., 1990; Neubauer 2008). Model regressions were fit using Minitab 17. Variance Inflation Factors (VIF) were used to assess multi-collinearity between SOM and SIM accumulation rates; regression models with low VIF

(<10) were selected as the best fitted models (Freund and Wilson, 2003). In the top-down models, accretion rates were reported in terms of cm yr^{-1}, and SOM and SIM accumulation as kg m^{-2} yr^{-1}, such that the relationship occurs on a 1:1 scale. For example, a SOM coefficient of 0.75 means that every 0.75 kg of SOM equates to 0.75 cm of accretion.

A bottom-up modelling approach following Morris et al., (2016) was compared to the multiple linear regression equations using observations of LOI and DBD to derive the packing densities for SOM and SIM (see section 2.2 for density definitions). Packing densities can be used to estimate the potential volume (i.e., accretion) occupied by a given mass of SOM or SIM; see Morris et al. (2016) for the rationale and derivation of this approach. Briefly, the model states that a soil's bulk density should be roughly equal to the combined packing densities of the SOM and SIM, and that these should be related to the soil's organic content. The model is simplified to the following form:

$$DBD = \frac{1}{\frac{LOI}{k_1} + \frac{1 - LOI}{k_2}} \qquad (Eq. 2)$$

The k_1 and k_2 terms are the SOM and SIM self-packing densities, and are assumed to be additive (i.e., they should not change when combined). The values for each term were derived from a non-linear curve fitting routine in Minitab 17 using DBD and LOI observations from the 735 core intervals across all 23 sites. Comparisons were also made with results from Morris et al. (2016) in which 5,075 LOI and DBD samples from 33 North American estuarine wetlands were used to identify the values of k_1 and k_2 as 0.085 and 1.99 g cm^{-3}.

The utility of the three model types [1: top-down/multiple linear regression, 2: mangrove bottom-up (these data), and 3: Morris et al. (2016) bottom-up] was evaluated using different timescales within our dataset. SOM and SIM accumulation rates from 10-, 50-, and 100-year timescales were used from each study site to estimate the corresponding accretion rates. These rates represent three cumulative depths within each core, and are different from the inputs used in the multiple regression models that were based

on observations from individual soil intervals. The modelled and observed results were regressed to identify how well the models performed based on the level of correlation and how close the slope was to a value of 1.

3. Results

3.1 Gravimetric Results and Soil Classification Scheme

Dry bulk density in the Everglades sites was highest near the river mouths (e.g., 0.59±0.15 g cm^{-3} WSC-10, 0.87±0.14 g cm^{-3} WSC-13) and decreased upstream (e.g., 0.16±0.02 g cm^{-3} WSC-1, 0.14±0.03 g cm^{-3} WSC-2) (Table 1). Values in the Ten Thousand Islands were similar for the four island sites (e.g., 0.21±0.03 g cm^{-3} TTI-5) and increased at the mainland site (0.64±0.24 g cm^{-3}). The inverse of this pattern was evident in the LOI percentage of total soil mass; values increased with distance upstream in the Everglades sites (e.g., 13±2% WSC-13, 86±1% WSC-1), and in the TTI sites the percentage was the same on the four islands (e.g., 49±5% TTI-5) but decreased at the mainland site (18±10% TTI-1). The DBD and LOI% of the Mexico cores were reflective of the landscape heterogeneity in terms of hydrology, with no spatially significant pattern as a linear function of distance from the lagoon mouth or from open water. For soil core intervals across all sites, DBD ranged from 0.07 to 1.17 g cm^{-3}, and LOI varied from 8.6 to 87.1%.

All mangrove sites were subsequently classified according to the mean LOI% of the core intervals (Fig. 2) as Organic (82±4%; n=160), Intermediate (56±8%; n=379) and Mineral (23±10%; n=196).

3.2 Radiometric Results

A net decrease in excess ^{210}Pb with soil depth was seen in each of the soil cores (Fig. S1). The organic and intermediate soil class sites along with the single mineral TTI site (TTI-1; Table 1) exhibited log-linear profiles with high r^2 values. The lack of a high correlation coefficient for the decay profiles of the four Everglades mineral sites (r^2 range: 0.36 to 0.78) occurs because of the closer proximity to the

Gulf of Mexico and storm deposition events that introduce pulses of marine SIM that is low in excess ^{210}Pb (e.g., Smoak et al., 2013). Visible laminations in these cores indicated that these sediments are not mixed. A total of 465 samples were dated based on the presence of excess ^{210}Pb.

The inventory of excess ^{210}Pb was 26.3 ± 7.8 dpm cm^{-2} for the Florida sites and 8.5 ± 3.4 dpm cm^{-2} for the Mexico sites. The lower inventories in the Yucatan peninsula cores may indicate less excess ^{210}Pb in the predominantly marine influence on atmospheric source, however the inventories in two of the study sites were extremely low (core AG: 4.5 dpm cm^{-2}; core SK: 6.0 dpm cm^{-2}). These low inventories and high correlation coefficients of the natural logarithm of ^{210}Pb versus depth (Fig. S1), suggests that erosion has depleted the inventory or that there was a lack of sediment deposition and accumulation until relatively recently. The lack of a complete inventory violates one of the assumptions necessary for application of the CRS model, and thus maximum age and rates were calculated using the CIC model (e.g., Smoak and Patchineelam, 1999).

3.3 Rates of SOM, SIM, and Accretion

Soil organic matter accumulation rates were relatively constant across the study region with a 100-year mean (± SD) of 240 ± 74 g m^{-2} yr^{-1} and a range from 99 (core AG) to 366 g m^{-2} yr^{-1} (core WSC-10) (Table 2). Rates for individual soil intervals ranged from 50 (WSC12, years 1908-1926) to 1126 g m^{-2} yr^{-1} (WSC12, years 1944–1945) across all sites. There was no significant difference ($p>0.05$) in mean (± SE) SOM accumulation rates between the organic (192 ± 23 g m^{-2} yr^{-1}), intermediate (265 ± 20 g m^{-2} yr^{-1}), and mineral (234 ± 36 g m^{-2} yr^{-1}) soil classes (Fig. 3a).

Mineral sediment accumulation rates showed substantial variability across the study region with a 100-year mean (± SD) of 361 ± 470 g m^{-2} yr^{-1} and ranged from 28 (WSC-2) to 1,739 (WSC-13) g m^{-2} yr^{-1}. The median (and inter-quartile range) of 100-year SIM accumulation rates was 199 (92–400) g m^{-2} yr^{-1}. Rates for individual soil intervals ranged from 13 (WSC-2A, years 1916–1929) to 6,555 (WSC-13, years 1963-1965) g m^{-2} yr^{-1} across all sites. There was a significant increase ($p<0.001$) in mean (± SE) SIM

accumulation rates between the organic (45 ± 5 g m^{-2} yr^{-1}), intermediate (216 ± 30 g m^{-2} yr^{-1}), and mineral (888 ± 267 g m^{-2} yr^{-1}) soil classes (Fig. 3b).

The average (± SD) 100-year accretion rate for all sites is 2.3 ± 0.6 mm yr^{-1}, and is only slightly lower if normalized for density (2.1 ± 0.5 mm yr^{-1}). Site averages over 100 years ranged from 1.2 (site AG in Celestun) to 3.4 mm yr^{-1} (site WSC-9 on the Harney River). Density-corrected rates for individual soil intervals of approximately 100-years or less, ranged from 0.7 (core WSC 2, years 1916–1929) to 12.3 mm yr^{-1} (core TTI2, years 1984–1985) across all sites. There was no significant ($p>0.05$) difference in mean (± SE) accretion rates between the organic (1.9 ± 0.2 mm yr^{-1}), intermediate (2.6 ± 0.2 mm yr^{-1}), and mineral (2.2 ± 0.2 mm yr^{-1}) soil classes (Fig. 3c).

3.4 Model Results

All dated samples approximately 100 years old or younger were used in a multiple linear regression model assessing accretion rates as a function of the combination of SOM and SIM accumulation rates for each soil class (Organic response variable n=65; Intermediate n= 203; Mineral n=105). Each model showed significant and high correlation values for the overall model and the individual predictor variables (Table 3). Correlation between predictor variables (SOM and SIM) was minimal, with variance inflation factors of 3.45, 1.60, and 2.06 for the organic, intermediate, and mineral soil classes respectively (Table 3).

The best-fitted values for the non-linear mixing model (Eq. 2; Fig. S2) are: k_1 (SOM) = 0.114 ± 0.002, and k_2 (SIM) = 5.327 ± 0.631 g cm^{-3}. The use of an r^2 value to evaluate the performance of non-linear models has been strongly rejected in the statistical literature (Spiess and Neumeyer, 2010, and references therein). Thus, in this analysis the standard error of the regression model (S) was used, which indicates the mean value of the response variable (DBD) residuals in units of g cm^{-3}. The value of S for this model was 0.067 g cm^{-3} indicating that 95% of DBD observations (~2 × S) are within 0.134 g cm^{-3} of the value estimated by the model.

4. Discussion

4.1 SOM and SIM are non-additive contributors to soil volume

If the contributions of SOM and SIM to soil volume and accretion are assumed to be additive, then a site with a high rate of mass accumulation should have a higher accretion rate than a site with a lower rate of mass accumulation. There are several lines of evidence indicating that this additive relationship is not present in these study sites. First, there are numerous sites where a greater mass accumulation rate did not equate to a greater accretion rate (Table 2; Fig. 3). For example, a mass accumulation rate of 320 g m^{-2} yr^{-1} equated to an accretion rate of 2.2 mm yr^{-1} at site WSC-1; much higher mass accumulation rates of 1988 and 830 g m^{-2} yr^{-1} equated to a just slightly higher accretion rate of 2.5 mm yr^{-1} at WSC-13 and a slightly lower rate of 1.9 mm yr^{-1} at TTI-1 (Table 2). If additivity was valid for these soils, then the highest accretion rates would be expected in the mineral soil-class sites that exhibit the highest SOM and SIM accumulation rates. Instead, this was not the case; there was no statistically significant difference in accretion rates among soil classes (Fig. 3).

Secondly, individual interval-level accretion rates are not proportionally related to overall mass accumulation. If the two mass constituents made additive volume contributions, then a strong linear relationship should be present between accretion and both the SOM and SIM rates. Instead, accretion rates are well-predicted solely by SOM accumulation rates, with 73 to 93% of the variation accounted for by changes in SOM values (Fig. 4a). Moreover, the slopes of the regressions are nearly equal to 1 for all three-soil classes. In contrast, the addition of SIM has very little influence on accretion, indicated by low correlation coefficients and slopes significantly different from 1 (Fig. 4b).

Furthermore, the lack of an additive relationship between SOM and SIM is demonstrated in the top-down model coefficients for the predictor variables (Table 3). The SOM coefficients (m_1) are large and relatively similar (range: 0.747±0.025 to 0.947±0.045), indicating that SOM is predicted to make a consistent contribution to accretion across soil classes. Moreover, the SIM coefficients (m_2) decrease

significantly from organic (1.255±0.387) to intermediate (0.164±0.040) to mineral (0.018±0.004) soil classes (Table 3). Organic matter produces roughly the same amount of accretion across soil classes. However, the accretion contribution of SIM decreases substantially as the supply increases, likely because its consolidated mass is capable of compressing the organic matter or because its finer grain size can occupy the void spaces within and between SOM structures. According to this model, SIM contributes meaningfully to accretion, but with substantially decreasing influence in the transition from organic sites (large SIM coefficient multiplied by a very small SIM flux) to intermediate to mineral soil classes (very small SIM coefficient multiplied by a very large SIM flux) (Table 3).

A final argument against additivity of SOM and SIM can be identified in comparisons of the observed vs. modeled accretion rates when using the bottom-up model with k_1 and k_2 values derived from this dataset and a comparison with Morris et al. (2016). Table 4 depicts the r^2 and slope of comparisons between modeled and observed accretion rates. The bottom-up model explicitly assumes the additive relationship (Morris et al., 2016). A slope of 1 should be obtained if the model output values are the same as those observed in the soil cores. For both bottom-up models the slope values are near to 1 for the organic soil class, but well above 1 for the mineral soil class. The k_1 and k_2 values from Morris et al. (2016) over-estimate the observed accretion rates by 65±18% while values derived from this dataset over-estimate the observed values by 23±12% (Table 1.4). Because the bottom-up model assumes an additive relationship between the two constituents, and given that SOM flux is relatively constant across all soil classes (Fig. 1.3), the model's accuracy decreases when the SIM input increases.

4.2 SOM drives accretion; SIM drives bulk density

A large difference between particle and packing densities was observed in the soil of these study sites. For instance, the generally reported range of SOM particle densities (1.14 – 1.2 g cm^{-3}) (e.g. DeLaune et al. 1983; Turner et al. 2006) is an order of magnitude (i.e. 10x) greater than the SOM packing density (see definition in Section 2.2 or Appendix 1) calculated here (0.114 g cm^{-3}); the lower the packing density, the greater the accretion contribution. This is consistent with the long-term preservation of plant

material in peat soil. Consequently, SOM packing densities can be highly variable, and contribute to both higher and lower accretion rates. Despite their low mass, these organic structures occupy large soil volumes that are occupied by water, gas or smaller SOM and SIM particles. This high variability of potential packing densities for SOM is likely the reason that all three modeling approaches used in these analyses have their weakest correlations in the organic soil class (Table 4). An implication of the high variability is that at some level, SOM packing density should reach a maximum where additivity would apply.

Figure 1.5 provides a simple illustration of these physical interactions controlling bulk density. Panel 5a depicts the regression of DBD versus both the SOM and SIM fractions of DBD. The SIM fraction has a high, significant correlation with a slope of 1, whereas there is no correlation with the SOM fraction. Similarly, for the radiometric observations (Fig. 1.5b) there is a positive, highly significant relationship between DBD and SIM accumulation rates, whereas there is generally only a weak correlation between SIM accumulation and accretion rates (Fig. 1.4b). In contrast, SOM accumulation has no capacity to predict DBD (Fig. 1.5c), but is an excellent predictor of accretion rates (Fig. 1.4a).

Previous research has identified SOM as the limiting factor for accretion in tidal marsh environments when utilizing top-down assessments (Turner et al., 2006; Neubauer, 2008; Nyman et al., 1990). While supporting the notion that SOM drives accretion in locations with low mineral sediment availability, Morris et al. (2016) suggested that accretion rates would be higher if more SIM were available. However, these results indicate an alternative relationship, where the addition of mineral sediment does contribute to accretion, but with a measure of decreasing efficacy (see previous section, 4.1). Although the underlying cause for the difference between these results and those of Morris et al. (2016) is unknown, two possible explanations can be advanced. First, most of the data for the Morris et al. study were sampled in marsh environments (although some observations from brackish tidal mangroves and mixed mangrove and marsh locations in ENP were cited). Mangrove wetlands may have a wider range of packing densities than those currently measured in marshes due to the fact that they are

forested wetlands with a wide range of organic material compositions (wood, roots and recalcitrant leaves with high C:N ratios). A second possibility is local and regional differences in soil formation processes under steady state vs. pulse inputs. These carbonate platform mangrove sites lack a regular supply of terrigenous sediments and the soil-building process occurs via production and accumulation of above- and below-ground organic matter (Chen and Twilley, 1999; McKee et al., 2007) and periodic subsidies (i.e., hurricanes, tropical storms) of SIM (Cahoon et al., 2003; Castañeda-Moya et al., 2010; Whelan et al., 2009). Conversely, soil building in wetlands with a regular supply of terrigenous mineral sediment is largely a constant, interactive undertaking between SOM and SIM, which may result in more consistent packing densities.

4.3 Accretion and historical rates of sea-level rise

Accretion rates are an important indicator of the degree of interaction between mangrove soil formation and SLR (Krauss et al., 2014; Woodroffe et al., 2016). The rate of SLR recorded at the Key West, FL, tide gauge increased from 2.3–2.8–6.3 mm yr^{-1} over the most recent 100, 50, and 10-year periods (Table 5). The 100-year and 50-year mean rates of accretion for the FL cores (2.2 and 2.8 mm yr^{-1}) are identical to rates of SLR over the corresponding timeframes. However, there is a lag of approximately 3 mm yr^{-1} between SLR and accretion in the most recent decade (Table 5). A longer time interval is necessary to evaluate if the rate of SLR in the past 10 years represents only periodic variability (i.e., El Niño or Atlantic Multi-decadal Oscillation) or a more enduring, long-term SLR acceleration (Haigh et al., 2014). Comparatively, satellite measurements using multiple altimeters provide a mean SLR rate of 3.2 ± 0.4 mm yr^{-1} for the Gulf of Mexico (GOM) over the last 20 years (NOAA Laboratory for Satellite Altimetry), which is similar to the 10-year accretion rates in south Florida (3.3 ± 0.5; Table 5).

Gaps in the long-term tide gauge record at the port of Progreso, Yucatan, Mexico, make it difficult to compare long-term and recent rates of SLR with accretion for the mangrove sites in Mexico. The longest available period (1952–1984) for the local rate of SLR (4.5 ± 0.9 mm yr^{-1}) is substantially higher than the 100-, 50-, and 10-year accretion rates of 1.7, 2.1, and 2.2 mm yr^{-1} respectively. These

accretion rates are also less than the above-mentioned rates of SLR at Key West and the 20-year satellite altimetry record for the GOM. Two possible explanations for these low accretion rates can be suggested. First, these rates are similar to 100-year rates for basin mangroves (1.3 and 1.0 mm yr^{-1}) noted by Lynch et al. (1989) in Terminos Lagoon. The multi-decadal to centennial durability of these sites suggests a decoupling between accretion and surface elevation change. If accretion was synonymous with surface elevation change then sites with low accretion rates would be expected to show signs of permanent submergence over long periods of time. While Surface Elevation Table (SET) records are not available at these sites, it is likely that they would indicate a strong belowground/ root-zone contribution to soil expansion occurring beneath the depth of the ^{210}Pb dates/ accretion rates. An alternative possibility concerns the relatively low rates of SOM accumulation in these sites that are all less than the mean for the entire dataset (Table 2). These low rates may reflect prevalent sulfate reduction and high rates of methane production that have been observed in these soils that are extensively influenced by fresh groundwater (Chuang et al., 2015).

Satellite altimetry measurements for the Caribbean Sea (1993–present) indicate SLR rates of 2.6 ± 0.4 mm yr^{-1} (NOAA Laboratory for Satellite Altimetry), which are identical to the 60-year accretion rates for Sian Ka'an (Table 2). However, like Celestun, this coast is highly influenced by groundwater (Lagomasino et al., 2015). Further work is required to determine how representative this core is for this coastal region.

4.4 Estimating future accretion requirements compared with sea-level rise

Projections of SLR in south Florida by the year 2060 range from 22.9–61.0 cm above 2010 levels, which equate to mean rates ranging from 4.6–12.2 mm yr^{-1} (Southeast Florida Regional Climate Change Compact, 2011). These rates are greater than any of the observed long-term (i.e., ≥50 years) rates in our record. To calculate the annual SOM and SIM fluxes required to achieve these accretion targets, the mean SOM and SIM proportions for each soil class (e.g., Fig. 2) were held constant and used in Equation 1. To meet the minimum projected accretion/SLR target of 4.6 mm yr^{-1}, the organic,

intermediate, and mineral soil classes would require the following respective annual rates of SOM/SIM accumulation: 452/99, 446/337, and 534/1787 g m^{-2} yr^{-1} (Table S1). The required rates of SIM accumulation are similar only to the observed 10-year averages for the three soil classes (μ±SD = 60±20, 365±284, and 1797±1273 g m^{-2} yr^{-1}). The required SOM accumulation rates are at the upper end of the observed 10-year average rates of 252±117 (organic), 403±114 (intermediate), and 470±92 (mineral) mm yr^{-1}. These estimates indicate that some of these sites may keep pace with a SLR rate of 4.6 mm yr^{-1} if the production and preservation of SOM observed over the most recent 10-year period is sustainable over longer periods of time.

To meet the maximum projected accretion target of 12.2 mm yr^{-1}, the organic, intermediate, and mineral soil classes require 1,184/260, 1,158/874, and 1,478/4,948 g of SOM/SIM m^{-2} yr^{-1} respectively (Table S1). To meet these mass input requirements, mangrove wetlands in the carbonate platforms of the Florida and Yucatan peninsulas need to receive annual accumulation rates equivalent to the mass of sediment deposition reported for hurricane Wilma in south Florida (i.e., 3.9–29.6 kg m^{-2} yr^{-1}) (Castañeda-Moya et al., 2010; Smoak et al., 2013; Whelan et al., 2009). While this underscores the importance of tropical cyclones in sedimentary processes, it also indicates both the uncertainty and unsustainability of such a sedimentary source over the long-term.

5. Conclusions

The findings from this research support the hypothesis that SOM is the dominant driver of accretion rates in carbonate platform mangrove soils. In contrast, the hypothesis that SOM and SIM contribute additively to soil volume, is not supported. Rather the two soil components interact with each other such that SOM is best able to consistently predict accretion, while the addition of SIM primarily increases soil bulk density. Mineral sediments make a substantive contribution to accretion, as demonstrated specifically by storm layers, but it does so with diminishing effectiveness in the transition from organic to mineral soil classes.

Overall, accretion in both the Florida and Yucatan sites on the Caribbean Sea is maintaining pace with regional SLR, whereas the sites in Celestun Lagoon exhibit an accretion deficit. As SLR accelerates, the SIM composition is likely to increase in the intermediate and organic soil classes across these regions. The bottom-up models suggest that this change could lead to increased accretion rates in these soil classes. However, the top-down models suggest that an increase of SIM in lower bulk-density organic and intermediate soils is unlikely to increase accretion rates. Additionally, alteration of the soil OM:IM ratios will impact soil biophysical structures and ecological processes including respiration rates (Troxler et al., 2015). Conversely, the increased supply of marine material including P, a limiting nutrient in these regions, may drive positive feedbacks between mangrove productivity and soil building (Castañeda-Moya et al., 2013, 2010; Rivera-Monroy et al., 2011).

References

Adame, M.F., Kauffman, J.B., Medina, I., Gamboa, J.N., Torres, O., Caamal, J.P., Reza, M., Herrera-Silveira, J. a., 2013. Carbon Stocks of Tropical Coastal Wetlands within the Karstic Landscape of the Mexican Caribbean. PLoS One 8, e56569. doi:10.1371/journal.pone.0056569

Adame, M.F., Teutli, C., Santini, N.S., Caamal, J.P., Zaldívar-Jiménez, A., Hernández, R., Herrera-Silveira, J. a., 2014. Root Biomass and Production of Mangroves Surrounding a Karstic Oligotrophic Coastal Lagoon. Wetlands. doi:10.1007/s13157-014-0514-5

Appleby, P.G., Oldfield, F., 1978. The calculation of Lead-210 dates assuming a constant rate of supply of unsupported 210Pb to the sediment. Catena 5.

Binford, M.W., 1990. Calculation and uncertainty analysis of 210Pb dates for PIRLA project lake sediment cores. J. Paleolimnol. 3:253–267.

Bouillon, S., Borges, A. V., Castañeda-Moya, E., Diele, K., Dittmar, T., Duke, N.C., Kristensen, E., Lee, S.Y., Marchand, C., Middelburg, J.J., Rivera-Monroy, V.H., Smith, T.J., Twilley, R.R., 2008. Mangrove production and carbon sinks: A revision of global budget estimates. Global Biogeochem.

Cycles 22, 1–12. doi:10.1029/2007GB003052

Breithaupt, J.L., Smoak, J.M., Smith, T.J., Sanders, C.J., 2014. Temporal variability of carbon and nutrient burial, sediment accretion, and mass accumulation over the past century in a carbonate platform mangrove forest of the Florida Everglades 119, 2032-2048. doi:10.1002/2014JG002715

Cahoon, D.R., Hensel, P., Rybczyk, J., McKee, K.L., Proffitt, C.E., Perez, B.C., 2003. Mass tree mortality leads to mangrove peat collapse at Bay Islands, Honduras after Hurricane Mitch. J. Ecol. 91, 1093–1105. doi:10.1046/j.1365-2745.2003.00841.x

Callaway, J., DeLaune, R., Patrick Jr, W., 1997. Sediment accretion rates from four coastal wetlands along the Gulf of Mexico. J. Coast. Res. 13, 181–191.

Castañeda-Moya, E., Twilley, R.R., Rivera-Monroy, V.H., 2013. Allocation of biomass and net primary productivity of mangrove forests along environmental gradients in the Florida Coastal Everglades, USA. For. Ecol. Manage. 307, 226–241. doi:10.1016/j.foreco.2013.07.011

Castañeda-Moya, E., Twilley, R.R., Rivera-Monroy, V.H., Marx, B.D., Coronado-Molina, C., Ewe, S.M.L., 2011. Patterns of Root Dynamics in Mangrove Forests Along Environmental Gradients in the Florida Coastal Everglades, USA. Ecosystems. doi:10.1007/s10021-011-9473-3

Castañeda-Moya, E., Twilley, R.R., Rivera-Monroy, V.H., Zhang, K., Davis, S.E., Ross, M., 2010. Sediment and nutrient deposition associated with hurricane Wilma in mangroves of the Florida coastal everglades. Estuaries and Coasts 33, 45–58. doi:10.1007/s12237-009-9242-0

Chambers, L.G., Osborne, T.Z., Reddy, K.R., 2013. Effect of salinity-altering pulsing events on soil organic carbon loss along an intertidal wetland gradient: a laboratory experiment. Biogeochemistry 115, 363–383. doi:10.1007/s10533-013-9841-5

Chen, R., Twilley, R., 1999. Patterns of mangrove forest structure and soil nutrient dynamics along the Shark River estuary, Florida. Estuaries and Coasts 22, 955–970.

Childers, D., Boyer, J., Davis, S., Madden, C., 2006. Relating precipitation and water management to nutrient concentrations in the oligotrophic “upside-down” estuaries of the Florida Everglades. Limnol. Oceanogr. 51, 602–616.

Chuang, P.-C., Young, M.B., Miller, L.G., Herrera-Silveira, J.A., Paytan, A., 2015. Methane and sulfate dynamics in sediments from mangrove-dominated tropical coastal lagoons, Yucatán, Mexico. Biogeosciences Discuss. 12, 17913–17951. doi:10.5194/bgd-12-17913-2015

Davies, B.E., 1974. Loss-on-ignition as an estimate of soil organic matter. Soil Sci. Soc. Am. Proc. 38, 150–151.

DeLaune, R.D., Baumann, R.H., Gosselink, J.G., 1983. Relationships among Vertical Accretion, Coastal Submergence, and Erosion in a Louisiana Gulf Coast Marsh. SEPM J. Sediment. Res. 53, 147–157. doi:10.1306/212F8175-2B24-11D7-8648000102C1865D

Ellison, J.C., Stoddart, D.R., 1991. Mangrove ecosystem collapse during predicted sea-level rise: Holocene analogues and implications. J. Coast. Res. 7, 151–165.

Freund, R.J., Wilson, W.J., 2003. Statistical methods. Second edition. Academic Press, Burlington, Massachusetts.

Furukawa, K., Wolanski, E., 1996. Sedimentation in mangrove forests. Mangroves Salt Marshes.

Gonneea, M.E., Paytan, A., Herrera-Silveira, J.A., 2004. Tracing organic matter sources and carbon burial in mangrove sediments over the past 160 years. Estuar. Coast. Shelf Sci. 61, 211–227. doi:10.1016/j.ecss.2004.04.015

Haigh, I.D., Wahl, T., Rohling, E.J., Price, R.M., Pattiaratchi, C.B., Calafat, F.M., Dangendorf, S., 2014. Timescales for detecting a significant acceleration in sea level rise. Nat. Commun. 5, 3635. doi:10.1038/ncomms4635

Herrera-Silveira, J.A., 1996. Salinity and nutrients in a tropical costal lagoon with groundwarer

discharges to the Gulf of Mexico. Hydrobiologia 321, 165–176. doi:10.1007/BF00023172

Krauss, K.W., From, A.S., Doyle, T.W., Doyle, T.J., Barry, M.J., 2011. Sea-level rise and landscape change influence mangrove encroachment onto marsh in the Ten Thousand Islands region of Florida, USA. J. Coast. Conserv. 15, 629–638. doi:10.1007/s11852-011-0153-4

Krauss, K.W., McKee, K.L., Lovelock, C.E., Cahoon, D.R., Saintilan, N., Reef, R., Chen, L., 2014. How mangrove forests adjust to rising sea level. New Phytol. 202, 19–34. doi:10.1111/nph.12605

Kumara, M.P., Jayatissa, L.P., Krauss, K.W., Phillips, D.H., Huxham, M., 2010. High mangrove density enhances surface accretion, surface elevation change, and tree survival in coastal areas susceptible to sea-level rise. Oecologia 164, 545–53. doi:10.1007/s00442-010-1705-2

Lewis, R.R., Milbrandt, E.C., Brown, B., Krauss, K.W., Rovai, A.S., Beever, J.W., Flynn, L.L., 2015. Stress in mangrove forests: Early detection and preemptive rehabilitation are essential for future successful worldwide mangrove forest management. Mar. Pollut. Bull. 109, 764-771. doi:10.1016/j.marpolbul.2016.03.006

Lynch, J.C., Meriwether, J.R., McKee, B. a., Vera-Herrera, F., Twilley, R.R., 1989. Recent Accretion in Mangrove Ecosystems Based on 137 Cs and 210 Pb. Estuaries 12, 284-299. doi:10.2307/1351907

McCloskey, T., Liu, K., 2013. Sedimentary History of Mangrove Cays in Turneffe Islands, Belize: Evidence for Sudden Environmental Reversals. J. Coast. Res. 29, 971–983 doi:10.2112/JCOASTRES-D-12-00156.1

McKee, K.L., Cahoon, D.R., Feller, I.C., 2007. Caribbean mangroves adjust to rising sea level through biotic controls on change in soil elevation. Glob. Ecol. Biogeogr. 16, 545–556. doi:10.1111/j.1466-8238.2007.00317.x

Meriwether, J.R., Sheu, W.J., Hardaway, C., Beck, J.N., 1996. Coring sampler for chemical analyses of soft sediments. Microchem. Journal. 53, 201–206. doi:10.1006/mchj.1996.0029

Morris, J.T., Barber, D.C., Callaway, J.C., Chambers, R., Hagen, S.C., Hopkinson, C.S., Johnson, B.J., Megonigal, P., Neubauer, S.C., Troxler, T., Wigand, C., 2016. Contributions of organic and inorganic matter to sediment volume and accretion in tidal wetlands at steady state. Earth's Futur. 4, 110-121. doi:10.1002/2015EF000334. doi:10.1002/2015EF000334.

Neubauer, S.C., 2008. Contributions of mineral and organic components to tidal freshwater marsh accretion. Estuar. Coast. Shelf Sci. 78, 78–88. doi:10.1016/j.ecss.2007.11.011

NOAA Laboratory for Satellite Altimetry/ Sea Level Rise (accessed September, 2016). [Available at: http://www.star.nesdis.noaa.gov/sod/lsa/SeaLevelRise/LSA_SLR_timeseries_regional.php].

NOAA National Ocean Service (2016), Mean sea level trend Key West Florida. [Available at http://tidesandcurrents.noaa.gov/sltrends/ sltrends_station.shtml?stnid=8724580].

----- (2016), Mean sea level trend Progreso, Mexico. [Available at http://tidesandcurrents.noaa.gov/sltrends/sltrends_global_station.htm?stnid=920-001].

Nyman, J. a., Walters, R.J., Delaune, R.D., Patrick, W.H., 2006. Marsh vertical accretion via vegetative growth. Estuar. Coast. Shelf Sci. 69, 370–380. doi:10.1016/j.ecss.2006.05.041

Nyman, J., DeLaune, R., Jr, W.P., 1990. Wetland soil formation in the rapidly subsiding Mississippi River deltaic plain: Mineral and organic matter relationships. Estuarine, Coast. Shelf. 31: 57–69.

Rivera-Monroy, V.H., Twilley, R.R., Davis, S.E., Childers, D.L., Simard, M., Chambers, R., Jaffe, R., Boyer, J.N., Rudnick, D.T., Zhang, K., Castañeda-Moya, E., Ewe, S.M.L., Price, R.M., Coronado-Molina, C., Ross, M., Smith, T.J., Michot, B., Meselhe, E., Nuttle, W., Troxler, T.G., Noe, G.B., 2011. The Role of the Everglades Mangrove Ecotone Region (EMER) in Regulating Nutrient Cycling and Wetland Productivity in South Florida. Crit. Rev. Environ. Sci. Technol. 41, 633–669. doi:10.1080/10643389.2010.530907

Saha, A.K., Moses, C.S., Price, R.M., Engel, V., Smith, T.J., Anderson, G., 2012. A Hydrological Budget

(2002–2008) for a Large Subtropical Wetland Ecosystem Indicates Marine Groundwater Discharge Accompanies Diminished Freshwater Flow. Estuaries and Coasts. 35: 459–474. doi:10.1007/s12237-011-9454-y

Sanders, C.J., Eyre, B.D., Santos, I.R., Machado, W., Luiz-silva, W., Smoak, J.M., Breithaupt, J.L., Ketterer, M.E., Sanders, L., Marotta, H., Silva-Filho, E., 2014. Elevated rates of organic carbon, nitrogen, and phosphorus accumulation in a highly impacted mangrove wetland. Geophys. Res. Lett. 41. doi:10.1002/2014GL059789

Smith, T.J., Anderson, G.H., Balentine, K., Tiling, G., Ward, G. a., Whelan, K.R.T., 2009. Cumulative impacts of hurricanes on Florida mangrove ecosystems: sediment deposition, storm surges and vegetation. Wetlands 29, 24–34. doi:10.1672/08-40.1

Smoak, J., Breithaupt, J., III, T.S., Sanders, C., 2013. Sediment accretion and organic carbon burial relative to sea-level rise and storm events in two mangrove forests in Everglades National Park. Catena 104, 58–66. doi:DOI: 10.1016/j.catena.2012.10.009

Smoak, J., Patchineelam, S., 1999. Sediment mixing and accumulation in a mangrove ecosystem: evidence from 210Pb, 234Th and 7Be. Mangroves Salt Marshes 3, 17–27.

Southeast Florida Regional Climate Change Compact Technical Ad hoc Work Group. April 2011. A Unified Sea Level Rise Projection for Southeast Florida. A document prepared for the Southeast Florida Regional Climate Change Compact Steering Committee. 27 p. https://southeastfloridaclimatecompact.files.wordpress.com/2014/05/sea-level-rise.pdf

Spiess, A.-N., Neumeyer, N., 2010. An evaluation of R2 as an inadequate measure for nonlinear models in pharmacological and biochemical research: a Monte Carlo approach. BMC Pharmacol. 10, 6. doi:10.1186/1471-2210-10-6

Stalker, J.C., Price, R.M., Rivera-Monroy, V.H., Herrera-Silveira, J., Morales, S., Benitez, J. a., Alonzo-

Parra, D., 2014. Hydrologic Dynamics of a Subtropical Estuary Using Geochemical Tracers, Celestún, Yucatan, Mexico. Estuaries and Coasts 37, 1376–1387. doi:10.1007/s12237-014-9778-5

Troxler, T.G., Barr, J.G., Fuentes, J.D., Engel, V., Anderson, G., Sanchez, C., Lagomasino, D., Price, R., Davis, S.E., 2015. Component-specific dynamics of riverine mangrove CO2 efflux in the Florida coastal Everglades. Agric. For. Meteorol. doi:10.1016/j.agrformet.2014.12.012

Turner, E.R., Milan, C.S., Swenson, E.M., 2006. Recent volumetric changes in salt marsh soils. Estuar. Coast. Shelf Sci. 69, 352–359. doi:10.1016/j.ecss.2006.05.005

Whelan, K.R.T., Smith, T.J., Anderson, G.H., Ouellette, M.L., 2009. Hurricane Wilma's impact on overall soil elevation and zones within the soil profile in a mangrove forest. Wetlands 29, 16–23. doi:10.1672/08-125.1

Woodroffe, C., 1992. Mangrove sediments and geomorphology. Trop. Mangrove Ecosyst. 41, 7–41. doi:10.1029/CE041p0007

Woodroffe, C.D., Rogers, K., McKee, K.L., Lovelock, C.E., Mendelssohn, I. a., Saintilan, N., 2016. Mangrove sedimentation and response to relative sea-level rise. Ann. Rev. Mar. Sci. 8, 243-266. doi:10.1146/annurev-marine-122414-034025

Zaldivar-Jimenez, M. a., Herrera-Silveira, J. a., Teutli-Hernandez, C., Comin, F. a., Andrade, J.L., Molina, C.C., Ceballos, R.P., 2010. Conceptual framework for mangrove restoration in the Yucatan Peninsula. Ecol. Restor. 28, 333–342. doi:10.3368/er.28.3.333

Tables

Table 1.1 Average loss-on-ignition (LOI) percentage and dry bulk density (DBD) by site for each river/transect. Sites were classified as follows: Organic: LOI > 70%, Intermediate: LOI = 40-70%, and Mineral: LOI < 40%.

River/ Transect	Site	Latitude	Longitude	Distance from Ocean (km)	Mean LOI ± SD (%)	Mean DBD ± SD (g cm^{-3})	Site Classification
Shark	WSC-1	25°26'31.45"N	80°54'21.21"W	25	86 ± 1	0.16 ± 0.02	Organic
	WSC-2	25°24'36.63"N	80°57'49.98"W	18	84 ± 1	0.14 ± 0.03	Organic
	WSC-3	25°23'31.29"N	80°59'50.90"W	13	78 ± 3	0.15 ± 0.02	Organic
	WSC-4	25°22'18.08"N	81° 2'31.04"W	8	61 ± 3	0.18 ± 0.03	Intermediate
	WSC-5	25°21'50.74"N	81° 4'42.53"W	4	52 ± 12	0.20 ± 0.05	Intermediate
	WSC-6	25°21'14.97"N	81° 5'48.40"W	2	32 ± 4	0.31 ± 0.07	Mineral
Harney	WSC-7	25°25'0.81"N	81° 0'44.57"W	14	79 ± 2	0.14 ± 0.02	Organic
	WSC-8	25°25'24.42"N	81° 3'37.21"W	9	62 ± 5	0.21 ± 0.04	Intermediate
	WSC-9	25°25'53.38"N	81° 6'0.02"W	5	51 ± 8	0.20 ± 0.05	Intermediate
	WSC-10	25°25'2.60"N	81° 7'55.56"W	2	19 ± 5	0.59 ± 0.15	Mineral
Broad	WSC-11	25°30'0.05"N	81° 4'57.68"W	11	68 ± 6	0.18 ± 0.02	Intermediate
	WSC-12	25°29'13.80"N	81° 6'31.74"W	8	34 ± 7	0.32 ± 0.07	Mineral
	WSC-13	25°28'32.47"N	81° 8'41.53"W	2	13 ± 2	0.87 ± 0.14	Mineral
TTI	TTI-1	25°54'25.62"N	81°30'32.88"W	6	18 ± 10	0.64 ± 0.24	Mineral
	TTI-2	25°53'2.94"N	81°31'10.20"W	3.5	62 ± 2	0.20 ± 0.03	Intermediate
	TTI-3	25°52'27.54"N	81°31'9.96"W	2.5	49 ± 6	0.22 ± 0.04	Intermediate
	TTI-4	25°51'59.76"N	81°31'13.80"W	1.5	54 ± 4	0.21 ± 0.04	Intermediate
	TTI-5	25°51'13.62"N	81°31'32.22"W	0	49 ± 5	0.21 ± 0.03	Intermediate
Celestun	BP	20°57'44.53"N	90°20'21.09"W	2.5	65 ± 6	0.16 ± 0.02	Intermediate
	SIP	20°51'11.11"N	90°22'28.67"W	3	56 ± 15	0.18 ± 0.09	Intermediate
	PET	20°50'56.46"N	90°22'29.82"W	3	80 ± 2	0.11 ± 0.02	Organic
	AG	20°50'53.68"N	90°22'40.33"W	2.8	23 ± 10	0.53 ± 0.27	Mineral
Sian Ka'an	SK	19°48'1.76"N	87°33'1.68"W	0.1	65 ± 9	0.18 ± 0.03	Intermediate
All Sites					**53 ± 22**	**0.28 ± 0.21**	

Table 1.2. 100-year mean rates of accretion, soil organic matter (SOM), and soil inorganic matter (SIM) accumulation by Site. See footnotes for explanation of uncertainties. [The 100-year median (and inter-quartile range) values for SIM accumulation was 199 (99-402) g m^{-2} yr^{-1}].

Soil Class*	Location/ Transect	Site	Accretion[1] (mm yr^{-1})	Density-Normalized Accretion (mm yr^{-1})	SOM Accumulation[2] (g m^{-2} yr^{-1})	SIM Accumulation (g m^{-2} yr^{-1})
O	Shark	**WSC-1**	2.2 ± 0.1	1.9 ± 0.1	275 ± 18	45 ± 3
O	Shark	**WSC-2**	1.5 ± 0.1	1.4 ± 0.1	136 ± 12	28 ± 2
O	Shark	**WSC3**	1.5 ± 0.0	1.3 ± 0.0	165 ± 10	52 ± 3
I	Shark	**WSC-4**	3.2 ± 0.1	2.6 ± 0.1	325 ± 27	214 ± 19
I	Shark	**WSC-5****	2.8 ± 0.4	2.7 ± 0.4	267 ± 46	301 ± 104
M	Shark	**WSC-6**	2.2 ± 0.1	2.2 ± 0.1	214 ± 27	507 ± 64
O	Harney	**WSC-7**	1.9 ± 0.1	1.6 ± 0.1	181 ± 26	52 ± 8
I	Harney	**WSC-8**	2.4 ± 0.1	2.0 ± 0.1	295 ± 19	170 ± 11
I	Harney	**WSC-9**	3.4 ± 0.1	3.0 ± 0.1	329 ± 28	400 ± 30
M	Harney	**WSC-10**	3 ± 0.1	2.7 ± 0.1	366 ± 45	1688 ± 193
I	Broad	**WSC-11**	2.7 ± 0.1	2.4 ± 0.1	320 ± 23	143 ± 12
M	Broad	**WSC-12**	2.4 ± 0.1	2.4 ± 0.1	272 ± 46	550 ± 90
M	Broad	**WSC-13**	2.5 ± 0.1	2.1 ± 0.1	249 ± 45	1739 ± 341
M	TTI	**TTI1**	1.9 ± 0.1	1.7 ± 0.1	201 ± 18	629 ± 60
I	TTI	**TTI2**	2.7 ± 0.1	2.6 ± 0.1	319 ± 28	199 ± 17
I	TTI	**TTI3**	3.2 ± 0.1	2.8 ± 0.1	312 ± 35	347 ± 39
I	TTI	**TTI4**	2.1 ± 0.2	1.8 ± 0.2	216 ± 43	170 ± 37
I	TTI	**TTI5**	2.3 ± 0.0	2.0 ± 0.0	214 ± 13	246 ± 14
I	Celestun	**BP**	1.8 ± 0.1	1.6 ± 0.1	183 ± 17	99 ± 9
I	Celestun	**SIP**	2.0 ± 0.1	1.8 ± 0.1	150 ± 5	92 ± 3
O	Celestun	**PET**	2.4 ± 0.1	2.2 ± 0.1	204 ± 3	52 ± 1
M	Celestun	**AG**	1.2	1.2	99	217
I	Sian Ka'an	**SK*****	2.8	2.6	339	134
All Sites (± SD)			2.3 ± 0.6	2.1 ± 0.5	240 ± 74	361 ± 470

* O=Organic; I=Intermediate; M=Mineral

** WSC5 uncertainties are the St. Dev. of the means of 6 cores (Breithaupt et al., 2014).

*** Core SK was dated only to a maximum of 60 years old and was excluded from this analysis of 100-year means.

[1]Accretion uncertainties by site are calculated based on age error as profile depth divided by range of maximum ages for each core. Uncertainty of 0.0 indicates the measured uncertainty is < 0.01.

[2]Uncertainties for accumulation rates of organic matter and mineral sediment are their respective fractions of the calculated sediment mass accumulation error (Binford 1990).

Table 1.3. Multiple linear regression statistics and coefficients (Top-down model) for the fluxes of organic matter (SOM) (kg m^{-2} yr^{-1}) and mineral sediment (SIM) (kg m^{-2} yr^{-1}) vs. accretion rates (cm yr^{-1}) for each soil class. Uncertainties in model are ± 1 S.E. (Cores AG and SK from Mexico are excluded from these analyses because conditions violated assumptions necessary for application of the CRS model that was used to derive rates for individual depth intervals for the other cores). Criteria for evaluating Variance Inflation Factors (VIF) are provided in section 2.4.

							Accretion Prediction Models (Accretion = $m_1x_1 + m_2x_2 + b$)		
Soil Class	R^2 (Adjusted)	df	Model F Significance	SOM Significance	SIM Significance	VIF	SOM Coefficient (m_1)	SIM Coefficient (m_2)	Intercept (b)
Organic	0.87	2,78	***	***	**	3.45	0.766 (±0.082)	1.255 (±0.387)	-0.014 (±0.011)
Intermediate	0.80	2,224	***	***	***	1.60	0.947 (±0.045)	0.164 (±0.040)	-0.021 (±0.011)
Mineral	0.95	2,115	***	***	***	2.06	0.747 (±0.025)	0.018 (±0.004)	0.026 (±0.007)

** and *** indicate significance at p≤ 0.01 & 0.001 respectively

Table 1.4 Linear regression statistics for modelled vs. observed average accretion rates (by soil class) of samples from this dataset with ^{210}Pb ages of 10-, 50- and 100-years.

	Organic Soil Class			Intermediate Soil Class			Mineral Soil Class		
Model	r^2	Significance	Slope	r^2	Significance	Slope	r^2	Significance	Slope
This dataset: Top-Down	0.73	***	0.74 ± 0.12	0.89	***	1.07 ± 0.07	0.88	***	0.96 ± 0.10
This dataset: Bottom-Up	0.67	***	0.82 ± 0.15	0.91	***	0.96 ± 0.05	0.88	***	1.23 ± 0.12
Morris et al., 2016 Bottom-Up	0.67	***	0.96 ± 0.18	0.91	***	1.16 ± 0.06	0.86	***	1.65 ± 0.18

Table 1.5. Mean (± 95% C.I.) density-normalized accretion rates with local rates of sea level rise (recorded at Key West, FL[1] & Progreso, Mexico[2]) over the most recent 10-, 50-, and 100-year periods.

			Accretion Rates - Florida Sites			
Time Scale	Period	Key West, Fl SLR Trend	All Fl Cores	Organic Sites	Intermediate Sites	Mineral Sites
10-Year	2003-2012	6.3 ± 0.5	3.3 ± 0.5	2.5 ± 0.5	3.5 ± 0.7	3.5 ± 1.3
50-Year	1963-2012	2.8 ± 0.2	2.8 ± 0.3	2.0 ± 0.5	3.0 ± 0.5	3.0 ± 0.6
100-Year	1913-2012	2.3 ± 0.2	2.2 ± 0.5	1.6 ± 0.3	2.4 ± 0.4	2.2 ± 0.4

			Accretion Rates - Mexico Sites*			
Time Scale	Period	Progreso, MX SLR Trend	All MX Cores	Organic Sites	Intermediate Sites	Mineral Sites
10-Year	2003-2012	N/A	2.2 ± 0.9	2.5	2.4 ± 1.7	1.2
50-Year	1963-2012**	4.5 ± 0.9	2.1 ± 0.9	3.0	2.1 ± 1.3	1.2
100-Year	1913-2012	N/A	1.7 ± 0.7	2.2	1.7 ± 1.3	1.2

[1]Data accessed from NOAA National Ocean Service (2015), Mean sea level trend Key West Florida. [Available at http://tidesandcurrents.noaa.gov/sltrends/sltrends_station.shtml?stnid=8724580].

[2]Data accessed from NOAA National Ocean Service (2015), Mean sea level trend Progreso, Mexico. [Available at http://tidesandcurrents.noaa.gov/sltrends/sltrends_global_station.htm?stnid=920-001]

* Analysis excludes site SK because of dating concerns. Site AG was dated with the CIC model and thus shows a constant rate of accretion across timescales. See Results section 3.2.

** This 50-year period applies only to the accretion measurements. The Progreso tide gauge record only includes long-term, continuous data from 1952-1984; it is the trend for this period that is used as a comparison with accretion rates.

Table 1.6 Required SOM and SIM accumulation rates necessary to achieve accretion targets by soil class calculated using Equation 1 and terms from Table 3. The ratio of SOM:SIM were held constant based on their proportions for each soil class (see Fig. 2).

Accretion (cm yr^{-1})	Soil Class	SOM%	SIM%	m_1	SOM Flux (kg m^{-2} yr^{-1})	95% CI for SOM Flux (kg m^{-2} yr^{-1})	m_2	SIM Flux (kg m^{-2} yr^{-1})	95% CI for SIM Flux (kg m^{-2} yr^{-1})	b
0.457	O	82%	18%	0.766	**0.452**	0.39 - 0.54	1.255	**0.099**	0.09 - 0.12	-0.014
0.457	I	57%	43%	0.947	**0.446**	0.42 - 0.48	0.164	**0.337**	0.32 - 0.36	-0.021
0.457	M	23%	77%	0.747	**0.534**	0.51 - 0.56	0.018	**1.787**	1.71 - 1.88	0.026
1.219	O	82%	18%	0.766	**1.184**	1.02 - 1.41	1.255	**0.260**	0.22 - 0.31	-0.014
1.219	I	57%	43%	0.947	**1.158**	1.08 - 1.25	0.164	**0.874**	0.82 - 0.94	-0.021
1.219	M	23%	77%	0.747	**1.478**	1.41 - 1.55	0.018	**4.948**	4.72 - 5.20	0.026

Figures

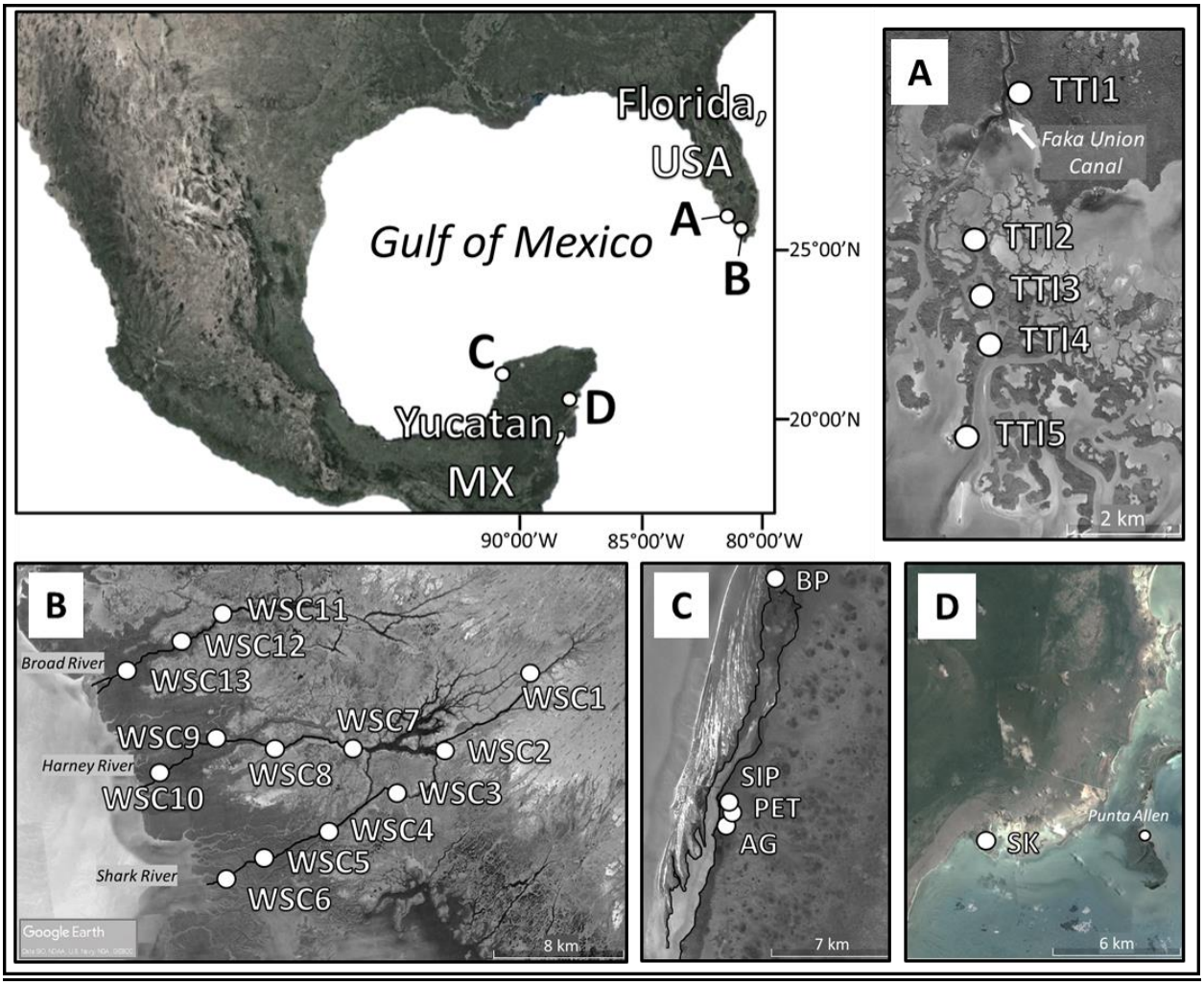

Figure 1.1: Map of soil core locations in Florida, USA and the Yucatan Peninsula in Mexico: Ten Thousand Islands (A), Everglades National Park (B), Celestun Lagoon (C), Sian Ka'an (D). Site coordinates are provided in Table 1.1

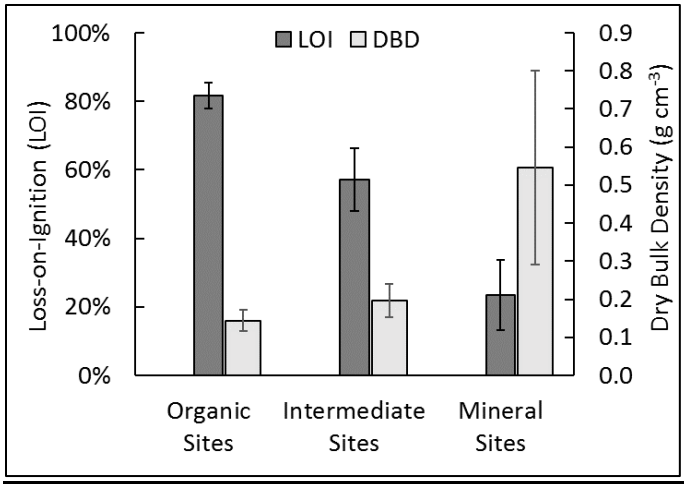

Figure 1.2 Mean (± 1 Std. Dev.) LOI and DBD for soil core intervals by Soil Class. Sample numbers for each soil class are: Organic = 160, Intermediate = 379, and Mineral = 196.

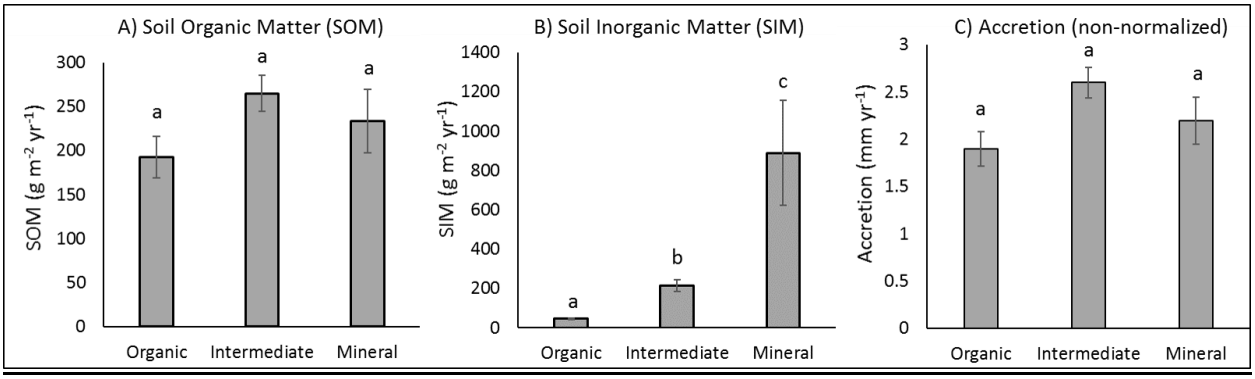

Figure 1.3 100-year mean accumulation and accretion rates (± 1 SE) by soil class. Different lower case letters indicate a significant difference ($p<0.05$).

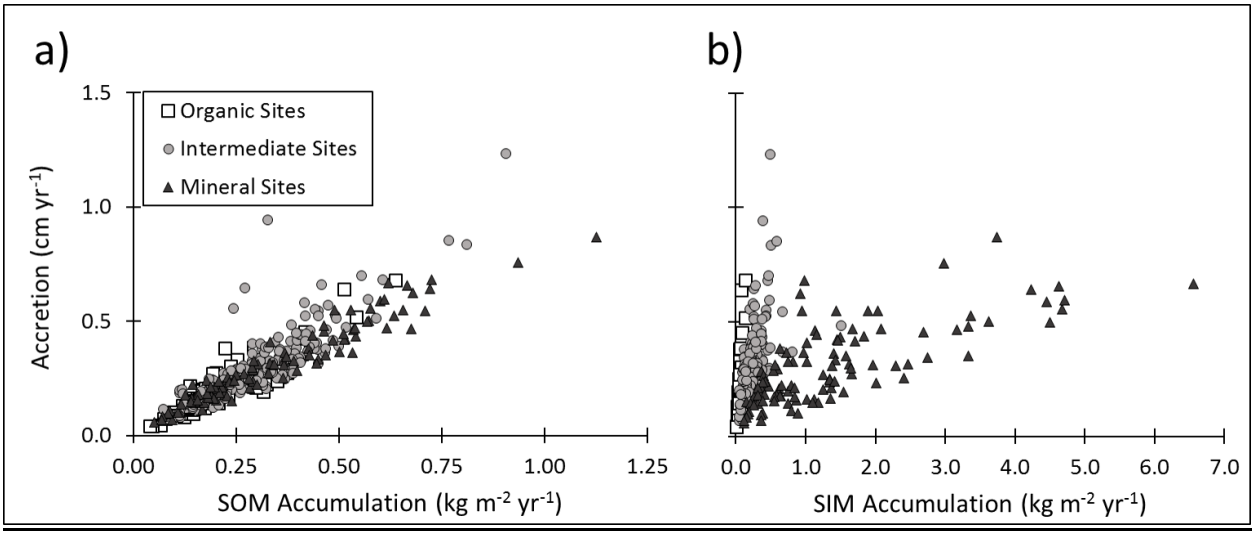

Figure 1.4 Accretion rates for soil core intervals (≤ 100 years old) as a function of a) organic (SOM) & and b) inorganic matter (SIM) accumulation rates. Statistics for Accretion vs SOM by soil class are: Organic: r^2=0.83, slope=0.98; Intermediate: r^2=0.73, slope=1.06, and Mineral: r^2=0.93, slope=0.80. For Accretion vs. SIM the statistics are: Organic: r^2=0.68, slope=4.38; Intermediate: r^2=0.32, slope=0.59, and Mineral: r^2=0.53, slope=0.10. All regressions showed significance of $p<0.0001$. Sample numbers (n) for each soil class are: Organic=64, Intermediate=202, and Mineral=104).

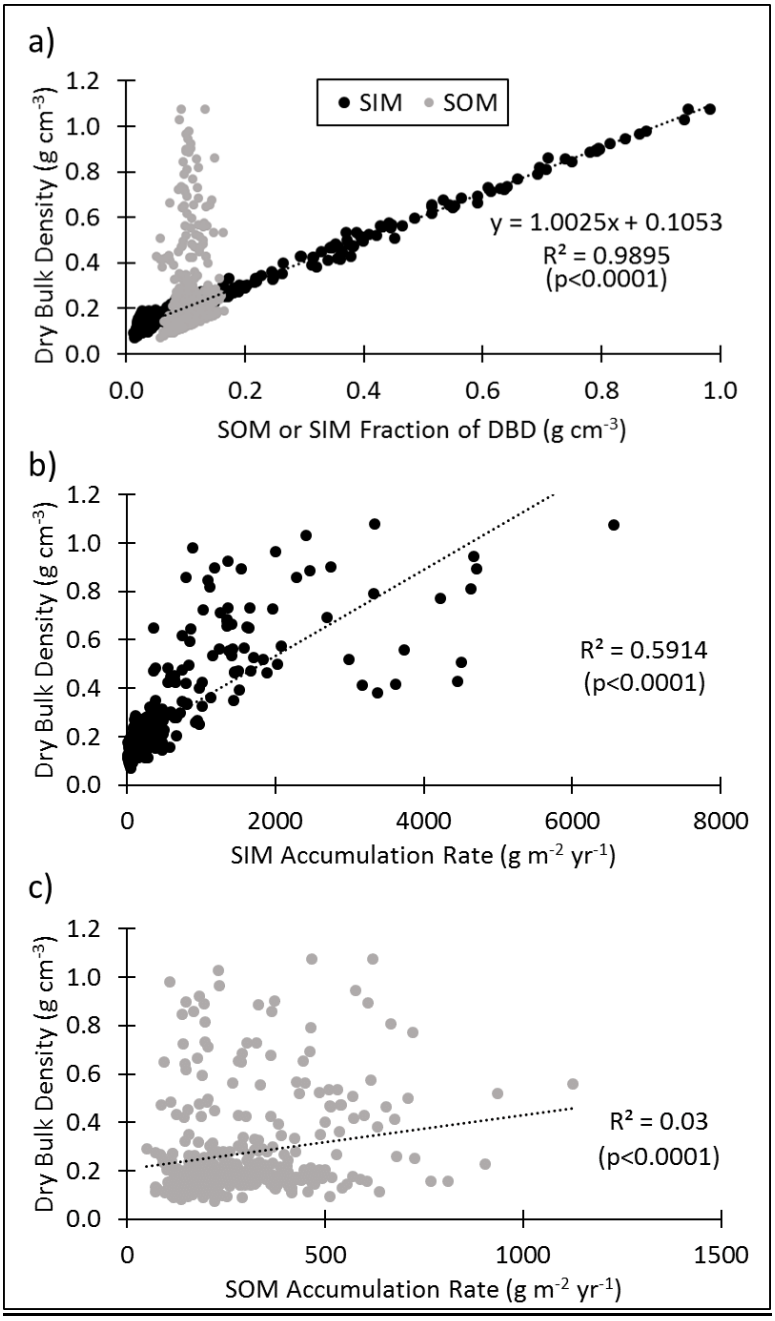

Figure 1.5 a) Total Dry Bulk Density as a function of the SOM & SIM fractions of Dry Bulk Density. b) Dry Bulk Density as a function of SIM accumulation rates, and c) Dry Bulk Density as a function of the SOM accumulation rate. (SOM and SIM accumulation rates are for all soil intervals ≤ 100 years old).

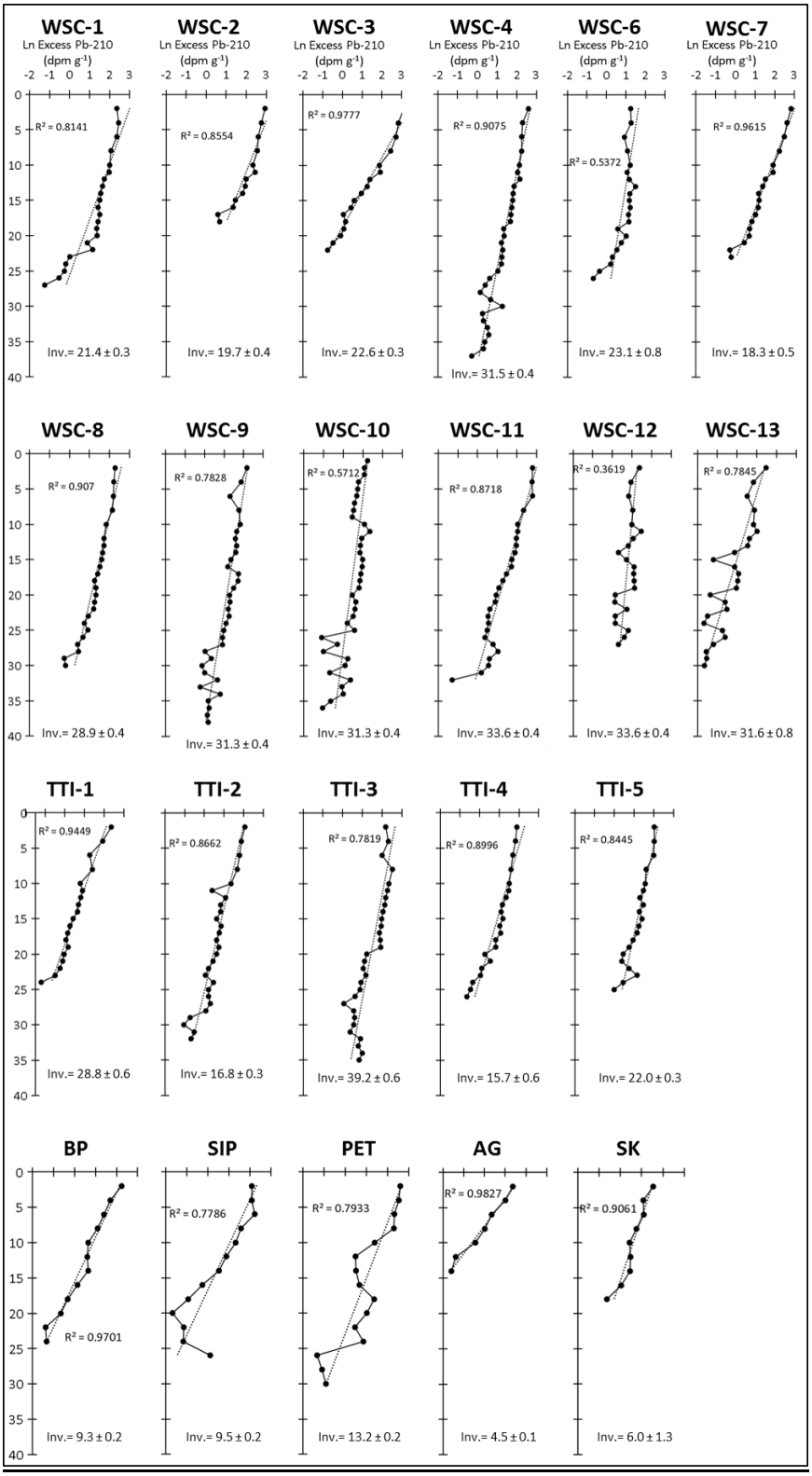

Figure 1.6 Depth profiles (cm) of excess ^{210}Pb activities (dpm g^{-1}) & total core inventories (dpm cm^{-2}). Site WSC-5 (not pictured) consists of 6 soil cores that were previously discussed in Breithaupt et al. (2014).

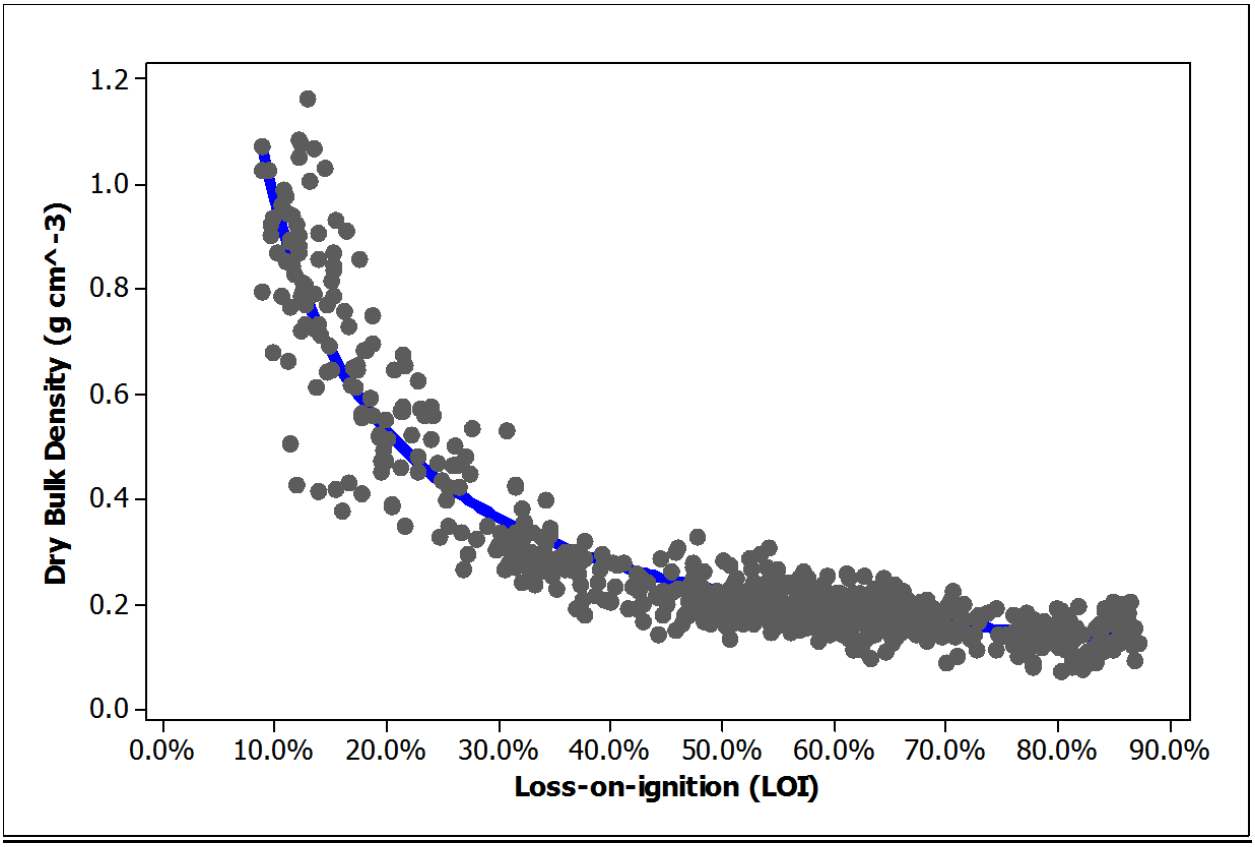

Figure 1.7 Bottom-up model of mangrove cores from this dataset; DBD = 1 / (LOI / k_1 + (1 - LOI) / k_2)). The best fit (S = 0.067 g cm^{-3}) produced the following values: k_1 = 0.11 ± 0.00, and k_2 = 5.337 ± 0.63 g cm^{-3}.

Chapter 2:
Spatial variability of organic carbon, calcium carbonate and nutrient burial rates spanning an estuarine gradient in the coastal Everglades

Abstract

Mangrove wetlands are globally important environments of biogeochemical cycling and are the object of intensive research related to the sequestration and exchange of carbon with oceans, continents, and the atmosphere. The objective of this research was to examine the spatial and temporal variability of burial rates of organic carbon (OC), $CaCO_3$, and nutrient [total nitrogen (TN) and phosphorous (TP)] across an ecosystem gradient of decreasing productivity and salinity in the coastal Everglades of southwestern Florida, USA. Results indicated only minor spatial variability in OC (116 ± 9 (1 SE) g m^{-2} yr^{-1}) and TN (6.2 ± 0.4 g m^{-2} yr^{-1}) burial rates. However, significant ($p<0.001$) regional differences in OC burial rates were observed relative to primary productivity. Over a centennial timescale, mid-stream sites sequestered roughly 22% of annual net primary production while upstream sites preserved less than 10%. Least efficient sequestration was seen in the oligohaline ecotone, where increases in groundwater salinities and the potential for sulfate reduction have been recorded in the past decade. These findings suggest that accelerating SLR will cause a substantial loss of historically sequestered carbon. Burial rates of both $CaCO_3$ (range: 13–1049 g m^{-2} yr^{-1}) and TP (range: 0.10–1.10 g m^{-2} yr^{-1}) decreased significantly with distance from the Gulf of Mexico (GOM). Core profiles of $CaCO_3$:TP potentially provided a novel method for estimating rates of dissolution of marine carbonate sediment in mangrove soils of varying organic concentrations. Estimated total dissolution rates over soil depths less than 40 cm range from 453 to 2439 g $CaCO_3$ m^{-2} yr^{-1}. These $CaCO_3$ sequestration/dissolution rates have important implications for the regional mangrove C budget because the carbon is non-mangrove in origin, and potentially represents a significant contribution of dissolved inorganic carbon/alkalinity to the nearshore environment.

1. Introduction

Mangrove wetlands are some of the most important locations of organic carbon (OC) sequestration and storage in the world on a per area basis (Donato et al., 2011; Mcleod et al., 2011). This is due in large part to high stocks of soil OC driven by high burial rates (Breithaupt et al., 2012; Chmura et al., 2003). Although the global average rate is relatively high, rates recorded in the literature vary substantially, from a low of 21 g m^{-2} yr^{-1} in scrub mangroves of Naples Bay, FL (Marchio et al., 2016) to high rates of 1020 and 1023 g m^{-2} yr^{-1} in the Jiulonjiang Estuary, China, and Cubatão, Brazil, respectively (Alongi et al., 2005; Sanders et al., 2014). This wide variability exists in part because of the extensive differences in mangrove forest structure that are driven by eco-geomorphological factors including tidal range, riverine influence, temperature, rainfall and evapotranspiration (Rovai et al., 2016; Twilley and Rivera-Monroy, 2009). However, the extent of the coupling between OC stocks and burial rates in mangrove vegetation and soils is unclear. For example, the two highest OC burial rates noted above were recorded in estuaries that have been extensively modified by anthropogenic activities, and it has been suggested that these extremes may include a substantial portion of non-mangrove OC (Sanders et al., 2014). Global comparisons indicate that approximately 10–15% of net annual mangrove production is buried over a centennial timescale (Bouillon et al., 2008; Breithaupt et al., 2012). For locations where site-specific C budgets have been conducted, estimates range from burial as 4% of gross primary production in Belize (Lovelock et al., 2015), 16–27% of net primary production in Malaysia (Alongi et al., 2004), 7-30% in China (Alongi et al., 2005), 4–12% in Thailand (Alongi et al., 2002) or 6–42% in the Herbert River estuary in Australia (Brunskill et al., 2002).

Mangroves in Everglades National Park (ENP) occupy 144,447 ha (Simard et al., 2006) of protected land in south Florida, USA. Recently, the extent of OC in ENP mangrove wetlands (above- and below-ground biomass and soils) has been estimated at 321 Mg ha^{-1}, with a value ranging from \$13,859–\$23,728 ha^{-1}, or a total value of \$2–\$3.4 billion USD based on an assessment of the North American socio-economic context as well as the protected status of these mangroves (Jerath et al., 2016). These mangroves have been subject to a number of substantial impacts since the beginning of the 20th Century.

These include extensive anthropogenic alteration of south Florida hydrology (McVoy et al., 2011), a steady rate of regional sea level rise (Maul and Martin, 1993), and numerous tropical storms & hurricanes (Smith et al., 1994, 2009). Mangroves in the southwest coast of the Everglades are estuarine in terms of hydrology and chemistry, and the relatively minor percentage of allochthonous sediment delivery is tidally dominated. Phosphorous, one of the primary limiting nutrients in this ecosystem (Boyer, 2006; Childers et al., 2006), is provisioned via storm surge deposition and tidal redistribution of carbonate marl sediment of marine origin, which decreases in the landward direction (Castañeda-Moya et al., 2010; Smith et al., 2009). As a result, the structure and composition of mangrove wetlands in this region is highly spatially variable (Castañeda-Moya et al., 2013; Chen and Twilley, 1999a). Much of the research conducted in past decades, continuing to the present, has sought to identify how geophysical conditions (including soil characteristics) influence the structure and productivity of mangrove forests (Thom, 1982; Boto and Wellington, 1984; Twilley, 1995; Chen and Twilley, 1999a; Rovai et al., 2016). Questions remain about the extent to which variability in above-ground forest structure and productivity indicates similar variability of burial rates of soil constituents like OC and $CaCO_3$ in peat-forming environments like the Everglades. The mangrove nutrient model (Chen and Twilley, 1999b; Twilley and Rivera-monroy, 2009) indicates that rates of mangrove production, decomposition and export, combined with addition of marine sediment from the GOM, explain the estuarine gradient in soil traits such as organic matter and nutrient concentrations with depth.

One hundred year OC burial rates have been measured previously (Breithaupt et al., 2014) in six cores within a 200-m footprint at a site on the Shark River where mangroves represent the highest standing above-ground biomass, tree height, and productivity in the Everglades (Simard et al., 2006; Castaneda-Moya et al., 2013). Soil at that site consists of 5.5 meters of peat above bedrock (Whelan et al., 2005) that has been accreting for the past 5,250 years, with specifically-mangrove peat accretion beginning 3,800 years ago (Yao et al., 2015). Breithaupt et al. (2014) reported a 100-year mean rate of 123±19 (SD) g OC m^{-2} yr^{-1} for six cores. This value is significantly lower than global expectations might

suggest (163 g m^{-2} yr^{-1}; Breithaupt et al., 2012) and raises the question of the extent to which the mean rate of 123 g m^{-2} yr^{-1} is representative of the region.

The broad objective of this study was to examine the spatial and temporal variability of OC, $CaCO_3$, and nutrient (TN & TP) burial rates across an estuarine gradient where productivity decreases in the landward direction. Based on the profound ecosystem-scale differences in above-ground vegetation characteristics (Simard et al., 2006; Castaneda-Moya et al., 2013) compared to the previous study (Breithaupt et al., 2014) at a single site with minimal above-ground variability, the research hypothesis is that a much greater variability of OC, TN & TP burial rates will be detected. Additionally, this research will build on previous extensive documentation of post-storm deposition rates of $CaCO_3$ and TP, to provide a broader understanding of their variability, including consideration of the stability of carbonate materials in mangrove soils.

2. Methods

2.1 Study Area

The saline coastal Everglades ecosystem is dominated by mangrove vegetation with peat soils ranging from 1–5.5 m thick that are situated atop carbonate bedrock (Scholl, 1964; Whelan et al., 2005; Yao et al., 2015). Hydrological characteristics are fundamental for understanding the organization and function of the ecosystem. Freshwater from the upstream Everglades marshes drains to the southwest coast via Shark River Slough and to the southeast via Taylor Slough. It has been estimated that the volume of fresh water reaching these mangroves has been reduced by up to 59% by Everglades drainage and impoundments during the 20th century (Smith et al., 1989). Under present day conditions the outflow through Shark Slough is ten-fold higher than that through Taylor Slough (Smith et al., 1989). Discharge is a combined result of surface and ground-water flow, precipitation, weather events that influence circulation, and semi-diurnal tides. As water from Shark Slough approaches the coast, it is further subdivided into five major outlets from north to south (along with their relative percentage of total

drainage from 1998–2000): Lostmans Creek (20%), Broad River (26%), Harney River (23%), Shark River (27%), and North River (4%) (Levesque, 2004).

Soil cores were collected from riverine mangroves along the Shark, Harney, and Broad Rivers in southwestern Everglades National Park, with riverine transect lengths of 25, 14, and 11 km respectively (Fig. 2.1; Table 2.1). See Chapter 1 for a more detailed description of the region and sites. Data for location WSC-5 has been previously reported in Breithaupt et al. (2014). Note that sites WSC-2, 4, 5, & 8 are co-located with stations of the United States Geological Survey (USGS), and Florida Coastal Everglades Long-Term Ecological Research (FCE-LTER) program, allowing comparisons with long-term ecosystem data.

Comparisons were made with measurements from the FCE-LTER for above-ground vegetation characteristics, total (above- and below-ground) net primary production (NPP) (Castañeda-Moya et al. 2013) and soil respiration (Troxler et al., 2015). The OC portion of NPP was assumed to be 44% of the total (Bouillon et al., 2008) and is referred to as CNPP hereafter. The carbon portion of soil CO_2 effluxes was up-scaled to annual rates by multiplying its molar fraction (27.29%) by the fluxes reported by Troxler et al. (2015) (μmol m^{-2} s^{-1}) and by the number of seconds in a year, and hereafter is referred to as $Resp_C$.

2.2 Mangrove above-ground vegetation characterization

Above-ground vegetation was characterized for sites WSC-7-10, 11, & 13 on the Harney and Broad Rivers in October 2015, using 20 x 20m plots. These surveys indicate the vegetation characteristics where soil cores were collected. They should not be interpreted as regional assessment of above-ground stocks because of variability with distance up/down river, and with distance from the creek edge (Simard et al., 2006). Characteristics that were measured include stem diameter at breast height (DBH), total basal area (m^2 ha^{-1}), total dry above-ground biomass (Mg ha^{-1}), stem density (stems ha^{-1}) and site complexity. Biomass was estimated using allometric equations specific to *Rhizophora mangle, Avicennia germinans*, and *Laguncularia racemosa* (Smith and Whelan, 2006), as well as *Conocarpus erectus* (Abohassan et al.,

2010). The complexity index for each site was calculated by multiplying total basal area by stem density by canopy height and by the number of different species present (Holdridge et al., 1971; Castañeda Moya et al. 2013). Tree height was estimated using an inclinometer based on measured distance from each trunk. Characteristics for the Shark River sites (WSC-2, 4, & 5) were previously collected by Castaneda Moya et al. (2013) using data collected from 2002–2004.

2.3 Soil characterization and dating

Soil dry-bulk density (DBD) and organic matter content have previously been calculated for site WSC-5 (Breithaupt et al., 2014) and the remaining sites (Chapter 1). Because of the strong decreasing gradient in soil organic matter content values as a function of upstream distance from the Gulf of Mexico (GOM) (Chen & Twilley, 1999b), sites were classified according to their mean loss-on-ignition (LOI) values as Upstream (>70%), Midstream (40–70%), and Downstream (<40%).

Sectioned core intervals were analyzed for OC and TN. Samples were acidified to remove carbonate material prior to OC measurements. Nitrogen measurements were conducted on non-acidified material. Analyses were done using a PDZ Europa ANCA-GL (Automated Nitrogen Carbon Analyzer-Gas Solids Liquids) elemental analyzer connected to a PDZ Europa 20-20 isotope ratio mass spectrometer. The analytical precision of duplicate analyses of standards was 0.28% for C and 0.02% for N.

The analysis of TP was conducted using a Perkin Elmer ELAN DRCe ICPMS (Dynamic Reaction Cell-equipped Inductively-Coupled Plasma Mass Spectrometer). The Laboratory Control Sample (LCS) was AGAL 12, which was digested and analyzed as part of each batch. Duplicates were analyzed every 10 samples. The calibration curve was 0.1, 1, 10, and 100 ppm phosphorus, which produced an r^2 greater than 0.9999.

In addition to the LOI measurement for organic matter, the $CaCO_3$ content was calculated via a secondary burn in a muffle furnace at 990° C for 1 additional hour (Dean, 1974). Although some of this

mass loss may be attributed to waters-of-hydration in clays, this is expected to be minimal in the coastal Everglades that lack a supply of terrigenous, mineral sediments. By multiplying the mass lost in the second burn (assumed to be CO_2) by 2.27, the total $CaCO_3$ content of the soils was estimated; (2.27 × 44 (CO_2 formula weight) = 100 ($CaCO_3$ formula weight) (Dean 1974). Values would be slightly different if soil concentrations of elemental carbonate compositions were known, including magnesium calcite, siderite, and dolomite.

Soil core intervals were dated using ^{210}Pb and the Constant-Rate of Supply model (Appleby 2001; Smoak et al., 2013). Full methods as well as profiles of excess ^{210}Pb activities are available in section 2.3 of Chapter 1. Soil mass accumulation rates were calculated by dividing the total mass (g) for a given unit area (cm^2 or m^2) by the age at depth (yrs). Burial rates of individual constituents (i.e., OC, TN, TP and $CaCO_3$) were calculated by multiplying the concentration (%) of each by the mass accumulation rate. For this paper, a flux is synonymous with burial rate, where positive values indicate addition to the soil and negative values indicate a loss.

2.4 Estimating $CaCO_3$ dissolution rates from $CaCO_3$:TP ratios

A first-order estimate of carbonate dissolution rates was derived for cores that exhibited a linear decrease above an asymptotic baseline in $CaCO_3$:TP vs. soil age (yrs). The slope of $CaCO_3$:TP as a function of soil age was calculated and used as a first-order estimate of dissolution (mols or g m^{-2} yr^{-1}):

$$Slope = \Delta \frac{CaCO_3\ flux}{TP\ flux\ yr^{-1}} \qquad (Eq.\ 1)$$

Changes to the $CaCO_3$ flux as a function of time can be solved for in Eq. 1 using the known slope and core-specific average TP flux. It was assumed that most of the change in $CaCO_3$:TP was driven by the dissolution of $CaCO_3$, and that the annual flux of TP was relatively constant within each core. These assumptions are supported by the small variability of the TP flux within each core (Table 2.4) and the observation that changes in the flux of $CaCO_3$ explain more than twice the variability in $CaCO_3$:TP than

changes in TP flux (Fig. 2.9). Lastly, the calculated annual change in the $CaCO_3$ flux was multiplied by the age of the slope to estimate the cumulative total dissolution occurring within a core.

2.5 Statistical analyses

All statistical analyses, including regression fitting, were conducted using Minitab 17. Differences in soil concentrations (TOC%, $CaCO_3$%, OC:TN, and TN:TP) or fluxes between the upstream, midstream, and downstream soil classes were tested using Welch's 1-way ANOVA with post hoc Games-Howell pairwise comparisons. Welch's ANOVA was used because of its power to detect differences even when homogeneity of variance is not established. This was particularly a concern for $CaCO_3$ and TP, which are highly variable across the regional gradient represented by these sites (Castañeda-Moya et al., 2010; Childers et al., 2006; Smith et al., 2009). The following transformations were used when data were found to be non-normally distributed: for timescale comparisons of mean rates by soil class, OC and TN values were raised to the power of -3.

Throughout this paper, reported uncertainties represent 1 standard error unless stated otherwise.

3. Results

3.1 Above-ground vegetation characteristics

Total dry above-ground biomass ranged from 95 (WSC-6/SRS-5) to 162.2 (WSC-5/SRS-6) Mg ha^{-1} (Fig. 2.2A). Similarly, basal area (m^2 ha^{-1}) was lowest at WSC-4/SRS-5 (22.3) and highest at WSC-5/SRS-6 (40.9) (Fig. 2.2B). Stem density (stems ha^{-1}) was lowest at WSC-9 on the Harney River (1500) and highest at site WSC-11 (9675) on the Broad River (Fig. 2.2C). Site WSC-2/SRS-4, an upstream site on the Shark River, had a similarly high stem density of 7746 stems ha^{-1}. Site WSC-9 had the lowest site complexity (11.7) and site WSC-11 had the highest complexity (108.9) (Fig. 2.2D). No significant difference was detected between upstream, midstream, or downstream classifications for any of the four characteristics ($p>0.05$) (Fig. 2.10), although the statistical power of these comparisons was limited because of the small sample size (n=2) for upstream & downstream sites.

3.2 Soil characteristics

The mean soil OC content decreased significantly ($p<0.05$) from upstream (40.4 ± 0.4%) to midstream (27.4 ± 0.7%) to downstream sites (9.3 ± 0.8%) (Table 2.1). The highest concentrations occurred in the upper Shark River sites (42%), and the lowest values were found at the river mouths (WSC-13: 3.5%, WSC-10: 7.1%, and WSC-6: 13.8%). Concentrations of $CaCO_3$ were opposite those of OC; the highest values occurred at the river mouths (WSC-13: 58.8 ± 0.85%, WSC-10: 41.8 ± 2.91%, and WSC-6: 22.3 ± 1.76%) and the lowest values occurred at sites on the upper Shark River (WSC-1 & 2: 6.9 ± 0.3%). Concentrations decreased from downstream (41.2 ± 2.8%), to midstream (19.4 ± 1.0%), to upstream (9.9 ± 0.5%) site classifications.

In general, OC and TN co-varied across sites within the region. The two lowest ratios were found at the mouth of the Shark (WSC-6: 17.2 ± 0.51) and Broad (16.2 ± 0.98) Rivers. The highest value was found at site WSC-3 on the Shark River (26.7 ± 0.34). There was no statistically significant difference between ratios of the upstream (23.7 ± 0.53) and midstream (22.7 ± 0.41) sites ($p>0.05$), but the downstream sites (19.4 ± 0.83) were significantly lower ($p<0.05$) (Table 2.1).

There was high regional variability in ratios of TN:TP, with the highest ratio occurring in the upper Shark River (WSC-1: 96.0 ± 3.5) and the lowest at the mouth of the Harney (WSC-10: 10.2 ± 0.4) (Table 2.1). Ratios decreased significantly ($p<0.05$) from upstream (81.3 ± 3.2) to midstream (34.4 ± 1.3) to downstream (12.9 ± 0.6).

3.3 Soil fluxes

The 100-year rates of TN burial varied substantially between cores, ranging from 3.5 (WSC-2) to 8.7 g m^{-2} yr^{-1} (WSC-9) (Table 2.2). However, there was no significant overall difference between rates in the upstream, midstream, or downstream soil classes ($p>0.05$) (Fig. 2.3A). In contrast, 100-year TP burial rates varied significantly as a function of distance from the Gulf of Mexico ($p<0.05$), increasing from 0.15

± 0.03 in the upstream sites, to 0.51 ± 0.05 in the midstream sites, and 1.09 ± 0.18 g m^{-2} yr^{-1} in the downstream sites (Fig. 2.3B).

Overall there was relatively little variability in 100-year OC burial rates, with a regional mean of 115.9 ± 8.8 g OC m^{-2} yr^{-1}. In contrast to soil OC concentrations, there was no consistent pattern in OC burial rates as a function of distance from the Gulf of Mexico. The two lowest rates were 69 (WSC-3, 13 km upstream) and 71 (WSC-13, 2 km upstream) g OC m^{-2} yr^{-1} (Table 2.2). The three sites with the highest burial rates were in the midstream site class (WSC-4: 157, WSC-9:152, and WSC-11:153 g OC m^{-2} yr^{-1}). Overall there was no significant difference in OC burial rates between site classes ($p>0.05$) (Fig. 2.3C). However, if site WSC-1 was treated as an outlier, the mean of the remaining three upstream cores (79.0 ± 5.3) was significantly lower than the midstream mean rate (144.1 ± 6.3) ($p=0.001$).

Rates of $CaCO_3$ burial showed substantial variability reflective of the GOM as its primary source. The mean 100-yr rates decreased significantly ($p<0.05$) from downstream (639.4 ± 233.6) to midstream (121.3 ± 31.7) to upstream (24.9 ± 4.6 g m^{-2} yr^{-1}) (Fig. 2.3D). Rates ranged from 13 (WSC-2) to 1049 (WSC-13) g m^{-2} yr^{-1}. The regional 100-yr mean was 261.9 ± 103.9 g m^{-2} yr^{-1} (Table 2.2).

Distance from the GOM was highly significant ($p<0.001$) when predicting 100-year mean fluxes of TP (r^2: 79.2), $CaCO_3$ (r^2: 75.4), and TN:TP (r^2: 86.8) (Table 2.3). For $CaCO_3$:TP, upstream distance explained 64.7% of the variability ($p<0.01$). Conversely, mean rates of OC and TN showed very weak, non-significant correlations with upstream distance. The ratio of OC:TN was modestly predicted by distance (r^2: 26.5), however the relationship was not significant ($p>0.05$).

3.4 $CaCO_3$:TP and carbonate dissolution

Seven of the 13 sites, consisting of upstream and midstream locations, had ratios of $CaCO_3$:TP that did not change substantially with depth, and that were relatively similar to one another (58.9 ± 1.5) (Table 2.4, Fig. 2.4A). The four downstream sites and one of the midstream sites (WSC-9) had ratios within their profile that were substantially elevated compared to the upstream baseline ratios (Fig. 2.4B-

E). The maximum ratios for these sites ranged from 233.0 at the mouth of the Shark River (WSC-6) to 420.5 and 429.2 at the mouths of the Harney (WSC-10) and Broad (WSC-13) Rivers respectively. Site WSC-13 had high values throughout the core, with a mean of 314.0 ± 6.3, and no readily discernible baseline or slope (Fig. 2.4F). Baseline ratios for sites 6, 9, 10 & 12 varied significantly [Range: 18.8 ± 1.6 (WSC-12) to 79.9 ± 6.2 (WSC-10)], but the slopes of the values vs. depth-age above each baseline were relatively similar [Range: -3.65 ± 0.84 (WSC-6) to -9.41 ± 1.64 (WSC-10a)] (Table 2.4). Two separate slopes were discernible for WSC-10. The first (WSC-10a) was from the surface to 18 cm (-9.41 ± 1.64), and the second (WSC-10b) was from 19-28 cm (-6.26 ± 1.06). The slope for WSC-9 was not significantly different from zero ($p>0.05$). The average of the four statistically significant slopes was -6.12 ± 1.22 (Table 2.4). No ratios were available for WSC-5 on the Shark River as this site represents previous work in which $CaCO_3$ was not measured (Breithaupt et al., 2014).

Assuming that changes in $CaCO_3$:TP are primarily caused by dissolution, estimated total annual $CaCO_3$ dissolution rates ranged from 455 at WSC-6 to a total of 3480 g m^{-2} yr^{-1} at WSC-10 (Table 2.4). Integrated, gross 100-year $CaCO_3$ burial rates were reduced by 20–72% if these core-specific dissolution rates are accounted for and removed (Table 2.2). Although high rates of $CaCO_3$ deposition/burial are observed in the uppermost intervals, $CaCO_3$:TP and estimated dissolution rates indicate that much of the material will not remain over 100-year timeframes.

4. Discussion

4.1 Spatial variability of above-ground vegetation and below-ground rates

One-hundred year OC burial rates in the southwestern coastal Everglades exhibit moderate spatial variability with a range of 69–157 g m^{-2} yr^{-1} (Table 2.2). The coefficient of variation (COV), which is the ratio of the standard deviation to the mean, was 0.27 for all sites in the study region over both the 10-year and 100-year timescales. Indeed, while there are some differences between individual cores, there was no statistical difference between soil-class burial rates; however, if core WSC-1 was treated as an outlier and

removed from consideration with the rest of the upstream sites (Fig. 2.3C), then the upstream sites were significantly lower than midstream sites (p=0.001). Previous measurements of OC burial rates in the southwestern coastal Everglades similarly identified minimal variability at the site level, with a COV of 0.15 in a 200-m spatial footprint (WSC-5; Breithaupt et al., 2014). Much greater spatial variability has been identified by recent measurements in mangroves of Naples Bay, FL, north of the Everglades, with a range in 100-year OC burial rates between impacted and pristine creeks, of 47–162 g m^{-2} yr^{-1}, and a COV of 0.48 (Marchio et al. 2016). Variability at those sites is even greater if low rates (21± 5 g m^{-2} yr^{-1}) from scrub mangroves (not sampled in our Everglades dataset) are included. Although the upstream Everglades has been extensively influenced by anthropogenic alterations to hydrology, the relatively small variability amongst these sites compared to those in Naples Bay, suggests that direct anthropogenic drivers may not have caused substantial changes in OC burial rates in the coastal Everglades in the past century.

The lack of substantial variability in OC burial rates is somewhat reflective of above-ground biomass variability at these locations (range=67 Mg ha^{-1}; COV=0.17) (Figs. 2.2A, 2.9). This may be because the locations of these soil cores and vegetation surveys are close to the river edges (<100 m). More variability would likely be noted if basin sites (Lugo and Snedaker, 1974), as well as locations further upstream in the northern rivers, were included. Remote-sensing assessments of mangrove characteristics across the full extent of the coastal Everglades have documented a range in the above-ground biomass of 0 – ~200 Mg ha^{-1} and a range in tree height of <1 – >18 m (Simard et al., 2006). Basal area was highest at site WSC-5 (40.9 m^{-2} ha^{-1}) (Castaneda-Moya et al., 2013), but variability was minimal at the remaining sites (COV=0.11). The greatest variabilities were in stem density (COV=0.69) and site complexity (COV=0.91). However, this variability could not be attributed to distance from the GOM; no statistical differences (p>0.05) in any of the vegetation characteristics were discernible by site classification (Fig. 2.10).

By contrast, there was substantial spatial variability in the concentrations and burial rates of TP and $CaCO_3$ (Tables 2.1 & 2.2), with significant differences (p<0.05) between site classes. Both

constituents were significantly negatively correlated with distance from the GOM ($p<0.001$) (Table 2.3). Castañeda-Moya et al. (2013) found that Soil TP concentration (mg cm^{-3}) explains 52% of variability in mangrove above-ground biomass across sites in Florida, Mexico and Micronesia. When our data are plotted against that relationship, seven of the sites are weakly explained by the model, with a standard error of the regression of 23.27 Mg ha^{-1} (Fig. 2.5). Two of the sites (WSC-10 & 13) fall well outside the predictions of the model. While each had high concentrations of TP, the above-ground biomass was 106 and 118 Mg ha^{-1}, less than the model predicts. A potential reason for this may be that the bio-available fraction of TP is much lower at these sites. Another may be due to the lingering impact of hurricane Wilma (2005) that caused substantial plant mortality near the GOM (Smith et al., 2009). Therefore, these severely impacted sites are likely still in a stage of recovery. Biomass at these sites is not as high as might be expected when compared with site WSC-5 where the biomass numbers are derived from pre-Wilma data (Castaneda-Moya et al., 2013).

4.2 Carbon Burial Efficiency

The site that is farthest upstream, WSC-1, had an OC burial rate (135 g m^{-2} yr^{-1}) that was higher than the remaining upstream sites (69–86 g m^{-2} yr^{-1}). The rate at WSC-1 is similar to rates measured for marshes of the central Everglades of approximately 130 g OC m^{-2} yr^{-1} measured over 25 years using ^{137}Cs (Craft and Richardson, 1993). The timescale difference in measurement techniques precludes direct comparisons; the 10–50 years OC burial rates at WSC-1 are 180 & 214 g m^{-2} yr^{-1}. The three remaining upstream sites, located near Tarpon Bay (Fig. 2.1b; WSC-2, 3, & 7), had rates of OC burial lower than at any other sites except the high-carbonate downstream site WSC-13 (Table 2.2). One hypothesis for the low rates in the sites around Tarpon Bay is that sea-level rise has introduced seawater sulfate into historically freshwater soils, which has led to enhanced soil OC oxidation (Chambers et al., 2015). This hypothesis is potentially supported by short-term data showing a 5–15 salinity increase in the annual maximum groundwater salinity between 2003–2008 at site WSC-2 (Saha et al., 2012). Site WSC-1 may represent a freshwater end-member that has yet to experience elevated seawater salinity. Surface water

salinity at this site was 0.67 ppt at the time of core collection in the regional dry season at high tide. If this SLR hypothesis for the low OC burial rates in the region around Tarpon Bay is true, then this oligohaline region of the Everglades appears to be a vulnerable source of OC where historically preserved soil carbon is either oxidized back to the atmosphere or exported as particulate and/or dissolved organic and inorganic carbon.

As noted in section 3.3, if WSC-1 is treated as an outlier, then OC burial rates are lowest in the remaining upstream sites and highest in the midstream sites. Additional evidence to support this interpretation of the spatial pattern of OC burial is found in data collected at the FCE LTER sites on the Shark River. Rather than comparing the magnitude of burial rates, comparisons were made of OC burial as a fraction of CNPP (above- and below-ground) (Castañeda-Moya et al., 2013). Figure 2.6A depicts the 100-year OC burial rates as a fraction of CNPP values. These values indicate the percentage of OC that can be expected to remain sequestered below-ground over the course of 100 years. This comparison assumes constant CNPP over the past century, which may be unlikely given the effect of disturbance events and an observed 5% reduction in ecosystem CO_2 uptake following substantial (i.e., +10 ppt) increases in salinity (Barr et al., 2012). At present however, global mangrove carbon budgets also rely on this assumption (Bouillon et al., 2008; Alongi, 2009) whereby the comparison serves as a good first order estimate. The upstream site (WSC-2) has the least efficient burial of OC (9%); WSC-4 is the most efficient (22%), and WSC-5 is intermediate (14%).

A similar characterization of the spatial variability of soil-carbon sequestration efficiency is discernible by comparisons of soil CO_2 effluxes (Troxler et al., 2015) with CNPP (Castañeda-Moya et al., 2013). At site WSC-2, where burial was the least efficient, the soil CO_2 fluxes as a fraction of NPP have been highest, twice that of the global estimate, and at the site where burial has been most efficient (WSC-4), the fluxes have been lowest; site WSC-5 again had values between the other two. There is a timescale uncertainty associated with these comparisons, as the soil CO_2 fluxes represent a series of five measurements over four years, and it is unlikely that these values are representative of the past century of

soil respiration at each site. However, this evidence from different methods presents an interesting indication of spatially variable belowground processes occurring in the peatlands of the coastal Everglades.

4.3 Potential $CaCO_3$ dissolution

Unlike soil OC, which is primarily related to local production, the carbonate mud in these mangrove locations is allochthonous in origin, primarily derived from the GOM. Therefore, in this environment, delivery is more important than production. Identification of baseline rates of $CaCO_3$ burial in these cores is relatively inconclusive on its own because of highly variable sedimentation rates. Patterns of change over time were more readily discerned by examining the molar ratio of $CaCO_3$ to TP. Rather than just comparing the magnitude of the fluxes, which is dependent on magnitude of depositional events, normalization to TP allows consideration of temporal $CaCO_3$:TP.

The wide range of values for these ratios across the southwestern Everglades and Florida Bay includes substantial differences with depth/age (Fig. 2.7). Maximum values observed in these cores are similar to ratios in Oyster Bay, Ponce de Leon Bay, and surface samples in Coot Bay (Fig. 2.1) (Kang and Trefry, 2013), suggesting those locations as potential sources. Values are substantially lower than those in Florida Bay sites that include sparse and moderate seagrass cover as well as some sites that are mudflat or hard bottom carbonate environments. However, values in the mangrove soil cores are like those found in northwestern Florida Bay in areas closest to the Everglades. The regional pattern of P concentrations in the sediment is different from, but likely linked to, water column P concentrations. Along this coast, Boyer (2006) noted an increase from south to north in water column P concentrations. This is likely due to strong P-sorption from carbonate production (Bosence, 1989) in southwest Florida Bay (Yates and Halley, 2006). Water column values indicate P-limitation in the southwestern mangrove rivers (Childers et al, 2006; Boyer 2006). However, inorganic/soluble reactive P may be released when P-laden carbonate sediment is introduced into an organic/acidic environment where dissolution can provide a source for mangrove utilization.

Tropical storms have been identified as a primary source of TP-rich carbonate sediment to the mangroves of the coastal Everglades (Castaneda-Moya et al, 2010), but questions remain about how readily available P is for uptake by mangroves. Since the beginning of the 20th century four major storms have made landfall in the coastal Everglades, each leaving a strong, spatially variable signature on the landscape (Smith et al., 2009). The $CaCO_3$:TP records indicate spatial variability of storm impacts, particularly regarding hurricane Wilma (Smith et al., 2009, Castaneda et al., 2010, Whelan et al., 2009). The 2005 occurrence of Wilma coincides with an observed $CaCO_3$:TP peak in each of the downstream cores (Fig. 2.4B–F). The influence of Hurricane Andrew is less noticeable in all cores, but is represented by peaks in cores 6, 10, & 12. A peak coinciding with hurricane Donna occurs in sites 10 & 13, and the 1935 Labor Day storm appears to be marked by nearby peaks above and below the 1935 date. Smoak et al. (2013) found that even in the years immediately following a hurricane, a storm's signature was not confined to a single time interval; rather fine-grained carbonate marl appears to become dispersed within older age intervals. We suggest that the higher ratios observed in storm deposits are due to higher ratios of the source material derived from nearshore coastal locations (Figs. 2.1a & 2.7) where presumably there has been less dissolution. It is unlikely that source differences alone could produce the significant linear decline in ratios detected here (Fig. 2.4 caption). Instead, if it is assumed that changes in $CaCO_3$:TP within these cores are driven primarily by allochthonous-deposition events followed by dissolution of the carbonate, the slopes provide an estimate of the stability of the carbonate once it is introduced to mangrove soils of varying organic content throughout the region.

Based on this interpretation, subsequent to the introduction of sediment with a high $CaCO_3$:TP ratio via storms or strong tidal conditions, mangrove peat soils are unstable with respect to carbonate, and cause its dissolution (and decreasing $CaCO_3$:TP ratios). Observations of carbonate loss have also been reported in mangroves of the Herbert River estuary in north Queensland, Australia (Brunskill et al., 2002). It has long been recognized that mangrove peats can be strongly acidic, with pH ranges reported from 3.5–8.3 (Davis, 1946; Middelburg et al., 1996). Acid is produced by root excretions and decaying

organic matter (Egler 1952). These include carbonic acid formed by aerobic respiration, nitric acid formed by nitrification, and sulfuric acid following oxidation of sulfides and iron sulfides (Aller 1982; Walter & Burton 1990; Middelburg et al., 1996). Our first order estimation of carbonate dissolution rates (Table 2.4) is similar to the range of rates (6–1363 g m^{-2} yr^{-1}) that have been reported in carbonate bottom sediments in the Bahamas, the Florida Atlantic reef tract and Florida Bay, including seagrass beds (Burdige et al., 2008; Ku et al., 1999; Walter and Burton, 1990; Yates and Halley, 2006). The rates estimated for core WSC-10 are higher than previous observations, but might be expected because that location receives a relatively large amount of carbonate annually while also having relatively high soil organic content.

Slightly different dissolution rates, combined with the spatial heterogeneity of $CaCO_3$ burial rates (Table 2.2) contribute to a range of inflection-point depths between 13–18 cm, where the slope meets an asymptotic baseline (Fig. 2.4). Ratios are stable below these depths, and, according to this interpretation, dissolution appears to largely cease in each core. These depths are concurrent with sediment ages of 30–50 years, and indicate that a 50-year estimate is necessary to assess long term carbonate preservation rates. The $CaCO_3$:TP stability below these depths may also be an indication of the stability of the soil organic matter, suggesting that greater respiration of labile material occurs in the shallower depths and contributes to carbonate dissolution. The substantial dissolution correction of carbonate burial in these cores is concordant with previous findings regarding the loss of up to half of gross carbonate production in shallow, terrestrial environments (Aller, 1982).

Higher soil organic content (LOI%) results in decreased ratios of $CaCO_3$:TP, explaining 69% of the variability (Fig. 2.8a) of the five sites with elevated ratios (Fig 2.4b–f) and 89% of the variability in regional non-mangrove sediments of the freshwater Everglades and Florida Bay (Kang & Trefry, 2013) (Fig. 2.8B). Based on this explanation, the consistently high ratios throughout core WSC-13 can be attributed to greater preservation due to lower concentrations of organic matter (Table 2.1) (Chapter 1). This reasoning is supported by findings from Biscayne Bay, where peat soils had pH ranges of 4.9–6.0

and carbonate mud-dominated sediments at nearby locations and depths had pH values nearer to 7.0 (Zieman, 1972). Baseline ratios of $CaCO_3$:TP are remarkably stable (Fig. 2.4 b–e), suggesting a change to conditions more suitable for carbonate preservation relative to TP. This may indicate extensive sulfate reduction, which, in the presence of excess calcium, can lead to carbonate precipitation (Baumgartner et al., 2006; Berner et al., 1978) and may simply offset any dissolution that would ordinarily occur from root exudations. Another possibility may be that dissolution of carbonate in the upper intervals produces sufficient alkalinity to buffer acid introduction from peat degradation or root exudation. This latter explanation may also provide reasons for different baseline ratios (Table 2.4). For instance, site WSC-13 has both a high baseline ratio and the highest concentration of $CaCO_3$; in this site there may be sufficient alkalinity production to buffer acid production.

Finally, the accretion potential of organic and mineral sediment fractions have been modeled for these sites (Chapter 1). Results of substituting these mineral dissolution rates for accretion rates indicate the potential vertical loss each year in the intervals above the baseline ratios of $CaCO_3$:TP. Calculations indicate that WSC-6 may lose 0.3 mm yr^{-1}, WSC-9 0.6 mm yr^{-1}, WSC-10 1.2 mm yr^{-1}, and WSC-12 0.4 mm yr^{-1}. Therefore, shorter timescale assessments (i.e., <50 years) of accretion in sediments with high carbonate concentrations should be adjusted downward when making predictions of accretion for longer timescales. In addition to erosion diminishing a storm-layer's accretion contribution (Whelan et al., 2009), this evidence suggests that dissolution plays a substantive role as well.

4.4 Regional carbon budget implications

Spatial and temporal variability of both OC and $CaCO_3$ have important implications for the regional carbon budget (Troxler et al., 2013). These findings provide strong evidence of numerous regional differences in multiple pools of the mangrove carbon budget: production, burial, soil respiration, and potentially (by mass balance) aqueous export. Our estimate is that approximately 10–20% of carbon is buried for a century or more at these sites. The values from Troxler et al. (2015) suggest that 14–38% of fixed carbon is lost to the atmosphere via soil respiration, (this is a conservative estimate that does not

include respiration from roots/pneumatophores and dead woody debris). Troxler et al. (2013) estimated an aqueous flux of carbon (dissolved and particulate OC, and dissolved inorganic carbon) as 131 ± 155 g m^{-2} yr^{-1}, which equates to 15–41% of the Castaneda-Moya et al. (2013) measurements of annual production at these sites. These terms (burial, soil respiration, and aqueous fluxes) sum to 39–99% of production. The estimates of $CaCO_3$ dissolution contribute uncertainty to the budget because the carbon that it produces is not of mangrove origin and therefore should not be included in the mangrove aqueous-flux term. A number of studies have identified the porewater flux of DIC as the missing component of the mangrove carbon budget (Alongi, 2014; Bouillon et al., 2008; Maher et al., 2013), however preliminary data suggest that care should be taken to substantiate that the carbon in question is a product of mangrove production. Secondly, Smith et al. (2016) identified substantial variability in wet (25%) and dry season (100%) exchange of groundwater between the mangrove soils and the estuary in this region of ENP. If tidal pumping and porewater advection is sufficient, then the dissolution rates in these locations likely contribute substantial DIC/alkalinity to the nearshore environment (Maher et al., 2013; Sippo et al., 2016).

References

Abohassan, A., Tewfik, S.F.A., Wakeel, A.O.E., 2010. Effect of Thinning on the above Ground Biomass of (Conocarpus erectus L.) Trees in the Western Region of Saudi Arabia. J. King Abdulaziz Univ. Meteorol. Environ. 21, 3–17. doi:10.4197/Met. 21-1.1

Aller, R.C., 1982. Carbonate Dissolution in Nearshore Terrigenous Muds: The Role of Physical and Biological Reworking. J. Geol. 90, 79–95.

Alongi, Daniel. The energetics of mangrove forests. Springer Science & Business Media, 2009.

Alongi, D., Pfitzner, J., Trott, L., Tirendi, F., 2005. Rapid sediment accumulation and microbial mineralization in forests of the mangrove Kandelia candel in the Jiulongjiang Estuary, China. Est., Coast. & Shelf 63, 605–618. doi:10.1016/j.ecss.2005.01.004

Alongi, D., Trott, L., Wattayakorn, G., Clough, B., 2002. Below-ground nitrogen cycling in relation to net canopy production in mangrove forests of southern Thailand. Mar. Biol. 140, 855–864. doi:10.1007/s00227-001-0757-6

Alongi, D.M., 2014. Carbon cycling and storage in mangrove forests. Ann. Rev. Mar. Sci. 6, 195–219. doi:10.1146/annurev-marine-010213-135020

Alongi, D.M., Sasekumar, A., Chong, V.C., Pfitzner, J., Trott, L.A., Tirendi, F., Dixon, P., Brunskill, G.J., 2004. Sediment accumulation and organic material flux in a managed mangrove ecosystem: estimates of land–ocean–atmosphere exchange in peninsular Malaysia. Mar. Geol. 208, 383–402. doi:10.1016/j.margeo.2004.04.016

Appleby, P.G., 2001. Chronostratigraphic techniques in recent sediments. In: Smol, J.P., Birks, H.J.B., Last, W.M. (Eds.), Tracking Environmental Change Using Lake Sediments. Kluwer Academic Publishers, New York. Vol 1, Ch 9

Barr, J.G., Engel, V., Fuentes, J.D., Fuller, D.O., Kwon, H., 2012. Satellite-based estimates of light-use efficiency in a subtropical mangrove forest equipped with CO2 eddy covariance. Biogeosciences Discuss. 9, 16457–16492. doi:10.5194/bgd-9-16457-2012

Baumgartner, L.K., Reid, R.P., Dupraz, C., Decho, A.W., Buckley, D.H., 2006. Sulfate reducing bacteria in microbial mats : Changing paradigms , New Discoveries. Sedimentary Geology.185, 131–145. doi:10.1016/j.sedgeo.2005.12.008

Berner, R.A., Westrich, J.T., Graber, R., Smith, J., Martens, C.S., 1978. Inhibition of aragonite precipitation from supersaturated seawater: a laboratoy and field study. Am. J. Sci. 278, 816–837.

Bosence, D., 1989. Biogenic Carbonate Production in Florida Bay. Bull. Mar. Sci. 44, 419–433.

Boto, K.G., Wellington, J.T., 1984. Soil Characteristics and Nutrient Status in a Northern Australian Mangrove Forest. Estuaries 7, 61–69.

Bouillon, S., Borges, A. V., Castañeda-Moya, E., Diele, K., Dittmar, T., Duke, N.C., Kristensen, E., Lee, S.Y., Marchand, C., Middelburg, J.J., Rivera-Monroy, V.H., Smith, T.J., Twilley, R.R., 2008. Mangrove production and carbon sinks: A revision of global budget estimates. Global Biogeochem. Cycles 22, 1–12. doi:10.1029/2007GB003052

Boyer, J.N., 2006. Shifting N and P limitation along a north-south gradient of mangrove estuaries in South Florida. Hydrobiologia 569, 167–177. doi:10.1007/s10750-006-0130-3

Breithaupt, J.L., Smoak, J.M., Smith, T.J., Sanders, C.J., 2014. Temporal variability of carbon and nutrient burial, sediment accretion, and mass accumulation over the past century in a carbonate platform mangrove forest of the Florida Everglades JGR Biogeo. 119:2032-2048. doi:10.1002/2014JG002715

Breithaupt, J.L., Smoak, J.M., Smith, T.J., Sanders, C.J., Hoare, A., 2012. Organic carbon burial rates in mangrove sediments: Strengthening the global budget. Global Biogeochem. Cycles 26, 1–11. doi:10.1029/2012GB004375

Brunskill, G.J., Zagorskis, I., Pfitzner, J., 2002. Carbon Burial Rates in Sediments and a Carbon Mass Balance for the Herbert River Region of the Great Barrier Reef Continental Shelf, North Queensland, Australia. Estuar. Coast. Shelf Sci. 54, 677–700. doi:10.1006/ecss.2001.0852

Burdige, D.J., Zimmerman, R.C., Hu, X., 2008. Rates of carbonate dissolution in permeable sediments estimated from pore-water profiles: The role of sea grasses. Limnol. Oceanogr. 53, 549–565. doi:10.4319/lo.2008.53.2.0549

Castañeda-Moya, E., Twilley, R.R., Rivera-Monroy, V.H., 2013. Allocation of biomass and net primary productivity of mangrove forests along environmental gradients in the Florida Coastal Everglades, USA. For. Ecol. Manage. 307, 226–241. doi:10.1016/j.foreco.2013.07.011

Castañeda-Moya, E., Twilley, R.R., Rivera-Monroy, V.H., Zhang, K., Davis, S.E., Ross, M., 2010.

Sediment and nutrient deposition associated with hurricane Wilma in mangroves of the Florida coastal Everglades. Estuaries and Coasts 33, 45–58. doi:10.1007/s12237-009-9242-0

Chambers, L.G., Davis, S.E., Troxler, T.G., 2015. Sea Level Rise in the Everglades: Plant-Soil-Microbial Feedbacks in Response to Changing Physical Conditions, in: Microbiology of the Everglades Ecosystem. CRC Press, Boca Raton, pp. 89–112.

Chen, R., Twilley, R., 1999a. Patterns of mangrove forest structure and soil nutrient dynamics along the Shark River estuary, Florida. Estuaries and Coasts 22, 955–970.

Chen, R., Twilley, R.R., 1999b. A simulation model of organic matter and nutrient accumulation in mangrove wetland soils. Biogeochemistry 44, 93–118. doi:10.1023/A:1006076405557

Childers, D., Boyer, J., Davis, S., Madden, C., 2006. Relating precipitation and water management to nutrient concentrations in the oligotrophic “upside-down” estuaries of the Florida Everglades. Limnol. Oceanogr. 51, 602–616.

Chmura, G.L., Anisfeld, S.C., Cahoon, D.R., Lynch, J.C., 2003. Global carbon sequestration in tidal, saline wetland soils. Global Biogeochem. Cycles 17. doi:10.1029/2002GB001917

Craft, C., Richardson, C.J., 1993. Peat Accretion and N , P , and Organic C Accumulation in Nutrient-Enriched and Unenriched Everglades Peatlands 3, 446–458.

Davis, John Henry. The peat deposits of Florida, their occurrence, development and uses. No. 30. Published for the Florida Geological survey, 1946.

Dean, W.E.J., 1974. Determination of carbonate and organic matter in calcareous sediments and sedimentary rocks by loss on ignition: Comparison with other methods. J. Sediment. Petrol. 44, 242–248. doi:10.1306/74D729D2-2B21-11D7-8648000102C1865D

Donato, D.C., Kauffman, J.B., Murdiyarso, D., Kurnianto, S., Stidham, M., Kanninen, M., 2011. Mangroves among the most carbon-rich forests in the tropics. Nat. Geosci. 4, 293–297.

doi:10.1038/ngeo1123

Egler, F.E. 1952. Southeast saline Everglades vegetation, Florida, and its management. Vegetatio 3: 213–265.

Holdridge, L.R., Grenke, W.C., Hatheway, W.H., Liang, T., Tosi Jr., J.A., 1971. Forest environments in tropical life zones: a pilot study. Pergamon Press Inc., New York

Jerath, M., Bhat, M., Rivera-monroy, V.H., Castañeda-moya, E., Simard, M., Twilley, R.R., 2016. The role of economic, policy, and ecological factors in estimating the value of carbon stocks in Everglades mangrove forests, South Florida, USA. Environ. Sci. Policy 66, 160–169. doi:10.1016/j.envsci.2016.09.005

Kang, W.-J., Trefry, J.H., 2013. Identifying increased inputs of terrestrial phosphorus to sediments of the southwestern Everglades and Florida Bay. Estuar. Coast. Shelf Sci. 129, 28–36. doi:10.1016/j.ecss.2013.06.003

Ku, T.C.W., Walter, L.M., Coleman, M.L., Blake, R.E., Martini, a. M., 1999. Coupling between sulfur recycling and syndepositional carbonate dissolution: evidence from oxygen and sulfur isotope composition of pore water sulfate, South Florida Platform, U.S.A. Geochim. Cosmochim. Acta 63, 2529–2546. doi:10.1016/S0016-7037(99)00115-5

Levesque, V.A., 2004. Water Flow and Nutrient Flux from Five Estuarine Rivers along the Southwest Coast of the Everglades National Park, Florida, 1997-2001 (No. Scientific Investigations Report 2004-5142).

Lovelock, C., Simpson, L., Duckett, L., Feller, I., 2015. Carbon Budgets for Caribbean Mangrove Forests of Varying Structure and with Phosphorus Enrichment. Forests 6, 3528–3546. doi:10.3390/f6103528

Lugo, A., Snedaker, S., 1974. The ecology of mangroves. Annu. Rev. Ecol. Syst. 5, 39–64.

Maher, D.T., Santos, I.R., Gleeson, J., Eyre, B.D., 2013. Groundwater-derived dissolved inorganic and organic carbon exports from a mangrove tidal creek : The missing mangrove carbon sink ? 58, 475–488. doi:10.4319/lo.2013.58.2.0475

Marchio, D., Savarese, M., Bovard, B., Mitsch, W., 2016. Carbon Sequestration and Sedimentation in Mangrove Swamps Influenced by Hydrogeomorphic Conditions and Urbanization in Southwest Florida. Forests 7, 116. doi:10.3390/f7060116

Maul, G. A., and Martin, D.M., 1993. Sea level rise at Key West, Florida, 1846-1992: America's longest instrument record? Geophys. Res. Lett. 20, 1955. doi:10.1029/93GL02371

Mcleod, E., Chmura, G.L., Bouillon, S., Salm, R., Björk, M., Duarte, C.M., Lovelock, C.E., Schlesinger, W.H., Silliman, B.R., 2011. A blueprint for blue carbon : toward an improved understanding of the role of vegetated coastal habitats in sequestering CO2. Frontiers in Ecology and the Environment, 9 (10), 552-560. doi:10.1890/110004

McVoy, Christopher, et al. Landscapes and hydrology of the predrainage Everglades. Gainesville: University Press of Florida, 2011.

Middelburg, J., Nieuwenhuize, J., Slim, F., Ohowa, B., 1996. Sediment biogeochemistry in an East African mangrove forest (Gazi Bay, Kenya). Biogeochemistry 34. doi:10.1007/BF00000899

Rovai, A.S., Riul, P., Twilley, R.R., Castañeda-Moya, E., Rivera-Monroy, V.H., Williams, A.A., Simard, M., Cifuentes-Jara, M., Lewis, R.R., Crooks, S., Horta, P.A., Schaeffer-Novelli, Y., Cintrón, G., Pozo-Cajas, M., Pagliosa, P.R., 2016. Scaling mangrove aboveground biomass from site-level to continental-scale. Glob. Ecol. Biogeogr. 25, 286–298. doi:10.1111/geb.12409

Saha, A.K., Moses, C.S., Price, R.M., Engel, V., Iii, T.J.S., 2012. A Hydrological Budget (2002 – 2008) for a Large Subtropical Wetland Ecosystem Indicates Marine Groundwater Discharge Accompanies Diminished Freshwater Flow 459–474. doi:10.1007/s12237-011-9454-y

Sanders, C.J., Eyre, B.D., Santos, I.R., Machado, W., Luiz-silva, W., Smoak, J.M., Breithaupt, J.L., Ketterer, M.E., Sanders, L., Marotta, H., Silva-filho, E., Al, S.E.T., 2014. Elevated rates of organic carbon, nitrogen, and phosphorus accumulation in a highly impacted mangrove wetland. Geophys. Res. Lett. 41. doi:10.1002/2014GL059789

Scholl, D., 1964. Recent sedimentary record in mangrove swamps and rise in sea level over the southwestern coast of Florida: Part 1. Mar. Geol. 1, 344–366.

Simard, M., Zhang, K., Rivera-Monroy, V.H., Ross, M.S., Ruiz, P.L., Castañeda-Moya, E., Twilley, R.R., Rodriguez, E., 2006. Mapping height and biomass of mangrove forests in Everglades National Park with SRTM elevation data. Photogramm. Eng. Remote Sens. 72, 299–311.

Sippo, J.Z., Maher, D.T., Tait, D.R., Holloway, C., Isaac, R., 2016. Are mangroves drivers or buffers of coastal acidification? Insights from alkalinity and dissolved inorganic carbon export estimates across a latitudinal transect . Global Biogeochem. Cycles 30, 753–766. doi:10.1002/2015GB005324

Smith, C.G., Price, R.M., Swarzenski, P.W., Stalker, J.C., 2016. The Role of Ocean Tides on Groundwater-Surface Water Exchange in a Mangrove-Dominated Estuary: Shark River Slough, Florida Coastal Everglades, USA. Estuaries and Coasts. doi:10.1007/s12237-016-0079-z

Smith, T., Robblee, M., Wanless, H., Doyle, T., 1994. Mangroves, hurricanes, and lightning strikes. Bioscience 44, 256–262.

Smith, T.J., Anderson, G.H., Balentine, K., Tiling, G., Ward, G. a., Whelan, K.R.T., 2009. Cumulative impacts of hurricanes on Florida mangrove ecosystems: sediment deposition, storm surges and vegetation. Wetlands 29, 24–34. doi:10.1672/08-40.1

Smith, T.J., Whelan, K.R.T., 2006. Development of allometric relations for three mangrove species in South Florida for use in the Greater Everglades Ecosystem restoration. Wetl. Ecol. Manag. 14, 409–419. doi:10.1007/s11273-005-6243-z

Smith III, T., Hudson, H., Robblee, M., Powell, G.V.N., Isdale, P.J., 1989. Freshwater flow from the Everglades to Florida Bay: a historical reconstruction based on fluorescent banding in the coral Solenastrea bournoni. Bull. Mar. Sci. 44, 274–282.

Smoak, J., Breithaupt, J., III, T.S., Sanders, C., 2013. Sediment accretion and organic carbon burial relative to sea-level rise and storm events in two mangrove forests in Everglades National Park. Catena 104, 58–66. doi:DOI: 10.1016/j.catena.2012.10.009

Thom, B. G. "Mangrove ecology: a geomorphological perspective." Mangrove Ecosystems in Australia. Australian National University Press, Canberra. p (1982): 3-17.

Troxler, T., Gaiser, E., Barr, J., Fuentes, J., 2013. Integrated carbon budget models for the Everglades terrestrial-coastal-oceanic gradient: Current status and needs for inter-site comparisons. Oceanography 26, 98–107.

Troxler, T.G., Barr, J.G., Fuentes, J.D., Engel, V., Anderson, G., Sanchez, C., Lagomasino, D., Price, R., Davis, S.E., 2015. Component-specific dynamics of riverine mangrove CO2 efflux in the Florida coastal Everglades. Agric. For. Meteorol. doi:10.1016/j.agrformet.2014.12.012

Twilley, Robert, and Charles Hall. Properties of mangrove ecosystems related to the energy signature of coastal environments. University Press of Colorado, 1995.

Twilley, R.R., Rivera-monroy, V.H., 2009. Ecogeomorphic models of nutrient biogeochemistry for mangrove wetlands, First edit. ed, Coastal Wetlands: An integrated ecosystem approach. Elsevier. doi:10.1016/B978-0-444-53103-2.00023-5

Walter, L.M., Burton, E.A., 1990. Dissolution of recent platform carbonate sediments in marine pore fluids. Am. J. Sci. 290, 601–643.

Whelan, K.R.T., Smith, T.J., Cahoon, D.R., Geological, U.S., International, F., Ehan, O., Reseat, P.W., Ave, B., 2005. Groundwater control of mangrove surface elevation : shrink and swell varies with

soil depth. Estuaries 28, 833–843.

Yao, Q., Liu, K., Platt, W.J., Rivera-Monroy, V.H., 2015. Palynological reconstruction of environmental changes in coastal wetlands of the Florida Everglades since the mid-Holocene. Quat. Res. doi:10.1016/j.yqres.2015.03.005

Yates, K.K., Halley, R.B., 2006. Diurnal variation in rates of calcification and carbonate sediment dissolution in Florida Bay. Estuaries and Coasts 29, 24–39.

Zieman, J.C., 1972. Origin of circular beds of thalassia (spermataphyta: hydrocharitaceae) in south Biscayne Bay, Florida, and their relationship to mangrove hammocks. Bull. Mar. Sci. 22.3, 559–574.

Tables

Table 2.1 Mean (± 1SE) soil content of organic carbon (TOC), calcium carbonate ($CaCO_3$), and nutrient ratios by site and site classification. Sites that are co-located with sites of the United States Geological Survey (USGS) and Florida Coastal Everglades Long-Term Ecological Research program (FCE-LTER) (indicated by superscript lowercase letters) are provided below the table. Loss-on-ignition and dry-bulk-density values for these cores are provided in Chapter 1.

River	Site Classification	Site	Distance from GoM (km)	TOC (%)	$CaCO_3$ (%)	Molar OC:TN	Molar TN:TP
Shark	Upstream	WSC-1	25	42.5 (0.17)	6.9 (0.30)	22.3 (0.83)	96.0 (3.50)
	Upstream	WSC-2[a]	18	42.4 (0.22)	6.9 (0.29)	23.4 (0.49)	85.8 (2.08)
	Upstream	WSC-3	13	39.1 (0.42)	5.8 (0.68)	26.7 (0.34)	80.7 (2.62)
	Midstream	WSC-4[b]	8	29.3 (0.27)	20.6 (0.74)	22.7 (0.59)	40.3 (2.0)
	Midstream	WSC-5[c*]	4	24.2 (1.43)	n/a	21.3 (0.57)	27.0 (0.65)
	Downstream	WSC-6	2	13.8 (0.29)	22.3 (1.76)	17.2 (0.51)	17.0 (0.29)
Harney	Upstream	WSC-7	14	37.1 (0.15)	12.2 (0.51)	22.7 (0.29)	57.4 (3.33)
	Midstream	WSC-8[d]	9	29.8 (0.24)	15.5 (0.80)	24.5 (0.37)	34.6 (0.63)
	Midstream	WSC-9	5	22.6 (0.52)	23.7 (1.47)	20.6 (0.39)	28.9 (0.91)
	Downstream	WSC-10	2	7.1 (0.46)	41.8 (2.91)	21.9 (1.05)	10.2 (0.41)
Broad	Midstream	WSC-11	11	32.6 (0.46)	12.4 (0.32)	24.9 (0.34)	41.8 (1.54)
	Downstream	WSC-12	8	15.9 (0.79)	14.4 (2.15)	21.0 (0.78)	16.5 (0.54)
	Downstream	WSC-13	2	3.5 (0.19)	58.8 (0.85)	16.2 (0.98)	10.5 (0.44)
	Upstream			40.4 (0.4) A	9.9 (0.5) A	23.71 (0.53) A	81.33 (3.21) A
	Midstream			27.4 (0.7) B	19.4 (1.0) B	22.66 (0.41) A	34.35 (1.34) B
	Downstream			9.3 (0.8) C	41.2 (2.8) C	19.39 (0.83) B	12.92 (0.57) C

Site co-locations: [a)] USGS SH2 & FCELTER SRS-4, [b)] FCELTER SRS-5, [c)] USGS SH3 & FCELTER SRS-6, & [d)] USGS SH4.
*Data taken from Breithaupt et al., (2014).

Table 2.2 100-year mean accumulation rates of organic carbon, total nitrogen, total phosphorous, and calcium carbonate by site and by site classification. Uncertainties for means of all sites represent 1 standard error.

			Accumulation Rate (g m^{-2} yr^{-1})				
River	**Site Classification**	**Site**	**TN**	**TP**	**TOC**	**$CaCO_3$**	**Corrected $CaCO_3$**
Shark	Upstream	WSC-1	7.1	0.18	135	27	--
	Upstream	WSC-2	3.5	0.10	69	13	--
	Upstream	WSC-3	3.8	0.11	83	25	--
	Midstream	WSC-4	7.2	0.48	157	119	--
	Midstream	WSC-5*	7.0	0.56	123	N/A	--
	Downstream	WSC-6	6.2	0.79	94	251	122
Harney	Upstream	WSC-7	4.5	0.21	86	35	--
	Midstream	WSC-8	6.8	0.44	137	86	--
	Midstream	WSC-9	8.7	0.69	152	221	170
	Downstream	WSC-10	7.2	1.59	130	1039	544
Broad	Midstream	WSC-11	7.1	0.40	153	59	--
	Downstream	WSC-12	6.5	0.87	118	219	62
	Downstream	WSC-13	5.4	1.10	71	1049	--
		All Sites	**6.2 (0.4)**	**0.58 (0.12)**	**115.9 (8.8)**	**261.9 (103.9)**	**192.6 (88.2)**

* WSC-5 data taken from Breithaupt et al., 2014

Table 2.3 Regression statistics for 100-year mean soil fluxes (y) vs. upstream distance (x). Significance values are indicated by ** (p<0.01), *** (p<0.001), & NS (not significant; p>0.05).

Flux (y)	Equation	r^2	Significance
TN	y = 6.937 - 0.07528 x	0.117	NS
TP	$\log_{10}$y = 0.0612 - 0.04610 x	0.715	***
OC	y = 119.0 - 0.336 x	0.005	NS
CaCO3	$\log_{10}$y = 2.78 – 0.767x	0.754	***
OC:TN	y = 19.69 + 0.2202 x	0.265	NS
TN:TP	y = 6.547 + 3.505 x	0.868	***
CaCO3:TP	$\log_{10}$y = 2.185 - 0.02923 x	0.605	**

Table 2.4. Core-specific mean TP fluxes, baseline and slope molar $CaCO_3$:TP along with interval-specific and total core estimates of $CaCO_3$ dissolution rates. All parenthetical values represent 1 SE. All rates are in units of mol or g m^{-2} yr^{-1}. No $CaCO_3$ data were available for site WSC-5.

		$CaCO_3$:TP		Δ $CaCO_3$ Flux			Total Annual $CaCO_3$ dissolution	
Core	μ TP Flux	Baseline	Slope	mol	g	Slope Age (Yrs)	mol	g
WSC_1, 2, 3, 4, 7, 8, & 11	--	58.9 (1.5)	--		--			
WSC_13	--	314.0 (6.3)	--		--			
WSC_6	0.028 (0.003)	43.5 (3.9)	-3.7 (0.8)	-0.10	-10.37	44	-4.5	-452.8
WSC_9	0.027 (0.002)	62.8 (1.6)	-6.1 (3.2)	-0.16	-16.48	29	-4.9	-485.8
WSC_10a	0.068 (0.006)	79.9 (6.2)	-9.4 (1.6)	-0.64	-63.98	38	-24.4	-2439.4
WSC_10b	"	"	-6.3 (1.1)	-0.43	-42.88	30	-12.8	-1278.6
WSC_12	0.033 (0.003)	18.8 (1.6)	-5.2 (1.2)	-0.17	-17.17	48	-8.2	-824.7
Average	0.039 (0.10)	57.6 (1.5)	-6.1 (1.2)	-0.24	-23.81			

Figures

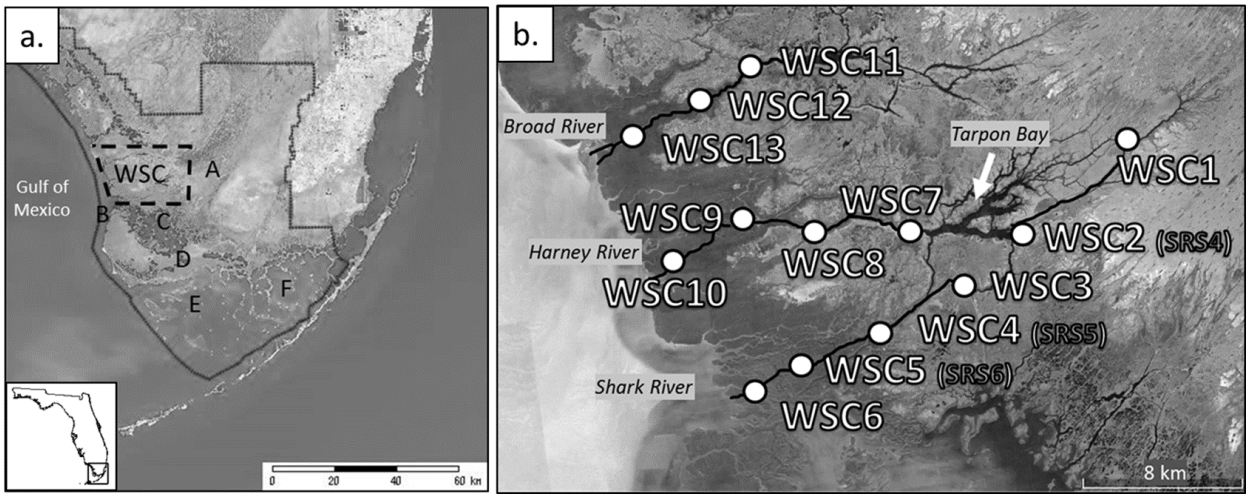

Fig. 2.1 a) Everglades National Park and b) WSC core sampling locations on the Shark, Harney, and Broad Rivers. Capital letters in panel a) represent sampling locations of $CaCO_3$:TP ratios from Kang and Trefry (2013): A: Shark River Slough, B: Ponce de Leon Bay, C: Oyster Bay, D: Coot Bay, E: northwest Florida Bay, and F: northeast Florida Bay. Map created using "Florida Coastal Everglades LTER Mapserver project". http://fcelter.fiu.edu/gis/everglades-map/ (20 December 2016).

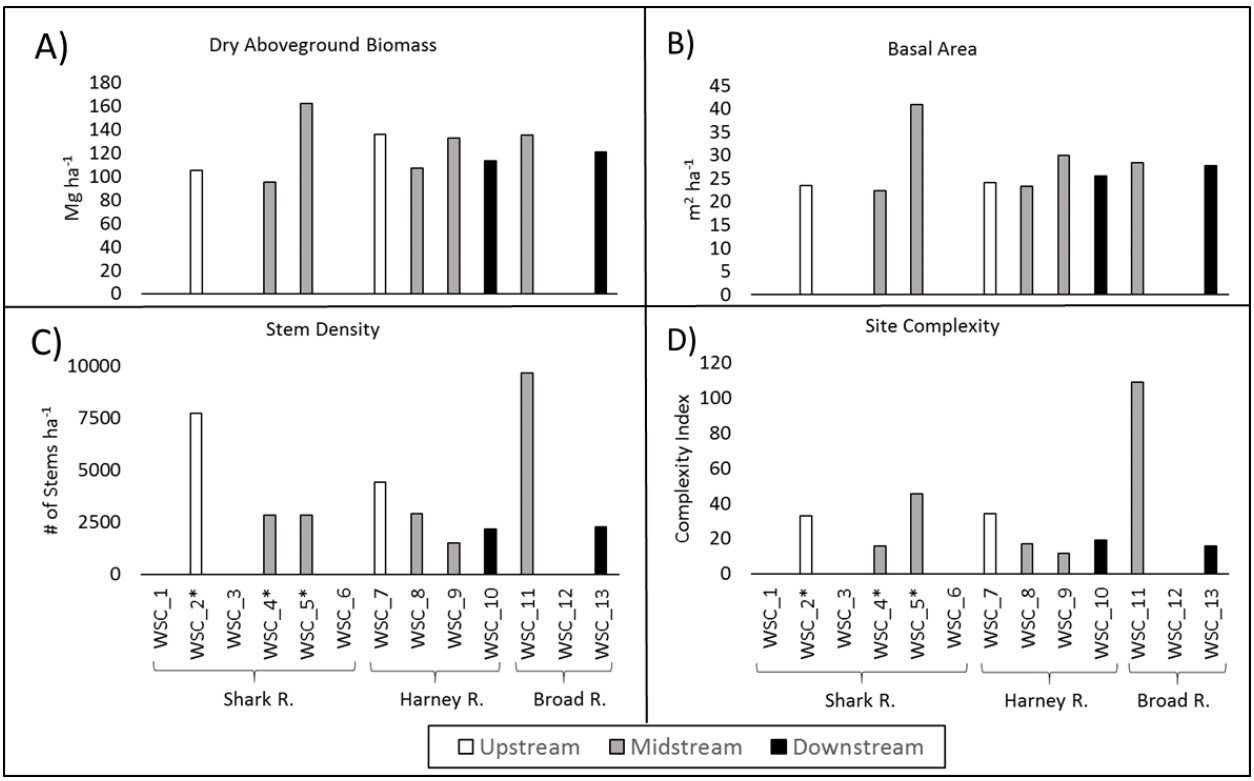

Figure 2.2 Above-ground biomass characteristics by site for each river and soil class: A) dry above-

ground biomass, B) basal area, C) stem density, and D) site complexity. Asterisks (WSC2, 4, & 5) indicate data collected from 2002-2004 by Castañeda-Moya et al., (2013).

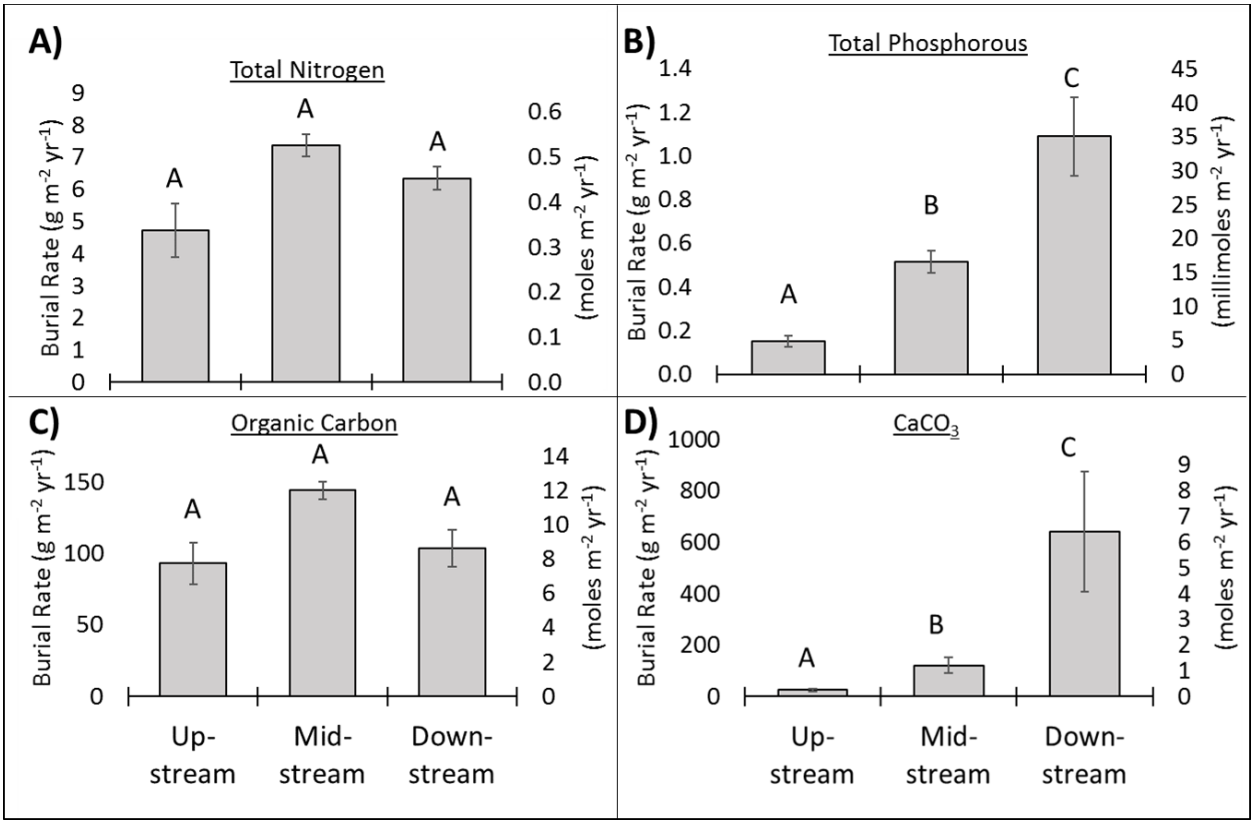

Figure 2.3 Mean (± 1 SE) burial rates by site classification. Different capital letters above error bars indicate significant difference ($p<0.05$). Rates are provided in mass units on the primary axis, and molar units on the secondary axis.

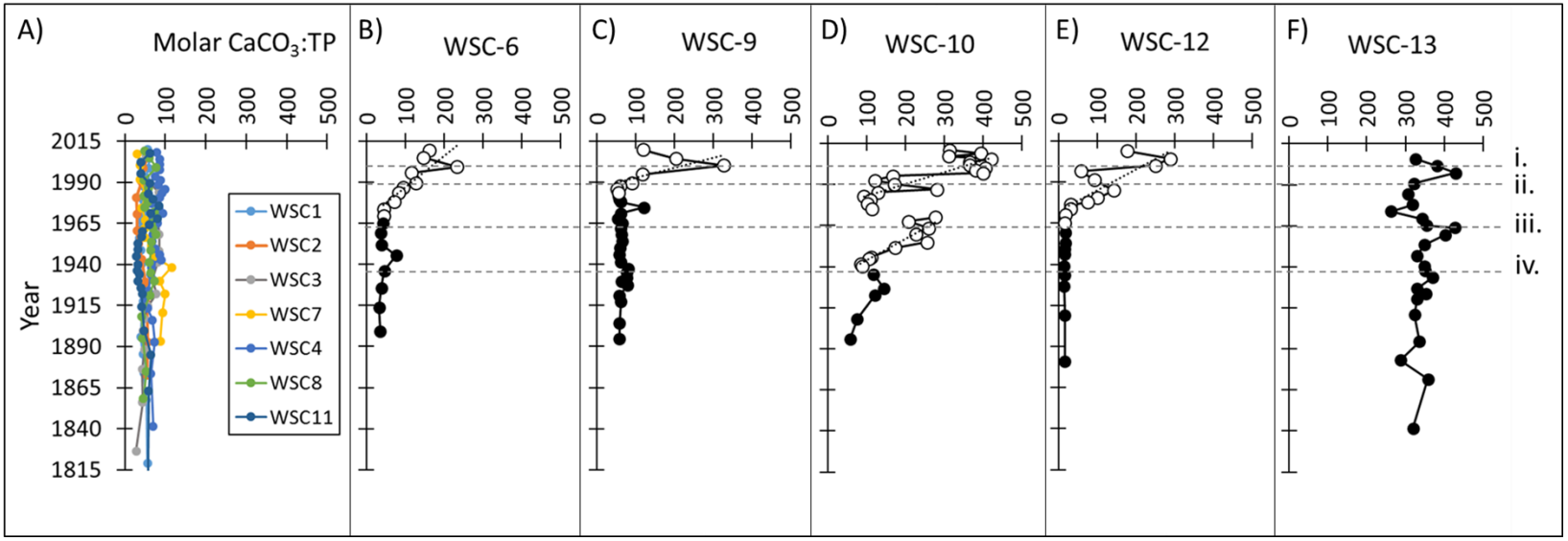

Figure 2.4 Plots of $CaCO_3$:TP vs. age/depth by site. Closed colored circles (Panel A) represent baseline values for sites with no discernible slope. For panels B-F, closed black circles represent baseline values and open white circles represent slopes. Slope statistics are: (B) WSC-6: r^2=0.70, p: 0.002; (C) WSC-9: r^2=0.37, p: 0.108; (D) WSC-10a (upper): r^2=0.67, p: 0.000; WSC-10b (lower): r^2=0.81, p: 0.000; & (E) WSC-12: r^2=0.66, p: 0.001. Dashed lines represent hurricanes: (i) Wilma, 2005, (ii) Andrew, 1992, (iii) Donna, 1960, & (iv) Labor Day, 1935.

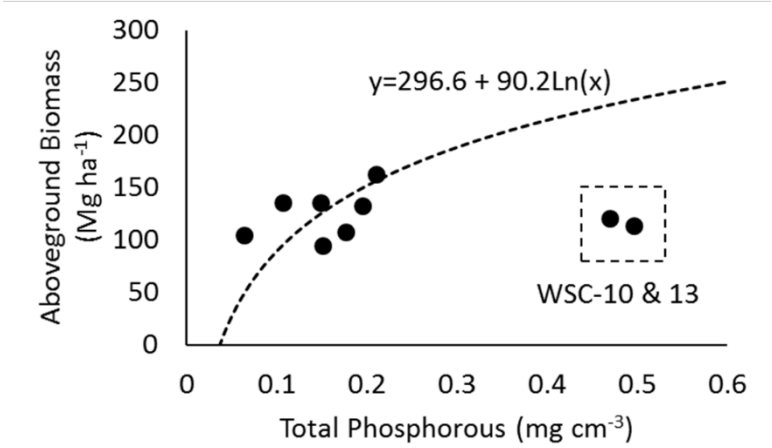

Fig. 2.5 Above-ground biomass (y) as a function of soil total phosphorous (x) (black circles) compared with model from Castañeda-Moya et al. (2013) (dashed line). The standard error of the regression (S) was 23.27 Mg ha^{-1}. Outlier sites WSC-10 & 13 are noted in the dashed square.

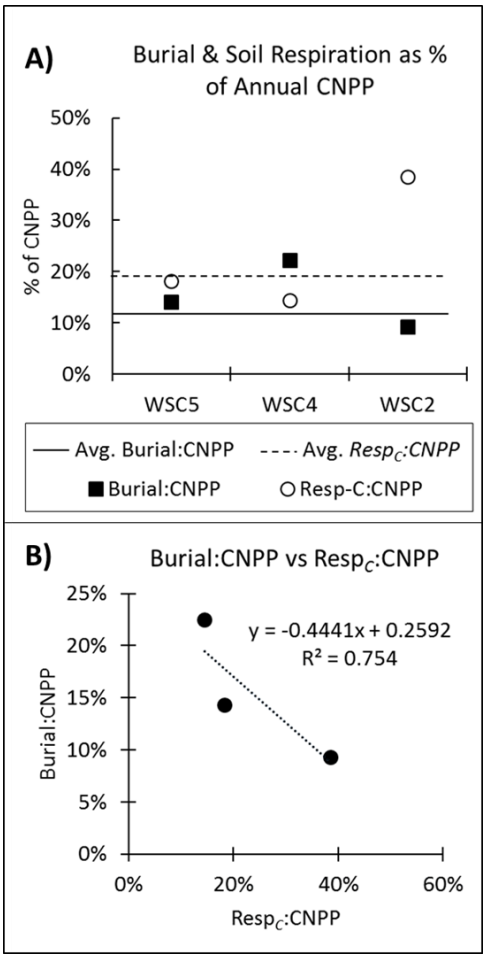

Figure 2.6 a) Organic carbon burial and soil C respiration (Troxler et al., 2015) as a fraction of site-specific above- and below-ground mangrove carbon net primary productivity (CNPP) (Castañeda-Moya

et al., 2013). Solid line (12.1%) represents global average burial:CNPP (Breithaupt et al., 2012). Dashed line (19.3%) represents global average $Resp_C$:CNPP (Bouillon et al., 2008). b) Correlation between site-specific ratios of burial:CNPP and $Resp_C$:NPP.

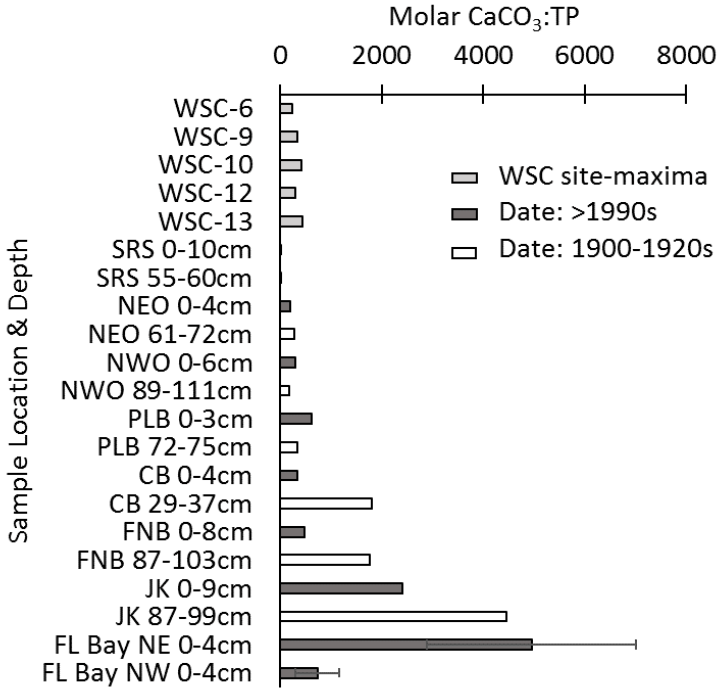

Figure 2.7 Comparison of maximum $CaCO_3$:TP ratios in WSC cores with regional ratios measured at different depths, and surface samples (0-4cm) from sites across northeast and southwest Florida Bay. Non-WSC data are compiled from Kang & Trefry (2013).

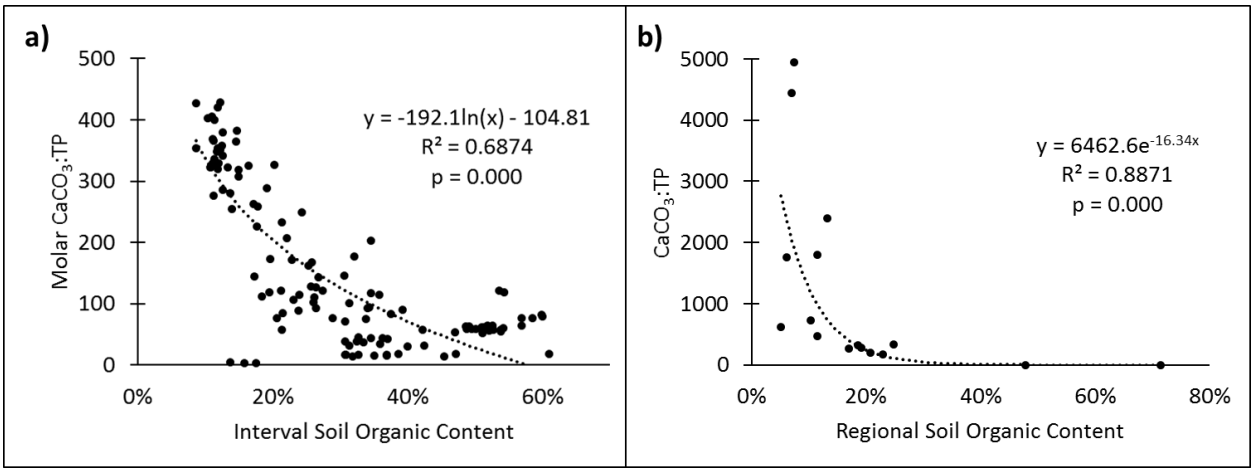

Figure 2.8 Molar $CaCO_3$:TP as a function of soil organic matter (OM%) for a) individual soil core intervals, and b) samples throughout Florida Bay and SW Everglades compiled from Kang & Trefry (2013).

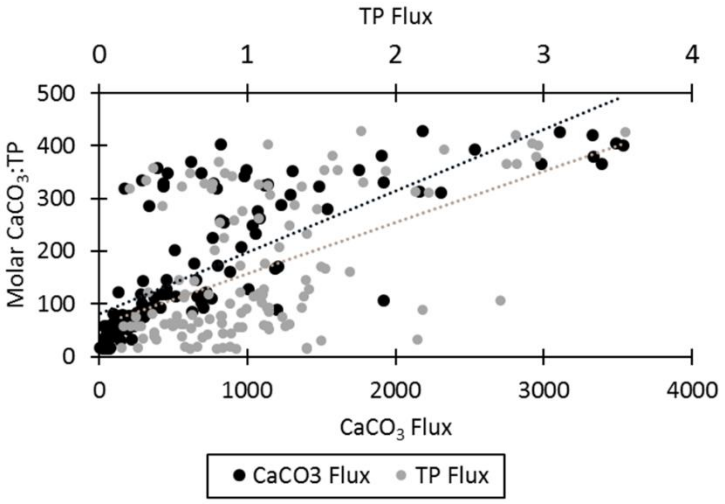

Figure 2.9 Regressions of molar $CaCO_3$:TP with the flux of $CaCO_3$ (black circles; R^2: 0.58) and TP (gray circles; R^2: 0.26).

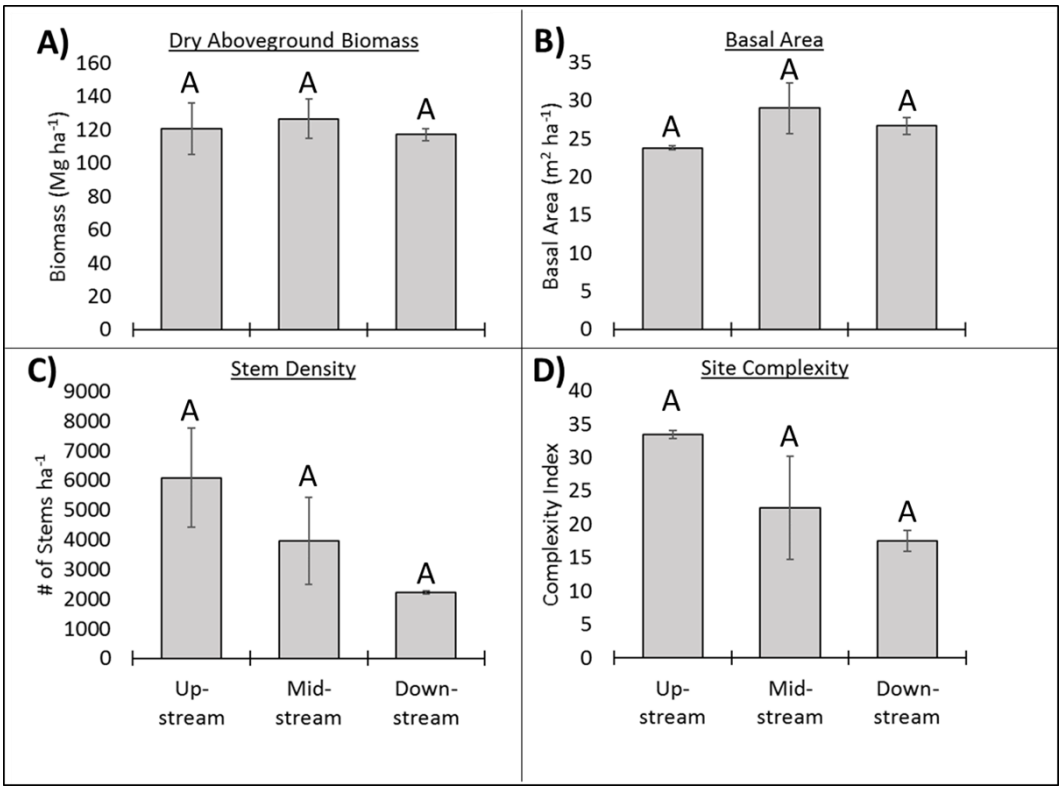

Figure 2.10 Mean above-ground vegetation characteristics by site classification: A) dry above-ground biomass, B) basal area, C) stem density, and D) site complexity. Same capital letters by stream position indicate no significant difference was detected ($p>0.05$). Note that site WSC-11 data was withheld from the stem density and site complexity mean for the Midstream positions because its values were so much higher than the others in observed in the system (Fig. 2.1C & D).

Chapter 3:
Bias in timescale assessments of coastal wetland sea-level rise vulnerability

Abstract

There is growing concern that accelerating sea-level rise (SLR) will exceed the vertical growth capacity of coastal-wetland substrates by the end of this century. Vulnerability estimates are typically based on a comparison of SLR rates with accretion and/or surface-elevation-change rates derived from soil cores and/or surface elevation tables (SETs). It is unclear which of the multiple timescales represented by these methods is the most useful for quantifying wetland vulnerability. To examine the potential for timescale bias in these assessments, we analyzed rates of accretion and elevation change from six regions around the world. Rates for both processes vary significantly as a function of measurement timescale. Failure to account for this variability will produce biased projections of SLR impacts on coastal wetlands. Robust vulnerability assessments should combine accretion rates from multiple timescales with the longest available SET record to provide long-term context for ongoing, short-term observations.

1. Introduction

Coastal marshes and mangroves, and the numerous ecosystem services that they provide, have existed under various rates of SLR over recent millennia (Alongi, 2015; Kirwan et al., 2016; Reed, 2002; Woodroffe, 1990). However, there is growing concern that these wetlands will not be able to keep pace with the projected increase in rates of SLR in the current century (Cahoon et al., 2006; Ellison and Stoddart, 1991; FitzGerald et al., 2008; Lovelock et al., 2015; Sasmito et al., 2015). The vertical growth of coastal wetland substrates occurs through dynamic feedbacks related to the production/supply and retention/preservation of organic matter and mineral sediments relative to the accommodation space

created by rising water level (Kirwan et al., 2016; Kirwan and Megonigal, 2013; Krauss et al., 2014; Woodroffe et al., 2016). Some processes may add both mass and volume to the soil body, including autochthonous production and allochthonous deposition, while processes of erosion, decomposition and bioturbation subtract both mass and volume. Other processes may only change soil volume, such as auto-compaction or shrinking/swelling during drying and wetting. Additionally, displacement within or below the soil body (such as from ingrowth of roots, fluid withdrawal, or tectonic events and isostatic adjustments) drives changes to the surface height relative to sea level. The drivers of these changes to mass, volume, and surface elevation of the soil body are numerous and regionally variable depending on climate, hydrology, productivity, underlying geology, ecosystem type, and soil depth/age, among others. This spatio-temporal variability contributes to the difficulty in making vulnerability assessments of coastal wetlands to SLR, and is the reason for the growing global effort to pair wetland analyses with local rates of SLR (Webb et al., 2013).

Soil- and sea-level-change processes operate over a wide range of timescales that can broadly be categorized as sub-decadal (≤ 9 years), decadal 10–99 years), centennial (100–999 years) and millennial (≥ 1,000 years) (Fig. 3.1). These timescales have also been described in the context of their influences as contemporary (sub-annual to decadal), historical (multi-decadal to multi-centennial), and geological (multi-centennial to multi-millennial) time (Cowell and Thom, 1994; Parkinson et al., 1994). Rates of wetland soil accumulation have historically been measured retrospectively using soil cores and dating methods covering timescales ranging from decades to millennia (Table 3.1). In recent decades the coupled SET–Marker Horizon (MH) methodology has offered a time-series approach with repeated measurements of elevation and accretion that offer sub-annual resolution (Cahoon et al., 2006; Webb et al., 2013) (Table 3.1). An annual rate of accretion is calculated as the thickness of the soil above a reference plane, divided by the number of years that have passed since the age of the reference plane (Table 3.2). Methods typically employed to measure accretion include the combination of a soil core (including due diligence to avoid compaction during collection) with a dating mechanism such as surface marker horizons,

radionuclides, or historical event horizons. The annual rate of elevation change is also calculated as the change in the soil thickness above a reference plane whose depth is located within the soil column or at a fixed vertical position within deep consolidated sediments or bedrock (Table 3.2). The method most reliably used to measure wetland elevation change with high accuracy has been some variant of the SET, whose materials (pipe vs rod) and depth (shallow vs deep) have evolved in the last few decades (Cahoon et al., 2002) (Table 3.1). By making comparisons from measurements at different depths, whether between an SET and an MH or between SETs of different depths, it is possible to identify the depth and drivers that contribute to the observed change.

Throughout the literature there are several stated and inferred assumptions that apply to the utilization of these techniques (Table 3.1) for quantifying rates of soil-body change relative to sea-level change. Several studies have used 5–15-year records of accretion and/or elevation change for predicting vulnerabilities over 50–100 years (Lovelock et al., 2015; Rogers et al., 2012; Rybczyk and Cahoon, 2002; Sasmito et al., 2015), implicitly assuming that rates measured over relatively short-timescales are suitable for estimating longer-term changes. Similarly, a recent, high profile study identified no significant difference between short (mean record length: 2.1 years) and long (mean record length: 5.5 years) timescales of RSET measurements, based on a comparison of data from 34 sites in Micronesia, New Zealand, and Australia (Lovelock et al., 2015). By implication, this suggests that trends in elevation change do not vary over different lengths of time. Conversely, much of the literature has focused on high rates of diagenesis in young, recently deposited material (Aller, 2013) to the extent that rates measured over sub-decadal scales are sometimes disregarded altogether when making comparisons with longer timescales because of the assumption that a high percentage of it will be transformed and lost with increasing time (Heathcote et al., 2015; Morris et al., 2016). For radionuclide-derived accretion data, it has often been asserted that rates derived from the peak or first occurrence of ^{137}Cs or $^{239+240}$Pu (20- to 50-year timescale depending on date of measurement) should be in agreement with rates derived from ^{210}Pb (100 to 150-year timescale) (Corbett and Walsh, 2015; Sanders et al., 2016), which implicitly suggests

that accretion rates are the same over these different lengths of time. In general, throughout the literature the submergence potential of coastal wetlands has been separately calculated using SETs, MHs, ^{137}Cs, and ^{210}Pb, which raises the question of whether the calculations provided by each technique (and timescale) are equally comparable. Even in cases where MH accretion is not used on its own, but is combined with elevation change to identify shallow subsidence or root zone expansion, there remains a question of what length of record is most suitable for long-term vulnerability assessments. These assumptions about timing have important ecological and resource management implications that include the identification of equilibrium rates and differentiating periodic variations from the onset of permanent changes in ecosystem conditions.

The objective of this study was to examine rates of accretion and elevation change for the four timescales of relevance to coastal wetland formation (Fig. 3.1), over several spatial scales ranging from local to regional, in order to test the following null hypotheses:

i. There is no difference between accretion rates measured over different lengths of time.
ii. There is no difference between rates of elevation change measured over different lengths of time.

These hypotheses were tested by following several approaches using data derived from a review of the literature. First, average rates of elevation change were compared with timescale-averaged accretion rates from six regions around the world where sub-decadal, decadal, centennial, and millennial timescales were represented: 1) New York & Connecticut, USA (NY-CT), 2) Louisiana, USA (LA), 3) southwest Florida, USA (FL), 4) northwestern Mediterranean (Med.), 5) northeast Australia (N.Aust.), and 6) southeast Australia (S.Aust.) (Fig. 3.2). These regions represent a diversity of settings including latitude, geomorphology, sediment type/source, primary plant type, and ecosystem type. Second, within each region, temporal comparisons were made for sub-regions as well as for regionally-unique environmental categories such as marsh or mangrove ecosystem type. Lastly, three sites with relatively long SET-MH records, combined with numerous local radiometric measurements, were analyzed to compare predictions of future rates of accretion and elevation change.

2. Methods

2.1 Literature review

A literature review was conducted using a combination of Google Scholar searches and cross-referencing of cited papers. This process was done iteratively by region from November 2015 to April 2016. Search terms focused on processes and locations. The initial list of potential regions was identified based on literature reviews of SET-MH data (Lovelock et al., 2015; Sasmito et al., 2015; Webb et al., 2013). Subsequent searches related to locations included regional terms such as Louisiana, Florida, Gulf of Mexico, Long Island Sound, New York, Connecticut, Australia, Europe, Mediterranean, Venice, Ebro, Rhone, France, Spain, and Italy. Additionally, within each region search terms included coastal wetlands, mangroves, and marshes combined with process terms such as accretion or elevation change as well as less specific terms like soil accumulation or coastal change. Additional searches were conducted substituting technique terms for the process terms; these included marker horizons, feldspar horizons, elevation tables, SETs, Pb-210, 210Pb, Cs-137, 137Cs, Plutonium, C-14, 14C, & radiocarbon. In addition to these searches, numerous sources were identified by following cited references in the papers. Introduction and Discussion sections, which often provided broader regional contexts of contemporary or previous research results, were particularly useful. Only *in situ* observational research papers were used (no modeling, laboratory, or meso-cosm experiments) from coastal marsh and mangrove environments that measured accretion and/or elevation change in coastal wetlands. Measurements from unvegetated areas such as mud flats or sub-tidal marine sediments, including seagrass meadows, were excluded.

2.2 Regional focus

The goal of this research was to assess the role of timescales when interpreting local rates of soil change. Ideally such a comparison would be performed at the site-level, however there are relatively few coastal wetlands around the world where measurements have been conducted over the multiple timescales of interest. Therefore, we looked at temporal variability within individual regions ranging in scale from

approximately 200–2,000 km, to individual basins and sites ranging in scale from meters to kilometers. The six major regions were New York & Connecticut (NY-CT), Louisiana (LA), and Southwest Florida (FL) in the United States, Venice Lagoon, the Rhone delta, and the Ebro delta in the northwestern Mediterranean (Med.), and northeastern and southeastern Australia (NE. and SE. Aust.) (Fig. 3.2). These six regions were selected for the availability of data across multiple timescales and represent a diversity of settings including latitude (tropical and temperate, Northern and Southern hemispheres), coastal geomorphology (deltaic, open coast, embayment, carbonate platform), plant type (marsh and mangrove), and ecosystem type (e.g., high and low marsh, riverine and fringing mangroves). Although the dataset is not globally exhaustive, we believe that it is a comprehensive record of published values for each region. We included our own unpublished radionuclide accretion rates from sites in South Florida and Australia to supplement the representation of available timescales in the published literature for these regions. Additionally, although there is an abundance of published radiocarbon data for the Louisiana delta, no millennial timescale rates of marsh accretion were found for the region.

2.3 Regional environmental categories

The primary research goal of determining whether rates change as a function of timescale is potentially complicated by the fact that different rates of accretion or elevation change can occur as a function of environmental variables. Therefore, when possible, data were sub-categorized according to regionally-unique identifiers so that comparisons could be made with mean regional rates. The following environmental categories were identified: for NY-CT: high and low marshes; Louisiana: inland and streamside marshes; Florida: riverine, basin, over-wash island, and fringe mangroves (no records were found for scrub mangrove ecosystems); NW Mediterranean: riverine, impounded, and marine marshes; and for NE and SE Australia: mangrove, marsh, or mixed. When details in the literature were insufficient to assign data to a specific category, the data were recorded as Non-Categorized (N/C). For classification of high and low marshes in NY-CT, sampling locations were recorded as high marsh, low marsh or tidal freshwater marsh when provided by the authors, or based on plant species composition (Kirwan et al.,

2016). Application of the environmental categories was restricted to the sub-decadal and decadal timescales based on the potential for transition/succession from one category to another over the course of one hundred years or more (e.g., Clark and Patterson, 1984; McCloskey and Liu, 2013).

2.4 Timescale definitions

Data were categorized to four timescales according to the total length of the observed record. The four categories are Sub-Decadal (total record ≤ 9 years), Decadal (10–99 years), Centennial (100–999 years), and Millennial (≥ 1,000 years). For timescale categorization of ^{210}Pb rates, we assumed a conventional value of 100+ years (Baskaran, 2016; Corbett et al., 1998); the exception to this was if the CRS dating model was used to determine sub-decadal or decadal rates. Rates from individual measurements were recorded when available in the literature. Ideally these data were provided in tables or within the text of the papers. When values were not stated, the data were interpreted from figures using Get Data Graph Digitizer (http://getdata-graph-digitizer.com/). Values reproduced from this method were in good agreement with reported values, with uncertainties in the tenths decimal place of the scale used (i.e., mm or cm) for accretion or elevation. This uncertainty was often due to the large font size of individual data points relative to the figure scale. Uncertainties were potentially higher for figures with poorer digital resolution such as those in older references.

If individual measurements were not provided in the literature, we used the mean value reported by the authors. In instances where multiple rates and lengths of time were available for a single site or core (e.g., Breithaupt et al., 2014; Day, 1998; Kemp et al., 2015), each measurement was recorded and attributed to the same site. Including only one of the measured values would introduce a bias. In some cases, there was potential duplication of data between site-level papers and regional synthesis papers. If the timescales were determined to be equivalent, then we recorded only the site-level data. If the timescales were not equivalent, then we recorded both numbers, with one as site-specific and one as regional.

2.5 Data analysis and interpretation of literature data

While the goal was to extract rates that were already calculated by the authors, in several cases soil-core data provided in the papers were used to calculate accretion rates. In these situations, depth of the sample was divided by the age the authors derived for that depth. In each case we assigned the sample age to the bottom of the sampled interval (i.e., rather than to the sample mid-point). When recording the length of record for radiocarbon measurements, the age difference between the sampling date and 1950 was added to the radiocarbon age to account for the total depositional record. For each study we recorded the name of each unique sample when possible (more discussion about this follows below), site location, sampling date, measurement/dating method, length of the measured record, geomorphological setting, wetland type, ecological type, and the rate values. When a single site had measurements for more than one length of time, each was recorded as a separate line item in the dataset.

Whenever possible, line items in the dataset were entered to match the sample numbers collected by the primary researchers to improve the power of statistical comparisons. If a literature source provided a regional mean rate derived from "n" soil cores or SET stations, then that mean value was recorded n times in our database, where n is the number of soil cores or SET stations used to derive the site mean. For example, in marshes of Long Island Sound our search found only four published elevation change rates (Anisfeld et al., 2016; Wigand et al., 2014), however those four rates represent 12 SET stations. (Note that sample number adjustment for SETs was only applied to individual stations and did not extend to the arm or pin level). There are limitations to this approach, most notably a potential to minimize spatial variability over multiple samples. However, one reason to think our approach does not misrepresent the original data is that our use of mean values to represent the spatial variability is based on how the SET authors have presented the data: that is, stating the mean and uncertainty of multiple stations or multiple wetland environmental categories. We believe that this was the most consistent way to account for multiple sampling locations given the limited level of detail provided in the literature. The alternative approach of providing only a single line item in the dataset for each mean value, without

regard for the number of samples, would contribute a bias to the dataset by giving equal sample weighting to studies where the value is derived from one site and others that have used multiple sites. This adjustment was also necessary for some of the sites using radiometric dating techniques. A prominent example of this provides a total of three published mean values that represent 42 soil cores across a wide region of the Mississippi Deltaic Plain (Nyman et al., 1990). In other cases where only the minimum and maximum average values were provided (e.g., Milan et al., 1995), we divide the sample number equally between minimum and maximum values to include the range in the data, while altogether providing the same overall mean value reported by the study. If we did not make this adjustment, the reported literature values would incorrectly introduce a bias into the measurements. This is because the thematic focus is different among papers; some provide each of their measured rates and some choose only to provide a mean value.

The long timescale measurements obtained via radio carbon measurements require interpretational care. The goal for this project was to identify wetland accretion and elevation change. Over radiocarbon timescales in deltaic environments, particularly the NW Mediterranean and Louisiana, wetlands may occur intermittently as deltaic depositional environments change throughout the profile. Similarly, in these environments many measurements that have been made using radiocarbon are based on deltaic depositional and subsidence rates rather than wetland rates and therefore such results were excluded. To the extent that identifying the depositional environment in the literature is not a straightforward matter, the dataset for this timescale entails the most subjectivity in the interpretation of the published data. Therefore, of the entire dataset, this is the one timescale that potentially does not represent a regionally comprehensive collection of published rates. Similarly, because radiocarbon is often used to reconstruct SLR curves, the depth at which a radiocarbon sample is collected is often stated in reference to mean high water rather than the sediment surface. Additionally, the nonlinear radiocarbon calibration curve sometimes leads to multiple estimated age ranges for a sample. In such a case we recorded the mid-point of the ranges. Sometimes the authors assessed multiple lines of evidence to

identify the probability of one range being the most suitable (Donnelly et al., 2004); in this case we record the mid-point of the authors' assessment of the most likely age range.

2.6 Case study locations

As was noted earlier, many of the complications in this analysis are due to a dearth of research in which rate measurements have been made using multiple timescales at the spatial scale of a single site. Additional analysis was conducted using three SET-MH time-series with accompanying local radionuclide measurements as examples of the potential that can be achieved with local comparisons when making predictions of future accretion and elevation change. This was done for various lengths of time from 1–10 years (elevation change) and between 1 and several thousand years for accretion. The three sites were selected because of the length and resolution of the records, as well as different characteristics unique to each that provide case studies for broader consideration. We analyzed (a) a record of mangrove encroachment into saltmarsh from Kooragang Island, southeast Australia, with relatively low rates of both accretion and elevation change (Rogers et al., 2013), (b) a record for a restored salt marsh in Jarvis, CT, USA with high rates and a virtually unwavering trend over the SET-MH timescale (Anisfeld et al., 2016), and (c) a mangrove site in the Everglades, FL, USA (Whelan et al., 2009) because the record includes a well-documented disturbance event (Hurricane Wilma, 2005) that had a significant impact on the rates.

2.7 100-year projections of accretion and elevation change balances as a function of local SLR

For the three SET-MH records, projections of total accretion and elevation change 100 years into the future were made using iterative cumulative linear trends for all LORs of at least one year in duration. Only LORs of one year or greater were used because trends calculated over sub-annual timescales were shown to generate predictions 1–2 orders of magnitude greater than the remainder of the results. The accretion record was extended to include radionuclide LORs at the same/nearby stations (Breithaupt et al., 2014; Nydick et al., 1995; Saintilan and Wilton, 2001; van de Plassche, 2000; van De Plassche et al.,

1998; Yao et al., 2015). Projections were calculated by using the annual rate identified by the cumulative linear trend (SET-MH record) or net cumulative change (radionuclide record) (Table 3.2) for each LOR, and multiplying by 100 years.

A balance is calculated as the rate of elevation change or accretion minus the rate of SLR. A positive balance equates to the soil body rate of change exceeding SLR, and a negative balance equates to lagging behind SLR. While suggestions have been made regarding the most appropriate duration of SLR to include in this calculation (Alongi, 2015; Lovelock et al., 2015; Reed, 2002), this is likely a function of objectives. Here the goal is consideration of SLR and coastal wetland vulnerability in the coming century. Therefore, the LORs for accretion and elevation change are compared with the longest available local sea-level record. Balances were only calculated when a significant trend ($p<0.05$) was discernible for a particular soil body LOR. For this reason, a number of points are missing from the elevation balances for the Everglades because a significant trend was not detected in the SET record prior to the occurrence of a high sedimentation storm event. Reported uncertainties are based on propagating the errors in trends from both soil and sea level. Comparisons with regional relative sea level were made using tide-gauge records obtained from Newcastle V, Australia (Holgate et al., 2013),[62] (1.19 ± 0.20 mm yr^{-1} for the period 1966–2012), Bridgeport, CT, USA (NOAA National Ocean Service 8467150) (2.82 ± 0.16 mm yr^{-1} for the period 1964–2014) and Key West, FL, USA (NOAA National Ocean Service 8724580) (2.26 ± 0.05 mm yr^{-1} for the period 1913–2006).

3. Results

Within each of the regions, we found significant differences ($p < 0.05$) between timescale-averaged accretion rates, however the relationship between the differences was not the same in each region (Fig. 3.3; Table 3.3). Whenever available, millennial-scale measurements of accretion were the lowest. Sub-decadal rates were generally the highest, with the exception of LA where they provided a relatively low estimate, and N. Aust where sub-decadal and decadal accretion rates were not statistically different. Rates decreased progressively from sub-decadal to millennial timescales in NY-CT and FL. In

Med. and N. Aust., rates over the sub-decadal, decadal, and centennial timescales were similar to one another, but greater than millennial rates. In S. Aust. there was a general decrease from sub-decadal to millennial, however discernment of statistical differences was inhibited by very small sample numbers for the centennial and millennial timescales (Table 3.3). In LA, sub-decadal rates were significantly lower than decadal rates, but were not significantly different from the rates over centennial timescales.

The mean length-of record (LOR) for the elevation change data was 4.8 ± 2.9 years (Table 3.3). The shortest average LOR occurred in the FL data (2.9 ± 0.9 yrs) and the longest average was in NY-CT (8.3 ± 1.4 yrs) (Table 3.3). The longest individual records for these regions were available for Med. and S. Aust., with site LORs exceeding a decade (Fig. 3.4h, j). Mean rates of elevation change were equal to the highest rates of accretion in NY-CT and Med., whereas they were not statistically different from the lowest rates of accretion in LA, and both Australian regions. In FL the mean rates of elevation change were the same as centennial-scale accretion rates.

There were significant differences between environmental categories in each of the regions over the sub-decadal timescale, but only for Med. and S. Aust. over the decadal timescale. In NY-CT, accretion and elevation change were significantly different between the low marsh and high marsh, but there was no difference between the two processes within marsh type (Fig. 3.4a). In FL, rates of accretion were generally the same across mangrove ecosystem types, with the exception of some low values for non-categorized mangroves. Rates of elevation change were also not statistically different by mangrove ecosystem type. Rates of accretion were different than rates of elevation change in fringe and over-wash mangroves, but not in basin or riverine for the sub-decadal timescale (Fig. 3.4c). In LA, rates of accretion were not different between inland and streamside marshes, but were greater than streamside elevation changes as well as numerous non-categorized accretion and elevation change samples (Fig. 3.4e). There was a significant pattern of differentiation between the two processes at riverine, marine and impounded marshes in the Med. sites over both the sub-decadal and decadal timescales (Fig. 3.4g, h). Rates of mangrove accretion in N. Aust were different from rates of mangrove elevation change and from both

processes in the marsh sites (Fig. 3.4i). In S.Aust., mangrove accretion rates were greater than those in marsh; in the sites with mixed marsh and mangrove, accretion rates were not statistically different from either marsh or mangrove. Elevation change in the mangrove site was lower than the accretion rate, but no statistical difference was found between the two processes in the marsh or mixed sites. Mangrove accretion rates were higher than those for marsh sites over the decadal timescale in S.Aust. Low sample numbers precluded comparison with the other environmental categories in S.Aust. (Fig. 3.4l).

There was no discernible difference between sub-decadal and decadal rates for high and low marsh categories in NY-CT, all categories of both elevation change and accretion in Med., mangrove accretion in N.Aust, and marsh accretion in S.Aust (Fig. 3.4). However, significant timescale differences were detected for fringe and riverine mangroves in FL, non-categorized marsh sites in LA, and mangrove accretion in S.Aust. The remaining categories could not be differentiated due to low sample numbers available in the literature.

A comparison of site-level projections of accretion and elevation balances with sea-level were made using a combination of SET-MH and radionuclide records (Anisfeld et al., 2016; Rogers et al., 2013; Whelan et al., 2009) (See Methods; Extended Data Fig. 3.2). A balance indicates the extent that accretion or elevation exceeds (positive balance) or lags (negative balance) sea-level. Differences in projected elevation balances were 12.1 ± 3.5, 55 ± 23.6, and 26.6 ± 28.7 cm in Kooragang, Australia, Jarvis, CT, and Everglades, FL respectively (Fig. 3.6a, b, c). Accretion balances were generally higher than elevation balances over the SET-MH timescales with ranges of 26.5 ± 6.4, 40.4 ± 31.0, and 56.0 ± 18.9 cm over the given record. When radionuclide accretion rates were included, the range of projected accretion balances at the three respective sites increased to 35.4 ± 3.3, 132.9 ± 6.3, and 101.6 ± 12.1 cm (Fig. 3.6a, b, c).

4. Discussion

A conceptual model is introduced in which the mean rates for each timescale are displayed as a function of soil depth/ age (Fig. 3.5a). The resulting profiles indicate a timescale hierarchy (Woodroffe, 2002) for each region (Fig. 3.5b–g) or sub-region (Extended Data Fig. 3.1) and can be used to evaluate the null hypotheses. The first null hypothesis, that timescale does not influence mean accretion rates (gray profile in Fig. 3.5a), is not supported by the data. Four of the regions (LA, NY-CT, FL, and Med.) (Fig 3.5 b,c,f,g) and numerous sub-regions (Extended Data Fig. 3.1) exhibit significant differences across timescales. While two of the regional timescale hierarchies (N. & S.Aust.) have profiles that could be interpreted as supporting the null hypothesis over sub-decadal to centennial scales (Fig. 3.5d,e), millennial rates are significantly different from the sub-decadal rates. Additionally, the location-specific case studies (Fig. 3.6) indicate a wide range of 50-year accretion projections based on different LORs.

Numerous biogeochemical and geomorphological factors, of natural or anthropogenic derivation, drive the differences in timescale hierarchies (Figs. 3.1, 3.5b–g). A profile with a positive slope can indicate that addition of soil material or volume has increased in the shorter timescales, that the cumulative amount of degradation is greater for longer timescales, or some combination thereof. A negative slope could indicate that rates of material or volume addition have decreased over shorter timescales, that the rate of degradation/loss has decreased, or some combination of the two. Examples of temporal variability in natural ecosystem processes include peat formation, by which rates of diagenesis change exponentially with depth/age of the material (Aller, 2013) (e.g., FL, NY-CT), ecological transition (from high to low marsh, from marsh to mangrove etc.), unusually high deposition rates attributed to stochastic events such as storm surge (Smoak et al., 2013; Tweel and Turner, 2012), or broad spatial-scale climate oscillations such as sea-level change caused by El Niño (Rogers et al., 2013). Additional insights can be gleaned from rate comparisons as a function of the mineral vs. organic soil content over time (Anisfeld et al., 2016). Such comparisons may indicate wetlands changes such as responses to different periods of submergence, dependence on allochthonous supply or autochthonous production, and the durability/stability of the deposited materials. Anthropogenically-influenced changes may include

hydrological modifications that alter suspended sediment loads and flow/delivery patterns as well as increased or reduced fluid withdrawals (e.g., LA, Med.).

The second null hypothesis, that rates of elevation change do not vary with timescale, is also not supported by these data. A difficulty of testing this hypothesis is that there are few published SET datasets that are longer than ten years, and so statistical comparisons of mean rates by timescale have limited power to detect differences. Rather than comparing timescale-mean rates, evidence refuting the second null hypothesis is demonstrated by the three case studies in NY-CT, FL, and S.Aust. These depict a wide range in elevation-change and accretion trends calculated as a function of different LORs (Fig. 3.6a–c; 3.8). Observations from the Jarvis Marsh (Anisfeld et al., 2016) (Fig. 3.6b, 3.8b) are particularly informative. Even though the trends in elevation change show minimal variation over a nine-year period, the effect of projecting those trends 100 years into the future magnifies the differences by two orders of magnitude. This is the danger of long-term vulnerability projections, regardless of whether they are derived from SETs or any of the accretion timescale methods. The range of potential outcomes from these three case studies demonstrates the potential for biased vulnerability estimates. The consequences of misunderstanding this relationship on the scale of half a meter or more could be a matter of misjudging a wetland's viability by multiple decades depending on both the rate and trajectory of soil-body and sea-level change.

Equifinality and convergence are terms used to describe how numerous processes, feedbacks, and orders of events may contribute to the same long-term geologic outcome in different locations (Woodroffe, 2002). This equifinality applies to coastal wetlands in equilibrium with SLR, whereby overall surface elevation keeps pace, but different sub-regions or environmental types respond at different rates, leading or lagging changes in SLR. There are a number of feedback processes that occur over small spatial scales related to accommodation space, inundation times, plant productivity, and accretion of new mineral sediment (Cahoon and Reed, 1995; FitzGerald et al., 2008; Krauss et al., 2014; Morris et al., 2016; Nydick et al., 1995; Woodroffe et al., 2016). For substrates that are in equilibrium with sea level,

we contend that spatial complexity and these feedback processes are most important over shorter timescales. Environmental categories that are distinct in the short-term, can change in the long-term. For example, repeated transitions between high and low marsh (Clark and Patterson, 1984) or mangrove presence/absence (McCloskey and Liu, 2013) have been documented in the literature over centennial to millennial timescales. Similarly, in FL mangroves relatively high spatial variability in the decadal record of accretion rates is minimized over the centennial scale (Breithaupt et al., 2014). Sole reliance on a short-term record to project longer-term trends, might overlook the occurrence of these critically important feedbacks. A site with a short-term positive balance (accretion or elevation change) would be projected to rise out of the water, whereas a site with a short-term negative balance would be projected to fully submerge in the same number of years. Instead, as long as the wetland is in healthy equilibrium with SLR, long-term rates from both sites are expected to resemble the long-term rates of SLR (Kolker et al., 2009), accelerating as a location submerges and slowing as it emerges (Nydick et al., 1995). However, under future change, SLR is expected to exceed equilibrium conditions for wetlands. In such cases, the long-term rates [which are shown here to generally be the most conservative (Fig. 3.3)], would likely underestimate the potential of the wetland to respond to a higher rate of SLR.

A key question for vulnerability assessments is the detection of change in the long-term trends and the onset of deceleration or wetland collapse. Detection of acceleration in regional tide gauge trends will require several more decades of data, even assuming upper limits of IPCC sea-level projections (Church et al., 2013) by the end of the century (Haigh et al., 2014). If these uncertainties persist regarding sea-level, then they also pertain to assessments of soil accretion and elevation change, processes that are highly dependent on sea level. While the importance of making wetland comparisons with local rates of sea-level change has been recognized (Cahoon, 2015), it is less clear what duration of a local record is most useful (Reed, 2002). This may be particularly relevant for mangrove-vulnerability assessments in the Indo-Pacific (Lovelock et al., 2015) where evidence suggests that relative sea level has been anomalously high over the past two decades (Merrifield, 2011).

There are several steps that can be taken to improve our understanding of temporal dynamics of soil body change in coastal wetlands, and our ability to predict their vulnerability to future change. First, ideally a study like this would analyze data from numerous sites where side-by-side comparisons of timescale techniques are available within a small spatial footprint. The case studies (Fig. 3.6) demonstrate the strength of this approach, allowing for comparisons of elevation change with accretion over numerous lengths of time. One of the findings of this research is just how sparse such data are (Table 3.3). We recommend that the growing global effort to pair local tide gauges with SET-MH stations (Webb et al., 2013) be made more robust by also utilizing all available timescale techniques to understand site-specific variability. Second, one of the most persistent difficulties for detecting a true change in the rates recorded in the geologic record is the question of apparent change driven by post-depositional diagenesis (Aller, 2013; Bianchi et al., 2016). Because radiometric dating has been conducted in coastal wetlands for several decades, there is an opportunity to conduct repeated site-specific measurements using the same initial method to identify whether rates are the same as those in previous decades. If they are not, then observed differences would provide a means of empirically quantifying decadal-scale rates of processes like diagenesis, reduced sedimentation, or accelerated sedimentation at these sites. Third, the concerns about timescale bias raised in this paper also apply to the burial/ sequestration rates of atmospheric CO_2 in wetland soils (Grimsditch et al., 2013; Mcleod et al., 2011). These measurements have been conducted using the full suite of radiometric techniques (Breithaupt et al., 2012; Chmura et al., 2003; Ouyang and Lee, 2014) as well as SETs (Lovelock et al., 2013; Webb et al., 2013) (Fig. 3.1, Table 3.1). Because carbon sequestration is of interest in the context of climate change, "permanence" for this sequestration is targeted for at least 100 years (Emmer et al., 2015). It is therefore imperative that the most robust application of timescale techniques is used to inform environmental policy decisions and provide the greatest assurance regarding the stability/permanence of carbon market investments.

We conclude that a combination of timescales should be utilized for measuring accretion and elevation change to avoid biased assessments of coastal wetland vulnerability. The adage that the past is

the best predictor of the future is complicated by predictions of unprecedented change in rates of SLR in coming decades. Use of the full suite of timescale hierarchies that operate in coastal wetlands is necessary for identifying the processes that contribute to the upper and lower bounds of potential wetland responses to future global changes. Long timescale measurements provide a baseline for comparison. Medium and short timescales, with adequate resolution, make it possible to ascertain when a true change in rates of accretion and/or elevation change begins to occur (i.e., acceleration, deceleration or collapse).

References

Aller, R.C., 2013. Sedimentary diagenesis, depositional environments, and benthic fluxes, 2nd ed, Treatise on Geochemistry: Second Edition. Elsevier Ltd. doi:10.1016/B978-0-08-095975-7.00611-2

Alongi, D.M., 2015. The impact of climate change on mangrove forests. Curr. Clim. Chang. Reports. doi:10.1007/s40641-015-0002-x

Anisfeld, S.C., Hill, T.D., Cahoon, D.R., 2016. Elevation dynamics in a restored versus a submerging salt marsh in Long Island Sound. Estuar. Coast. Shelf Sci. doi:10.1016/j.ecss.2016.01.017

Baskaran, M., 2016. Radon: A tracer for geological, geophysical and geochemical studies. doi:10.1007/978-3-319-21329-3

Bianchi, T.S., Schreiner, K.M., Smith, R.W., Burdige, D.J., Woodard, S., Conley, D.J., 2016. Redox effects on organic matter storage in coastal sediments during the Holocene: a biomarker/proxy perspective. Annu. Rev. Earth Planet. Sci. 44, 25pp. doi:10.1146/annurev-earth-060614-105417

Breithaupt, J.L., Smoak, J.M., Smith, T.J., Sanders, C.J., 2014. Temporal variability of carbon and nutrient burial, sediment accretion, and mass accumulation over the past century in a carbonate platform mangrove forest of the Florida Everglades. Journal of Geophysical Research: Biogeosciences 119, 2032-2048. doi:10.1002/2014JG002715

Breithaupt, J.L., Smoak, J.M., Smith, T.J., Sanders, C.J., Hoare, A., 2012. Organic carbon burial rates in mangrove sediments: Strengthening the global budget. Global Biogeochem. Cycles 26, 1–11.

doi:10.1029/2012GB004375

Cahoon, D.R., 2015. Estimating Relative Sea-Level Rise and Submergence Potential at a Coastal Wetland. Estuaries and Coasts 38, 1077–1084. doi:10.1007/s12237-014-9872-8

Cahoon, D.R., Hensel, P.F., Spencer, T., Reed, D.J., McKee, K.L., Saintilan, N., 2006. Coastal Wetland Vulnerability to Relative Sea-Level Rise: Wetland Elevation Trends and Process Controls, in: Wetlands and Natural Resource Management. pp. 271–292. doi:10.1007/978-3-540-33187-2_12

Cahoon, D.R., Lynch, J.C., Perez, B.C., Segura, B., Holland, R.D., Stelly, C., Stephenson, G., Hensel, P., 2002. High-Precision Measurements of Wetland Sediment Elevation: II. The Rod Surface Elevation Table. J. Sediment. Res. 72, 734–739. doi:10.1306/020702720734

Cahoon, D.R., Reed, D.J., 1995. Relationships among Marsh Surface Topography, Hydroperiod, and Soil Accretion in a Deteriorating Louisiana Salt Marsh. J. Coast. Res. 11, 357–369.

Chmura, G.L., Anisfeld, S.C., Cahoon, D.R., Lynch, J.C., 2003. Global carbon sequestration in tidal, saline wetland soils. Global Biogeochem. Cycles 17. doi:10.1029/2002GB001917

Church, J.A., Clark, P.U., Cazenave, A., Gregory, J.M., Jevrejeva, S., Levermann, A., Merrifield, M.A., Milne, G.A., Nerem, R.S., Nunn, P.D., Payne, A.J., Pfeffer, W.T., Stammer, D., Unnikrishnan, A.S., 2013. Sea level change. Clim. Chang. 2013 Phys. Sci. Basis. Contrib. Work. Gr. I to Fifth Assess. Rep. Intergov. Panel Clim. Chang. 1137–1216. doi:10.1017/CB09781107415315.026

Clark, J.S., Patterson Iii, W.A., 1984. Pollen, Pb-210, and opaque spherules: an integrated approach to dating and sedimentation in the intertidal environment (Long Island). J. Sediment. Petrol. 54, 1251–1265. doi:10.1306/212F85B2-2B24-11D7-8648000102C1865D

Corbett, D.R., Burnett, W.C., Cable, P.H., Clark, S.B., 1998. A multiple approach to the determination of radon fluxes from sediments. J. Radioanal. Nucl. Chem. 236, 247–253. doi:10.1007/BF02386351

Corbett, D.R., Walsh, J.P., 2015. 210Lead and 137Cesium: Establishing a chronology for the last century, in: Handbook of Sea-Level Research. pp. 361–372. doi:10.1002/9781118452547.ch24

Cowell, P. J., & Thom, B.G., 1994. Morphodynamics of coastal evolution, in: RWG Carter and CD Woodroffe (Ed.), Coastal Evolution: Late Quaternary Shoreline Morphodynamics. Cambridge University Press, Cambridge, United Kingdom and New York, NY, USA, pp. 33–86.

Day, J.W.J.E.A., 1998. Relative sea level rise and Venice lagoon wetlands. J. Coast. Conserv. 4, 27–34. doi:10.1007/BF02806486

Donnelly, J.P., Cleary, P., Newby, P., Ettinger, R., 2004. Coupling instrumental and geological records of sea-level change: Evidence from southern New England of an increase in the rate of sea-level rise in the late 19th century. Geophys. Res. Lett. 31, n/a-n/a. doi:10.1029/2003GL018933

Ellison, J.C., Stoddart, D.R., 1991. Mangrove Ecosystem Collapse during Predicted Sea-Level Rise: Holocene Analogues and Implications. Source J. Coast. Res. J. Coast. Res. 7, 151–165.

Emmer, I., von Unger, M., Needelman, B., Crooks, S., Emmett-Mattox, S., 2015. Coastal Blue Carbon in Practice: A Manual for Using the VCS Methodology for Tidal Wetland and Seagrass Restoration VM0033.

FitzGerald, D.M., Fenster, M.S., Argow, B. a., Buynevich, I. V., 2008. Coastal Impacts Due to Sea-Level Rise. Annu. Rev. Earth Planet. Sci. 36, 601–647. doi:10.1146/annurev.earth.35.031306.140139

Grimsditch, G., Alder, J., Nakamura, T., Kenchington, R., Tamelander, J., 2013. The blue carbon special edition - Introduction and overview. Ocean Coast. Manag. 83, 1–4. doi:10.1016/j.ocecoaman.2012.04.020

Haigh, I.D., Wahl, T., Rohling, E.J., Price, R.M., Pattiaratchi, C.B., Calafat, F.M., Dangendorf, S., 2014. Timescales for detecting a significant acceleration in sea level rise. Nat. Commun. 5, 3635. doi:10.1038/ncomms4635

Heathcote, A.J., Anderson, N.J., Prairie, Y.T., Engstrom, D.R., Del Giorgio, P.A., 2015. Large increases in carbon burial in northern lakes during the Anthropocene. Nat. Commun. 6, 10016. doi:10.1038/ncomms10016

Holgate, S.J., Matthews, A., Woodworth, P.L., Rickards, L.J., Tamisiea, M.E., Bradshaw, E., Foden, P.R., Gordon, K.M., Jevrejeva, S., Pugh, J., 2013. New Data Systems and Products at the Permanent Service for Mean Sea Level. J. Coast. Res. 288, 493–504. doi:10.2112/JCOASTRES-D-12-00175.1

Kemp, A.C., Hawkes, A.D., Donnelly, J.P., Vane, C.H., Horton, B.P., Hill, T.D., Anisfeld, S.C., Parnell, A.C., Cahill, N., 2015. Relative sea-level change in Connecticut (USA) during the last 2200 yrs. Earth Planet. Sci. Lett. 428, 217–229. doi:10.1016/j.epsl.2015.07.034

Kirwan, M.L., Megonigal, J.P., 2013. Tidal wetland stability in the face of human impacts and sea-level rise. Nature 504, 53–60. doi:10.1038/nature12856

Kirwan, M.L., Temmerman, S., Skeehan, E.E., Guntenspergen, G.R., Fagherazzi, S., 2016. Overestimation of marsh vulnerability to sea level rise. Nat. Clim. Chang. 6, 253–260. doi:10.1038/nclimate2909

Kolker, A.S., Goodbred, S.L., Hameed, S., Cochran, J.K., 2009. High-resolution records of the response of coastal wetland systems to long-term and short-term sea-level variability. Estuar. Coast. Shelf Sci. 84, 493–508. doi:10.1016/j.ecss.2009.06.030

Krauss, K.W., McKee, K.L., Lovelock, C.E., Cahoon, D.R., Saintilan, N., Reef, R., Chen, L., 2014. How mangrove forests adjust to rising sea level. New Phytol. 202, 19–34. doi:10.1111/nph.12605

Lovelock, C.E., Adame, M.F., Bennion, V., Hayes, M., O'Mara, J., Reef, R., Santini, N.S., O???Mara, J., Reef, R., Santini, N.S., 2013. Contemporary Rates of Carbon Sequestration Through Vertical Accretion of Sediments in Mangrove Forests and Saltmarshes of South East Queensland, Australia. Estuaries and Coasts 37, 763–771. doi:10.1007/s12237-013-9702-4

Lovelock, C.E., Cahoon, D.R., Friess, D.A., Guntenspergen, G.R., Krauss, K.W., Reef, R., Rogers, K., Saunders, M.L., Sidik, F., Swales, A., Saintilan, N., Thuyen, L.X., Triet, T., 2015. Supp Info. The vulnerability of Indo-Pacific mangrove forests to sea-level rise. Nature 526, 559-U217. doi:10.1038/nature15538

Lovelock, C.E., Cahoon, D.R., Friess, D. a., Guntenspergen, G.R., Krauss, K.W., Reef, R., Rogers, K., Saunders, M.L., Sidik, F., Swales, A., Saintilan, N., Thuyen, L.X., Triet, T., 2015. The vulnerability of Indo-Pacific mangrove forests to sea-level rise. Nature. doi:10.1038/nature15538

McCloskey, T., Liu, K., 2013. Sedimentary History of Mangrove Cays in Turneffe Islands, Belize: Evidence for Sudden Environmental Reversals. J. Coast. Res. doi:10.2112/JCOASTRES-D-12-00156.1

Mcleod, E., Chmura, G.L., Bouillon, S., Salm, R., Björk, M., Duarte, C.M., Lovelock, C.E., Schlesinger, W.H., Silliman, B.R., 2011. A blueprint for blue carbon: toward an improved understanding of the role of vegetated coastal habitats in sequestering CO2. Front. Ecol. Environ. 110621060659096. doi:10.1890/110004

Merrifield, M.A., 2011. A shift in western tropical Pacific sea level trends during the 1990s. J. Clim. 24, 4126–4138. doi:10.1175/2011JCLI3932.1

Milan, C.S., Swenson, E.M., Turner, R.E., Lee, J.M., 1995. Assessment of the 137Cs method for estimating sediment accumulation rates: Louisiana salt marshes. J. Coast. Res. 11, 296–307.

Morris, J.T., Barber, D.C., Callaway, J.C., Chambers, R., Hagen, S.C., Hopkinson, C.S., Johnson, B.J., Megonigal, P., Neubauer, S.C., Troxler, T., Wigand, C., 2016. Contributions of organic and inorganic matter to sediment volume and accretion in tidal wetlands at steady state. Earth's Futur. 4, doi:10.1002/2015EF000334. doi:10.1002/2015EF000334.Received

NOAA National Ocean Service (Accessed April 25, 2016), [Available at https://tidesandcurrents.noaa.gov/waterlevels.html?id=8467150].

NOAA National Ocean Service (Accessed April 25, 2016), [Available at https://tidesandcurrents.noaa.gov/stationhome.html?id=8724580].

Nydick, K.R., Bidwell, A.B., Thomas, E., Varekamp, J.C., 1995. A sea-level rise curve from Guilford,

Connecticut, USA. Mar. Geol. 124, 137–159. doi:10.1016/0025-3227(95)00037-Y

Nyman, J., DeLaune, R., Jr, W.P., 1990. Wetland soil formation in the rapidly subsiding Mississippi River deltaic plain: Mineral and organic matter relationships. Estuarine, Coast. Shelf Science 31, 57–69.

Ouyang, X., Lee, S.Y., 2014. Updated estimates of carbon accumulation rates in coastal marsh sediments. Biogeosciences 11, 5057–5071. doi:10.5194/bg-11-5057-2014

Parkinson, R., DeLaune, R., White, J., 1994. Holocene sea-level rise and the fate of mangrove forests within the wider Caribbean region. J. Coast. Res. 10, 1077–1086.

Permanent Service for Mean Sea Level (PSMSL), 2016, "Tide Gauge Data", Retrieved 25 Apr 2016 from http://www.psmsl.org/data/obtaining/stations/837.php)/.

Reed, D.J., 2002. Sea-level rise and coastal marsh sustainability: Geological and ecological factors in the Mississippi delta plain. Geomorphology 48, 233–243. doi:10.1016/S0169-555X(02)00183-6

Rogers, K., Saintilan, N., Copeland, C., 2012. Modelling wetland surface elevation dynamics and its application to forecasting the effects of sea-level rise on estuarine wetlands. Ecol. Modell. 264, 148–157. doi:10.1016/j.ecolmodel.2013.04.016

Rogers, K., Saintilan, N., Howe, A.J., Rodríguez, J.F., 2013. Sedimentation, elevation and marsh evolution in a southeastern Australian estuary during changing climatic conditions. Estuar. Coast. Shelf Sci. 133, 172–181. doi:10.1016/j.ecss.2013.08.025

Rybczyk, J.M., Cahoon, D.R., 2002. Estimating the potential for submergence for two wetlands in the Mississippi River Delta. Estuaries 25, 985–998. doi:10.1007/BF02691346

Saintilan, N., Wilton, K., 2001. Changes in the distribution of mangroves and saltmarshes in Jervis Bay, Australia. Wetl. Ecol. Manag. 9, 409–420. doi:10.1023/A:1012073018996

Sanders, C.J., Santos, I.R., Maher, D.T., Breithaupt, J.L., Smoak, J.M., Ketterer, M., Call, M., Sanders,

L., Eyre, B.D., 2016. Examining 239+240Pu, 210Pb and historical events to determine carbon, nitrogen and phosphorus burial in mangrove sediments of Moreton Bay, Australia. J. Environ. Radioact. 151, 623–629. doi:10.1016/j.jenvrad.2015.04.018

Sasmito, S.D., Murdiyarso, D., Friess, D. a., Kurnianto, S., 2015. Can mangroves keep pace with contemporary sea level rise? A global data review. Wetl. Ecol. Manag. doi:10.1007/s11273-015-9466-7

Smoak, J., Breithaupt, J., III, T.S., Sanders, C., 2013. Sediment accretion and organic carbon burial relative to sea-level rise and storm events in two mangrove forests in Everglades National Park. Catena 104, 58–66. doi:DOI: 10.1016/j.catena.2012.10.009

Tweel, A.W., Turner, R.E., 2012. Landscape-Scale Analysis of Wetland Sediment Deposition from Four Tropical Cyclone Events. PLoS One 7. doi:10.1371/journal.pone.0050528

van de Plassche, O., 2000. North Atlantic Climate–Ocean Variations and Sea Level in Long Island Sound, Connecticut, Since 500 cal yr A.D. Quat. Res. 53, 89–97. doi:10.1006/qres.1999.2099

van De Plassche, O., van Der Borg, K., de Jong, A.F.M., 1998. Sea level–climate correlation during the past 1400 yr. Geology 26, 319. doi:10.1130/0091-7613(1998)026<0319:SLCCDT>2.3.CO;2

Webb, E.L., Friess, D. a, Krauss, K.W., Cahoon, D.R., Guntenspergen, G.R., Phelps, J., 2013. A global standard for monitoring coastal wetland vulnerability to accelerated sea-level rise. Nat. Clim. Chang. 3, 458–465. doi:10.1038/nclimate1756

Whelan, K.R.T., Smith, T.J., Anderson, G.H., Ouellette, M.L., 2009. Hurricane Wilma's Impact on Overall Soil Elevation and Zones Within the Soil Profile in a Mangrove Forest. Wetlands 29, 16–23. doi:10.1672/08-125.1

Wigand, C., Roman, C.T., Davey, E., Stolt, M., Johnson, R., Hanson, A., Watson, E.B., Moran, S.B., Cahoon, D.R., Lynch, J.C., Rafferty, P., 2014. Below the disappearing marshes of an urban Estuary: Historic nitrogen trends and soil structure. Ecol. Appl. 24, 633–649. doi:10.1890/13-0594.1

Woodroffe, C.D., 2002. Coasts : form, process, and evolution. Cambridge University Press.

Woodroffe, C.D., 1990. The impact of sea-level rise on mangrove shorelines. Prog. Phys. Geogr. 14, 483–520. doi:10.1177/030913339001400404

Woodroffe, C.D., Rogers, K., McKee, K.L., Lovelock, C.E., Mendelssohn, I. a., Saintilan, N., 2016. Mangrove Sedimentation and Response to Relative Sea-Level Rise. Ann. Rev. Mar. Sci. 8, annurev-marine-122414-034025. doi:10.1146/annurev-marine-122414-034025

Yao, Q., Liu, K., Platt, W.J., Rivera-Monroy, V.H., 2015. Palynological reconstruction of environmental changes in coastal wetlands of the Florida Everglades since the mid-Holocene. Quat. Res. 83(3), 449-458. doi:10.1016/j.yqres.2015.03.005

Tables

Table 3.1. Description of methods used to measure accretion and surface elevation change in coastal wetlands, along with strengths, weaknesses, and assumptions of each.

Surface Marker Horizons — Variations: feldspar, sand, brick dust, tiles, cement		
Description A visibly-distinct layer is initially applied to the wetland surface. A sample is cored through/to the horizon and accretion is measured as thickness of sediment above the horizon since the time of horizon deployment. Core is replaced after measurement. Depth scale: < 5-10 cm	Assumptions • Material is deposited at the surface • Horizon does not influence deposition • Replacing cores after measurement does not influence future measurements • Auto-compaction not considered	Strengths (+) & Weaknesses (-) + May provide 5-10 years of data before horizon replacement (often less) + Potential for time-series analysis - Costly (time & money) long-term investment for regular, ongoing sampling - Capable of quantifying erosion, if it occurs after horizons have been established
^{137}Cs, $^{239+240}Pu$ — Variations: dating based on depth of tracer's first appearance (1953), peak occurrence (1963), or 1986 (Chernobyl)		
Description Gamma counting to identify Cs activities in soil intervals. Plutonium isotope ratios are detected using ICPMS following extensive sample preparation. Accretion calculated as depth above dated interval divided by total years. Depth scale: tens of cm	Assumptions • No compaction of soil during core collection • No vertical mixing of tracer • No auto-compaction • Dates indicate reservoir age: addition or loss of younger and older material can occur within the reservoir	Strengths (+) & Weaknesses (-) + Provides 20-50 years of data (depending on sampling date) + Dating calculations are easy to conduct - ^{137}Cs can be mobilized in saline, organic soils - Pu measurements are costly (time & money) - Tracer may not be found in arid climate soils with minimal atmospheric fallout/washout - ^{137}Cs has a half life of 30 years, so its signal will weaken in the coming century
^{210}Pb — Variations: CRS (variable sedimentation rates) & CIC (constant sedimentation rate) models		
Description Alpha or gamma spectroscopy used to establish activities of ^{210}Pb by depth. Dating models utilize decay constant and soil dry bulk density to establish mass sedimentation rates. Depth scale: tens of cm	Assumptions • See ^{137}Cs, $^{239+240}Pu$	Strengths (+) & Weaknesses (-) + Provides ~100+ years of vertical accretion and mass accumulation + CRS model potentially capable of sub-decadal resolution - May not be found in arid climate soils with minimal atmospheric fallout/washout
Historic Event Horizons — Variations: land-use change, hydrology change, pollen, volcanic eruption etc.		
Description Accretion calculated as depth to a distinct sedimentary layer of known origin, divided by years since that event. Depth scale: cm to m	Assumptions • See ^{137}Cs, $^{239+240}Pu$	Strengths (+) & Weaknesses (-) + When available, may provide rates over a range of ages from sub-decadal to millennial - Only opportunistically available
^{14}C (Accretion only) — Variations: can be combined with foraminifera analysis to infer elevation; not considered here.		
Description Macrofossils of organic (woody) or inorganic (molluscan) C are radio-carbon dated using AMS. The proximity of the dated material with the original soil surface is based on assumptions regarding stratigraphic proximity to other flora and fauna with less variable depth of soil occupation. Depth scale: Tens of cm to m	Assumptions • No compaction of soil during core collection • Particle ages are used to establish reservoir age • No vertical movement of chronometer following deposition • Dates indicate reservoir age: addition or loss of younger and older material can occur within the reservoir	Strengths (+) & Weaknesses (-) + Provides rates over a range of hundreds to thousands of years - Variable rates only provided when multiple macrofossils are dated - Uncertainties associated with dating roots that grow to various depths and mollusks capable of mobility. + For deep samples encompassing auto-compaction and long-term diagenesis, these accretion rates may be semi-synonymous with elevation change.
Surface Elevation Tables — Variations: Original, Shallow, and Deep Rod-SETs		
Description A vertical pipe or rod is driven to a known refusal depth and an arm is leveled in 4 positions, 90 degrees apart. The distance between the arm and the soil surface is measured and averaged using nine pins, Depth scale: Surface: mm to cm Soil depth: 2-40 m	Assumptions • Sampling is conducted under the same/consistent conditions whether seasonally or yearly • Although it is known that water levels influence surface elevation, sampling periods often cannot always be conducted at the same (tidal or seasonal) water level conditions.	Strengths (+) & Weaknesses (-) + Potential for time-series analysis with regular, relatively frequent sampling - Costly (time & money) long-term investment for regular, ongoing sampling - Inconsistent reference depths may complicate comparisons between sites for some of the early stations.

Table 3.2 Definition of terms related to measurements of accretion and elevation change in coastal wetlands.

Term	Definition
Accretion/ surface accretion	The thickness/ height of material added to the soil column above a given reference plane (in units of mm or cm yr^{-1}). Note that accretion is not a measurement of mass accumulation (units of g or kg yr^{-1}).
Compaction/ auto-compaction	The physical process of decreasing the volume occupied by a given unit of soil mass. Auto-compaction occurs as a result of the pressure applied via increasing overburden of new soil material. Note that water and increasing water depths do not drive compaction of the underlying soils because the porespace is occupied and supported by water.
Contraction/ shrinking/ consolidation	A decrease in the soil volume as a function of such processes as drying (loss of water volume), decomposition of organic matter (loss of soil mass), or rearrangement and increase of packing density of mineral particles.
Density normalization	A mathematical means of normalizing surface intervals to the same average dry bulk density as lower intervals in order to account for auto-compaction. Most frequently used with ^{210}Pb measurements.
Surface elevation change	The change in height of the wetland surface relative to a vertical reference plane. For early SETs the reference used was the initial height of the surface. Subsequent deployments have standardized the starting elevation to a vertical datum.
Erosion	The physical removal of material from the soil column.
Expansion/ swelling	The raising or increasing of elevation; may be caused by ingrowth of roots or addition of water to void spaces in formerly dry soils
Linear trend rate	For Marker Horizons or Surface Elevation Tables, the method of calculating the annual rate of change as the linear least squares regression of the observations of height vs. time. Less effected by outlier measurements.
Net change rate	The method of calculating the rate of change as the difference between the most recent measurement and the starting measurement divided by the number of years in the record. Can be highly influenced by outliers (e.g. storm deposition or droughts) in shorter datasets. This is the method used to calculate accretion rates for radionuclide-dated cores: thickness of soil column observed at time of sampling divided by the number of years above the reference plane.
Physical mixing, bioturbation	Following the geological law of superposition, the stratigraphy of wetland soils occurs with the oldest depositional layer at the bottom and the youngest, most recent depositional layers at the top. Physical (e.g. storm surge scouring) or biological disturbance (e.g. crab burrowing) contribute to rearranging this expected stratigraphy. The result may be a disturbance of a tracer used for dating the soil body, or the loss of material from within the soil body.
Reference plane	The depth above which changes to the height or thickness of the soil column are observed.
Degradation/decomposition/diagenesis	A continuum of processes that include the physical degradation of material as well biological and chemical transformation of complex compounds into simpler ones that in turn may be removed from the soil in a gaseous or dissolved state.
Sediment	Often geologically referring only to mineral material, but sometimes casually used to refer to any particulate material including organic matter
Sedimentation/ mass accumulation	The mass of soil that accumulates in a given area per unit time, generally in units of g m^{-2} yr^{-1}. See "sediment"; sometimes meant to describe only the rate of mineral sediment accumulation.
Subsidence (shallow and deep)	The sinking or decreasing of elevation. Due either to (a) shallow processes (such as compaction, dewatering or erosion) in the unsonsolidated soil above bedrock or the consolidated layer, or (b) deep processes related to bedrock/consolidated layer changes such as tectonic activity or flexural unloading.

Table 3.3 Mean and standard deviation (SD)[*] of length of record (years) and sample number for elevation change and sediment accretion rates (SAR) for each timescale[**] by region.

	Elevation Change			Sub-decadal SAR			Decadal SAR			Centennial SAR			Millenial SAR		
	Avg.	SD	n	Avg.	SD	n	Avg.	SD	n	Avg.	SD	n	Avg.	SD	n
New York & Connecticut, USA	8.3	1.4	12	7.6	2.5	17	43	13	38	237	208	96	1,450	338	35
Louisiana, USA	3.6	1.9	17	1.2	1.1	216	27	7	309	100	0	18			n/a
Southwest Florida, USA	2.9	0.9	21	2.9	0.9	26	29	19	30	106	24	19	3,131	1,334	14
Northwestern Mediterranean	6.6	3.6	92	3.3	1.7	44	12	7	50	322	347	6	1,991	264	4
Northeast Australia	3.6	1.3	52	3.0	0.0	12	26	22	5	100	0	10	7,405	1,168	8
Southeast Australia	3.8	2.1	90	3.1	0.3	91	27	22	15	108	11	2	1,620	424	2
Total	**4.8**	**2.9**	**229**	**2.8**	**1.9**	**406**	**25**	**13**	**447**	**193**	**187**	**151**	**2,619**	**2,107**	**63**

[*] Standard deviations of 0 indicate that multiple, identical values were entered (see Methods for further description).

[**] No radiocarbon rates of marsh accretion were found for Louisiana.

Figures

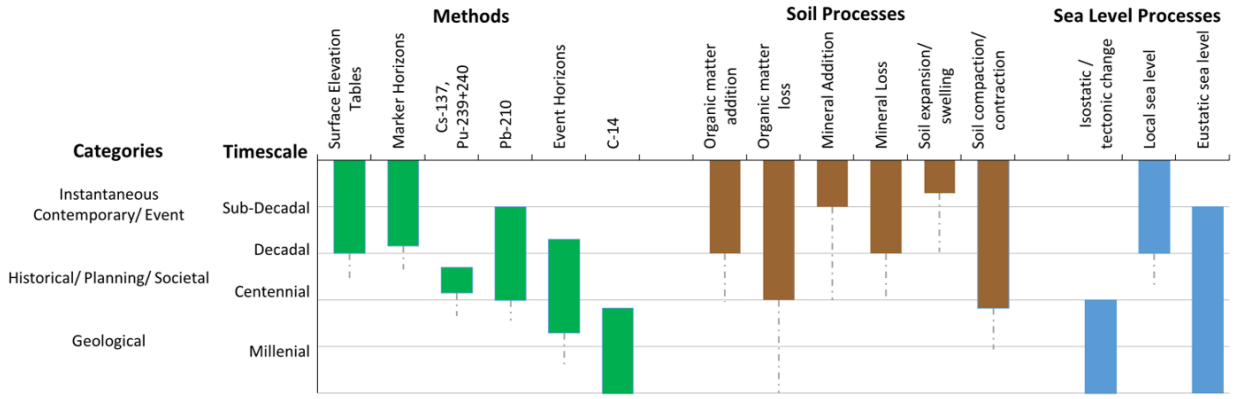

Figure 3.1 Timescales of processes affecting change of soil body accretion and elevation in coastal wetlands, and the methods used to measure them. The ranges represent the timescales over which a change in either the mass or volume of a soil body can be detected (using these methods). While the timescale of SET measurements represents the length of time over which observations have been made at a station, the tool measures changes occurring to the entire soil column, including material potentially deposited thousands of years ago. For Methods, dashed lines represent the upper limit of dating tools at present, noting that the utility of SET-MH stations will continue to increase as long as sampling continues in the future. For Soil and Sea-Level Processes, blocks represent predominant timescale of change, with dashed lines indicating full range of change (e.g. most soil organic matter diagenesis occurs in the first decade, but continues for thousands of years, even if at a slowing rate).

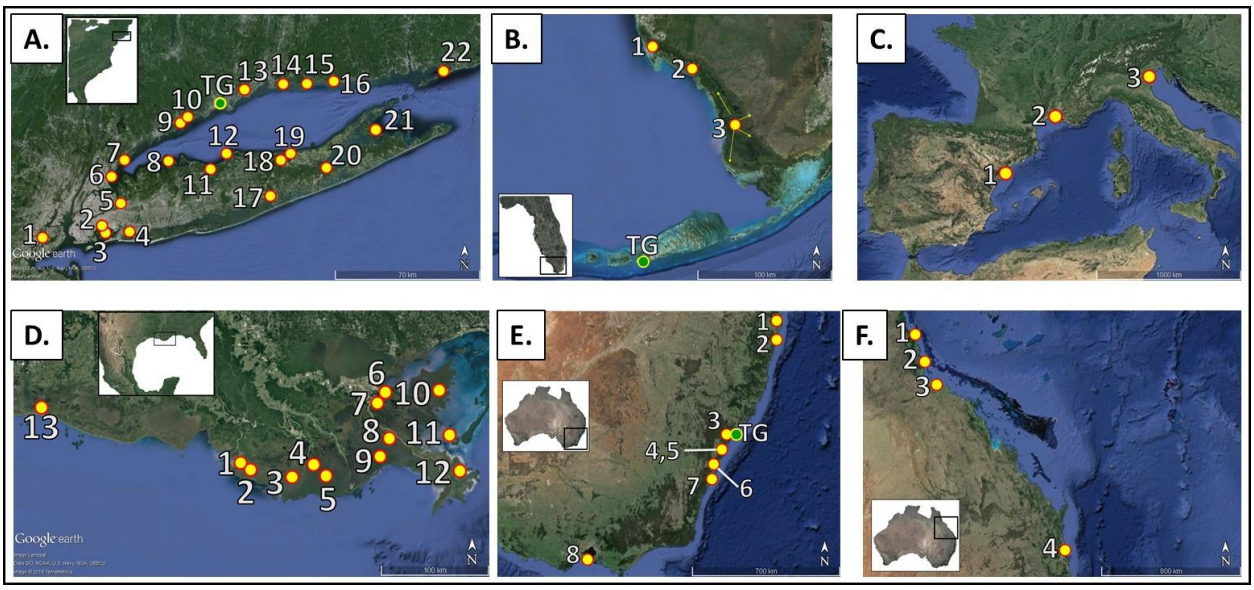

Figure 3.2 Location of regions examined in this study. Numbered place markers indicate locations of specific wetlands/ sub-regions where data was recorded from the literature. Green and yellow place markers indicate locations of tide gauges (TG) used for sea level comparisons. Locations in the maps are as follows: A) New York & Connecticut, USA: 1. Staten Island, NY, 2. Jamaica Bay, NY, 3. Hempstead Bay, 4. Alley Pond, NY, 5. Pelham Bay, NY, 6. Otter Creek, NY, 7. Marshlands Conservancy, Rye, NY, 8. Caumsett State Park, NY, 9. Norwalk, CT, 10. Westport, CT, 11. Nissequogue River, NY, 12. Flax Pond, NY, 13. Millford, CT, 14. Branford, CT, 15. Guilford, CT, 16. Clinton, CT, 17. Carmans River, NY, 18. Deep Pond, NY, 19. Fresh Pond, NY, 20. Hubbard County Park, NY, 21. Mashomack Preserve, NY, 22. Barn Island, CT , & Tide Gauge: Bridgeport, CT. B) Southwest Florida, USA: 1. Rookery Bay, 2. Ten Thousand Islands, 3. Southwest Everglades National Park, & Tide Gauge: Key West. C) Northwestern Mediterranean Sea: 1. Ebro River Delta, Spain, 2. Rhone River Delta, France, & 3. Venice Lagoon, Italy. D) Louisiana, USA: 1. Fourleague Bay, 2. Old Oyster Bayou, 3. Terrebonne, 4. Bayou Chitigue, 5. Lake Barre, 6. Violet, 7. Caernarvon, 8. West Point a la Hache, 9. Barataria Bay, 10. St. Bernard, 11. Breton Sound, 12. Delta National Wildlife Refuge, & 13. Cameron Parish. E) Southeast Australia: 1. Tweed River, 2. Evans Head, 3. Hunter River, 4. Parramatta River, 5. Sydney, 6. Minnamurra River, 7. Jervis Bay, 8. Western Port Bay, & Tide Gauge: New Castle V. & F) Northeast Australia: 1. Cairns, 2. Missionary Bay & Hinchinbrook Channel, 3. Magnetic Island, & 4. Moreton Bay.

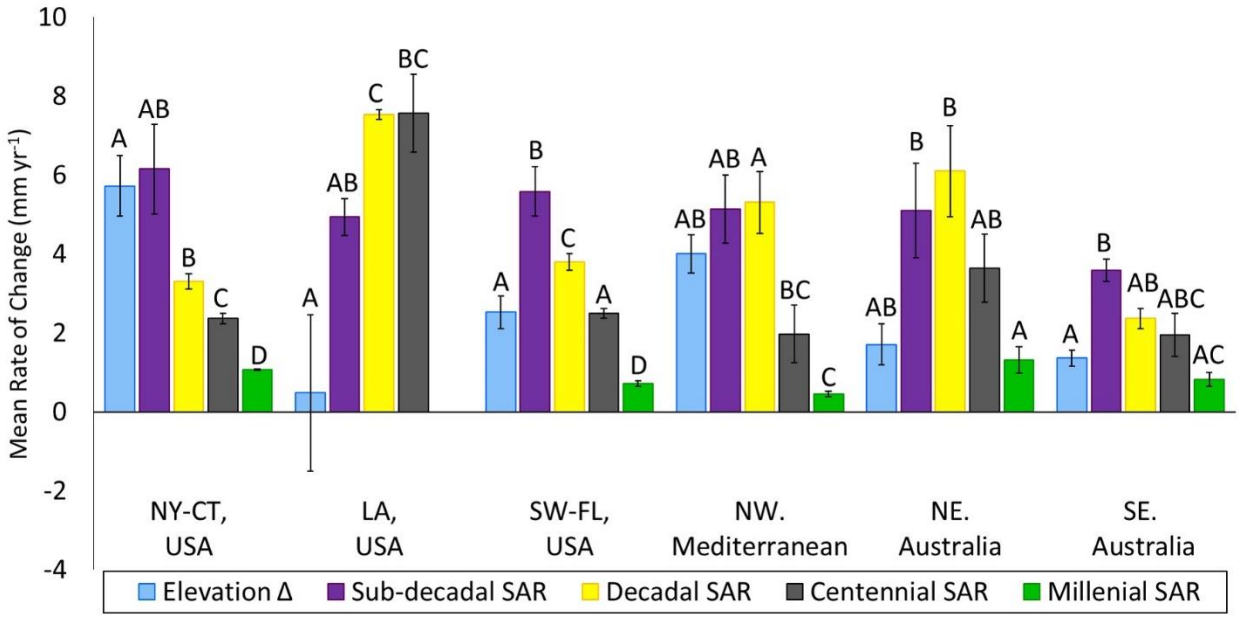

Figure 3.3 Average rates of elevation change (Elevation Δ) and sediment accretion (SAR) by timescale for each region. Different capital letters indicate significant difference ($p<0.05$) within regions. Error bars represent 1 SE.

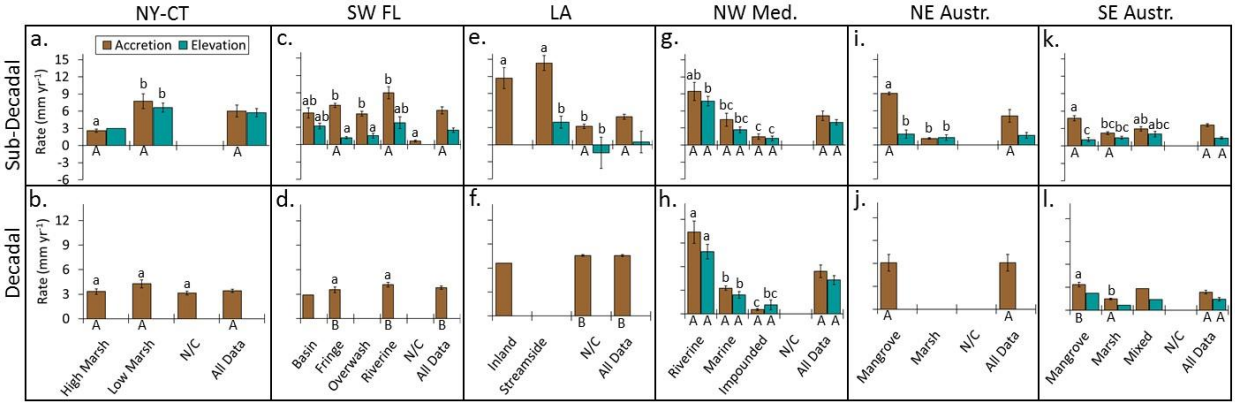

Figure 3.4 Comparison of average rates of accretion and elevation change for sub-decadal and decadal timescales for environmental categories within each region. Different lowercase letters (above columns) indicate significant difference ($p<0.05$) between environmental categories (x-axis) within regions for each timescale. Different capital letters (beneath columns) indicate significant difference ($p<0.05$) between timescales (y-axis) within environmental categories for each region. N/C indicates data that could not be categorized. Blank spaces indicate absence of data. Absence of upper or lowercase letters indicates that limited data precluded statistical comparison. Error bars represent 1 SE.

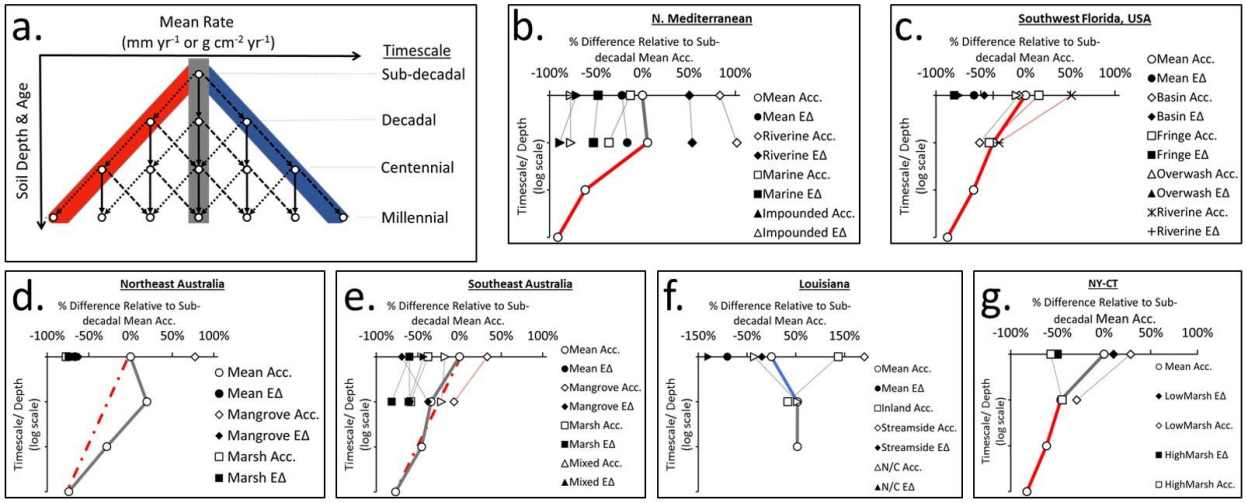

Figure 3.5 Conceptual model of timescale hierarchies of soil body rates as a function of depth/age. a, Potential profiles. The null hypothesis is represented by the gray profile, indicating no significant rate changes ($p<0.05$) over different depths or timescales. Red/ blue profiles indicate significantly decreasing/increasing rates. Potential profile variations reflect changes to rates of material delivery or degradation over time. b–g, Timescale hierarchies for the six study regions. Thick colored lines (red, blue, and gray) and open circle symbols indicate the statistical relationship for regional mean accretion rates as a function of timescale. Dashed lines indicate the relationship between the surface and bottom-most interval if the relationship is different than that between the bottom-most interval and the immediately-overlying intervals. Thin lines and additional symbols indicate the timescale relationship of elevation change (EΔ) and accretion (Acc.) rates for specific environmental categories within each region. "Not categorized" (N/C) represent rates that could not be assigned to a specific environmental category based on details provided in the literature.

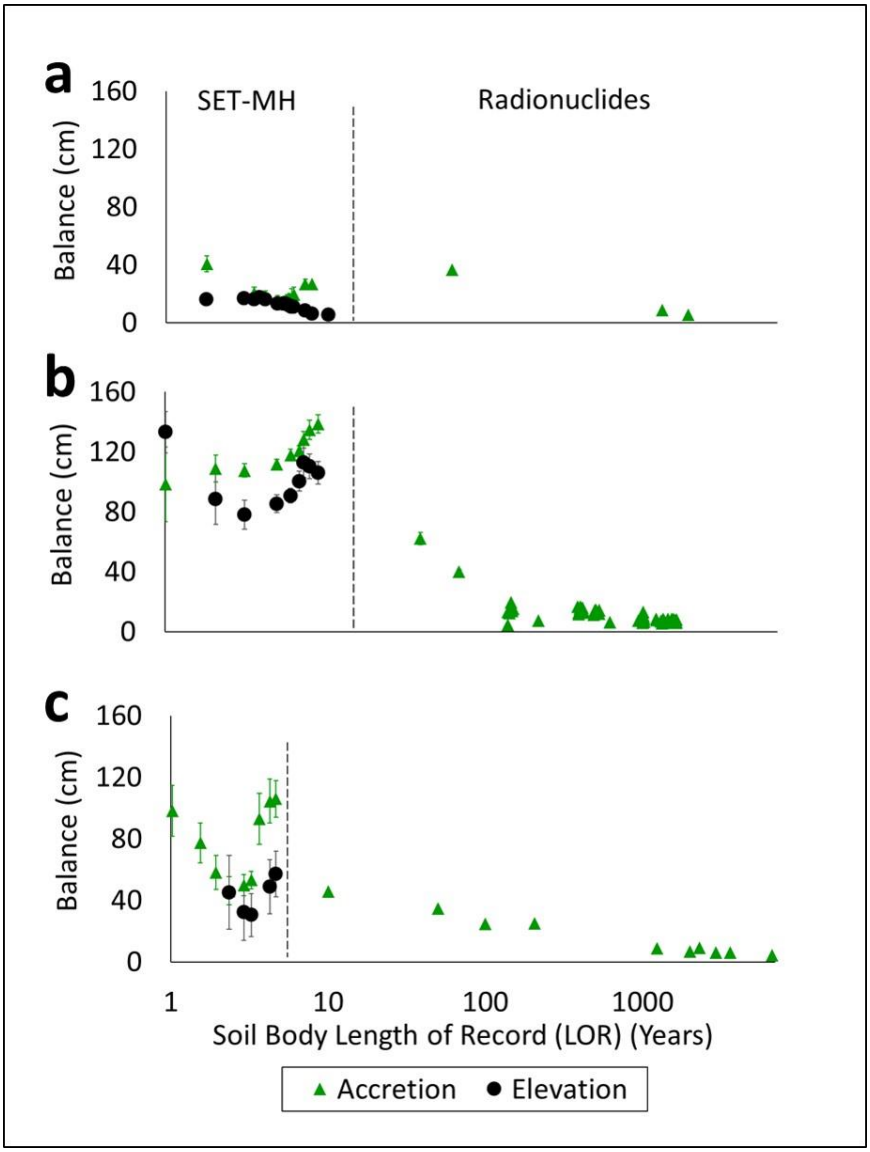

Figure 3.6 Timescale dependence of 100-year soil body balances relative to local sea-level. Accretion and elevation balances (See Methods) for a, Kooragang Island, Australia, b, Jarvis Marsh, CT, USA, and c, Everglades National Park, FL, USA. SET-MH measurements are to the left of the dashed line, and radionuclide measurements are to the right. Radionuclide measurements are provided from the same location for panel c, and from the nearest available locations for panels a (Sydney and Jervis Bay) and b (Guilford and Clinton, CT). Error bars represent 1 SE.

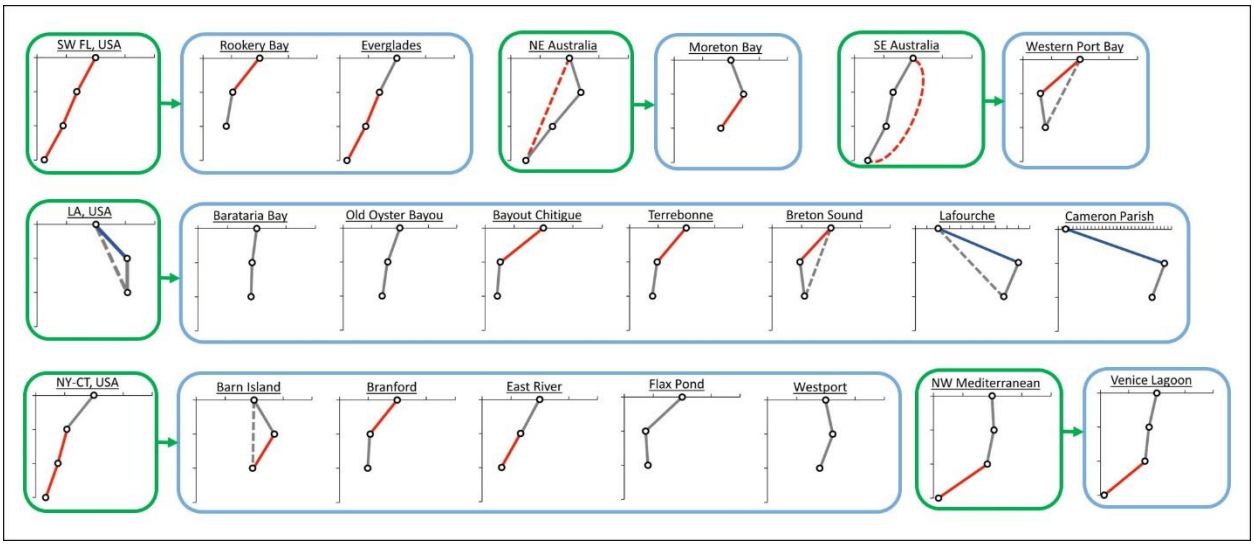

Figure 3.7 Site-specific timescale hierarchies. Sites included here have rates reported from three or more timescales. The X and Y axes are the same as those in Figure 3.5, but are simplified here for clarity. Note the substantially expanded x-axes for Lafourche and Cameron Parish sites in LA, USA (each tick-mark represents an additional 50% change relative to the position of the surface data point).

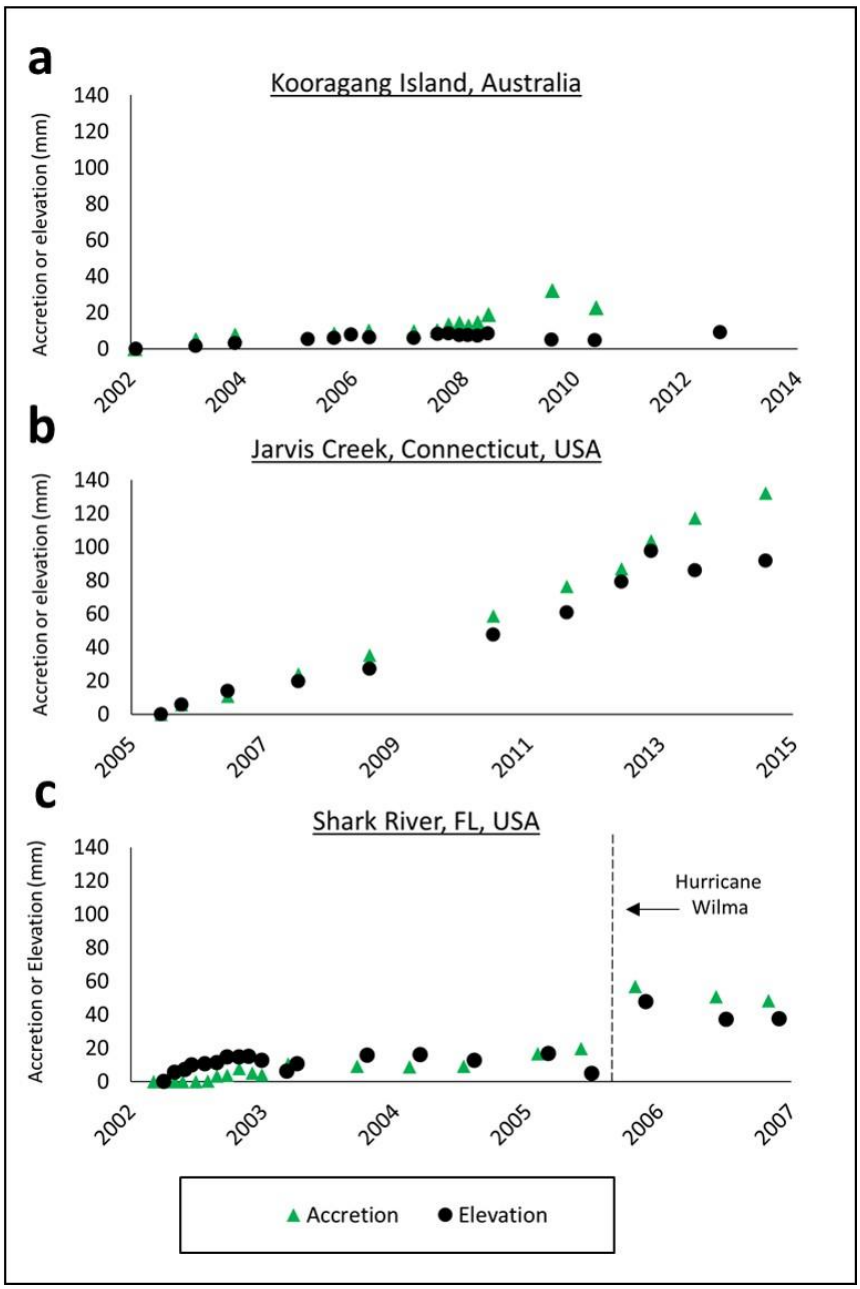

Figure 3.8 Case studies: raw accretion and elevation data (total mm relative to initial benchmark). Data reconstructed for a, Kooragang Island, Australia (Rogers et al., 2013), b, Jarvis Marsh, CT, USA (Anisfeld et al., 2016), and c, Everglades National Park, FL, USA (Whelan et al., 2009).

Conclusions

Key Findings

The following are primary conclusions reached for each chapter of this dissertation. From the first chapter: (a) the soil volume contributions made by SOM and SIM are not constant throughout the range of soil classes represented in the carbonate platform mangrove settings that were investigated. This is important because it appears to differ from previous findings from marsh environments in North America, and indicates an interactive contribution to soil volume from the two constituents. (b) The rate of SOM accumulation was consistently the best predictor of accretion rates. Conversely the rate of SIM accumulation was the best predictor of the soil density. (c) Based on historical rates of accretion and fluxes of SOM and SIM, there is evidence that sites in the intermediate and mineral soil classes can keep pace with 4.6 mm yr^{-1} of SLR. There are only three instances in the past 100 years (i.e., three dated soil core intervals) when any of the organic soil class sites have achieved a rate exceeding 4.6 mm yr^{-1}; these sites are less likely to keep pace with the low-end projection of future SLR for the region.

From the second chapter, the primary conclusions are: (a) 100-year average rates of OC and TN burial only show moderate spatial variability across the southwestern coastal Everglades. However, in the context of the regional landward gradient in NPP, there are substantial differences in OC burial efficiency. Organic carbon burial was least efficient near Tarpon Bay; increasing salinity (with the potential for sulfate reduction) has been observed in this oligohaline part of the ecotone in the past decade. These findings suggest that accelerating SLR may cause a substantial loss of historically sequestered carbon even in the absence of visible peat collapse. (b) In contrast, soil accumulation rates of $CaCO_3$ and TP decreased significantly as a function of distance from the GOM. These observations are consistent with previous characterizations of the region as an "upside down estuary" where the limiting nutrient (P) is provided from the marine environment, and often through the provision of storm-surge

sediment composed of marl with high concentrations of Ca-bound P. (c) Depth profiles of $CaCO_3$:TP in the downstream soil cores potentially provide a novel method for estimates of marine carbonate dissolution in mangrove soils of varying organic content. These first-order estimates of potential dissolution have important implications for the regional mangrove C budget because the carbon is non-mangrove in origin, and potentially represents a significant contribution of dissolved inorganic carbon/alkalinity to the nearshore environment.

The primary conclusions of the third chapter are: (a) rates of surface elevation change and accretion vary as a function of timescale. This finding was shown to be the case whether measurements were compared regionally or at individual locations, and whether comparisons are made over single years, decades, centuries or millennia. (b) The hierarchy of these timescale differences varies by region. This finding points to the importance of regional biogeochemical processes and eco-geomorphic histories, and indicates that identification of such hierarchies cannot be made *a priori* for different regions. (c) Ultimately because of these differences, the primary finding from this research was that multiple timescales and methods are needed to quantify past rates while simultaneously monitoring for future change.

Future directions

There are additional research activities that can be taken to further illuminate the findings from each chapter in this dissertation. Such work may consist of further examination of assumptions used to reach some of the existing conclusions or it may derive from new research questions generated. Future work stemming from Chapter 1 consists of the following: (a) examine whether the finding that SOM and SIM accumulation rates are not additive in predicting accretion rates applies to mangroves in other geomorphic settings where mangroves are found. Such research would include examination of how well the multiple linear regression models compare to measured rates in non-carbonate settings, as well as similar analysis of existing measurements in other regions to determine the respective accretion contributions of SOM and SIM in each. (b) This work has largely relied on a general characterization of

the SOM and SIM based on the LOI methodology. Future work should examine how much of the SIM is allochthonous marine material. Two potential alternative sources include allochthonous periphyton from upstream, freshwater ecosystems, as well as the possibility of $CaCO_3$ formation via the oxidation of organic matter. Useful techniques would include examination of the crystalline structure to differentiate calcite from aragonite as well as utilization of $\delta^{13}C$ values to potentially differentiate $CaCO_3$ formation from DIC (relatively enriched) versus that occurring from the oxidation of organic matter (relatively depleted). (c) Finally, there is opportunity for greater improvement in the models used to predict the non-additive SOM and SIM contributions to accretion. One specific opportunity is to use a linear derivation of the non-linear ideal mixing model to more easily identify different model fits according to a range of soil organic classes. Such an approach would be useful for considering the influence of auto-compaction on differences in the fits and SOM coefficients in the multiple linear regression models. (e) Finally, because the ultimate objective of much of this research is to understand the timing of wetland vulnerability, it will be important to explore modelling methods that consider variable accretion rates as a function of feedbacks with non-linear rates of SLR.

Future work to be conducted as follow-up to the research from Chapter 2 will consist of the following: (a) Increase the spatial coverage of soil cores and measurements of OC burial rates in locations that are both up- and downstream of the oligohaline ecotone. Such efforts would be fruitful for establishing a better understanding of the "baseline" rate of OC burial in regional freshwater peat, which is presently under-reported in the literature. Additionally, measurements in the oligohaline regions of other rivers such as Broad and Lostman's, would help to explain whether the low rates observed around Tarpon Bay in this research occur elsewhere in the region. (b) Just as more soil cores would help to illuminate regional patterns, additional measurements of soil CO_2 fluxes over greater spatial and temporal scales (months, seasons) would be useful to further constrain the relationship between burial rates and soil respiration. Particular locations that would be useful to examine include the upstream, freshwater peat locations as well as sites at the furthest downstream extent that are most exposed to coastal influences of

storms as well as the greatest tidal range. (c) One of the powerful controls on OC burial is tidal inundation depth, period, and frequency. Future work would benefit from knowledge of the surface elevation at each site in order to pair regional hydrology measurements with sites where these soil cores have been collected. (d) Finally, it would be fruitful to test the first-order carbonate dissolution rates estimated in this dissertation by making field measurements of porewater pH at various depths (as identified by the $CaCO_3$:TP slopes or asymptotes) at locations with varying soil organic content throughout the estuary.

Potential future work stemming from Chapter 3 consists of the following: (a) Undertake additional empirical studies of side-by side measurements made using multiple methods to determine location-specific changes as a function of time and the potential extent of post-depositional volume changes. (b) Utilize repeated radiometric measurements of rates at sites where the same techniques have been used previously (i.e., 10-20 years previously). (c) Finally, it would be potentially important to expand the scope of the study to the application of timescale relevance on measurements of OC burial rates.

Appendix 1

List of acronyms, abbreviations and uncommon terms

CSTN: Celestun Lagoon, Mexico

CNPP: net primary productivity of organic carbon (g OC m^{-2} yr^{-1})

DBH: diameter at breast height (cm)

Density: mass of sediment per unit volume. Four variations of density are discussed in this dissertation:

- DBD: dry-bulk density; mass of dry sediment per initial wet volume (g cm^{-3})
- Particle density: the respective mass: volume ratios of the SOM and SIM minus the mass and volume occupied by water and gas. This measurement represents only the volume occupied by the solid particles and is measured using crushed, homogenized material in a pycnometer
- Self-packing density: the *in-situ* volume occupied by SOM or SIM structures including soil, roots, branches, leaves, and rocks, including the occupied or unoccupied void spaces.
- SOM or SIM fraction of DBD: calculated as LOI × DBD (SOM fraction) or (1-LOI) × DBD (SIM fraction).

ENP: Everglades National Park, Florida, USA

FCE LTER: Florida Coastal Everglades Long-term Ecological Research

GOM: Gulf of Mexico

LOI: loss-on-ignition; mass loss as a fraction of total initial mass (g g^{-1}). Generally reported as a percentage.

LOR: length of record (years)

MH: marker horizon

NPP: net primary production (g OM m^{-2} yr^{-1})

OC: organic carbon

OM: organic matter

$Resp_C$: respired carbon (g OC m^{-2} yr^{-1})

SAR: sediment accretion rate; reported as both mm or cm yr^{-1}.

SET/RSET: surface elevation table/ rod-surface elevation table

SOM: soil organic matter; the material identified via loss-on-ignition (LOI)

SIM: soil inorganic matter; identified as the residual material following loss-on-ignition (LOI)

SK: Sian Ka'an Biosphere Reserve, Mexico

SLR/RSLR: sea-level rise/ relative sea-level rise

TN: total nitrogen

TP: total phosphorous

TTI: Ten Thousand Islands, Florida, USA

VIF: variance inflation factor; used to assess multi-collinearity between SOM and SIM accumulation rates for multiple linear regressions. A VIF of less than 10 indicates acceptable levels of collinearity.

WSC: Water, Sustainability & Climate grant-funded research sites in Everglades National Park (ENP)